Charge-transfer dynamics studied using resonant core spectroscopies

P. A. Brühwiler,* O. Karis,[†] and N. Mårtensson[‡]

Department of Physics, Uppsala University, Box 530, SE-751 21 Uppsala, Sweden

(Published 12 July 2002)

The authors review the use of core-level resonant photoemission and resonant Auger spectroscopy to study femtosecond charge-transfer dynamics. Starting from simple models of the relevant processes, they examine the rationale for this approach and illustrate the approximations and known subtleties for the inexperienced experimentalist. Detailed analysis of case studies of increasing complexity are taken up, as well as the connection to related approaches using both valence excitation and the core-level fluorescent channel.

CONTENTS

*Electronic address: paul.bruhwiler@fysik.uu.se
[†]Electronic address: olof.karis@fysik.uu.se
[‡]Also at the Swedish National Synchrotron Facility MAX-lab. Electronic address: nils.martensson@fysik.uu.se

I. INTRODUCTION

Charge-transfer dynamics is a topic with wide relevance in many fields, including, femtochemistry, photochemistry, surface reaction dynamics, molecular electronics, solar energy/photosynthesis, and photography (Miller *et al.*, 1995). A direct and appealing approach to studying such dynamics is the pump-probe measurement, in which an electron is optically excited ("pumped" to a higher state), and the excited state is probed as a function of time after the excitation. The use of lasers with pulse lengths as short as a few tens of fs for this is now well established. Systems to which this kind of technique has been applied recently include dye-sensitized semiconductor electrodes (Hannappel *et al.*, 1997), image-state wave packets at metal surfaces (Höfer, 1999), and hot electrons at noble-metal surfaces (Aeschlimann *et al.*, 2000). These methods have the appeal of operating in the time domain, which allows one to more or less directly derive relaxation times as low as around 10 fs.

Another option for looking at charge-transfer times in the fs regime has recently been successfully exploited, based on core-level excitation and decay (Björneholm *et al.*, 1992a). This method is analogous to the pump-probe technique, with an intrinsic time scale based on the lifetime of the intermediate (core-hole) state, leading to the descriptive name "core-hole clock." It is the shortness of this time scale compared to tens of fs which gives the approach a unique place in the study of electron-transfer dynamics. Besides that, it differs in two primary aspects from the more traditional pump-probe studies: (1) The measurement is carried out not in the time domain, but instead in the energy domain, so that it is often termed an excitation-decay, rather than a pump-

probe, measurement; (2) core electrons are involved, which enables the general atomic specificity unique to core spectroscopies.

The purpose of this article is to review developments in the study of charge-transfer dynamics using resonant core-level excitation-decay measurements and to present the basic principles, strengths, and limitations of this method, as well as a discussion of its future prospects. Time-independent theoretical treatments along similar lines are those of Ohno (1994) and Ueba (1991, 1992), and after submission of this review a time-dependent treatment was published by Gortel and Menzel (2001). We shall focus on studies in the soft-x-ray regime, primarily involving the C 1s and N 1s levels. We attempt to provide a unified view of the work that has been reported, with varied examples to give a feeling for the applications of the technique as well as its limitations, for example, as a function of system size.

Fundamental to our presentation is the concept of a "small" system, an atom or molecule, which is electronically coupled to a "large" system, such as a substrate or a matrix. The coupling is assumed to be weak enough that the small system can be described to a first approximation as if it were isolated, with the coupling effects as a perturbation which one would like to assess experimentally. More specifically, we focus here on cases of coupling strengths of the order of 0.1 eV, which are comparable to the core-state lifetimes employed in the examples. This regime is almost impossible to access by the more traditional band-structure technique of angle-resolved photoelectron spectroscopy, due to the need for presently unrealistic levels of energy and angle resolution. In addition, it is comparable to vibrational coupling effects, making it difficult to elucidate merely on the basis of, for example, linewidths in absorption spectra. Nevertheless, this regime of coupling strength is broad enough to encompass many interesting cases in widely divergent areas of chemical and condensed-matter physics.

The definition of charge transfer is also an important issue. It is clear in a quantum description that a charge which leaves one system for another does this via a coupling of the systems, which means that a return of the charge to the original state is a question of time (or probability), rather than a permanent state (May and Kühn, 2000). Temperature plays a role as well if the time scale is long enough, since, for example, the electron bath of the "large" system can eventually inject a charge back into the "small" system. However, it is the lifetime of this state which is generally of interest in the studies we describe here, and this lifetime will (also quite generally) be much shorter than the time scale of thermal excitations. This short discussion can be made more concrete by considering the classical double quantum well, as is done by Miller *et al.* (1995) in their Fig. 1.1. It is clear that an electron placed into this system spends time in each well, tunneling periodically between them in an easily described manner in the case of two identical potentials. For a case in which the available levels in one well are well separated (relative to the coupling strength) from those in the other, the electron will have a tendency to be localized in one of those two potential wells. This condition can be brought about in different ways, because the potential wells represent different species (one of which has been excited, as we shall focus on in this review), or because of the effects of other degrees of freedom such as vibrations (Miller *et al.*, 1995; May and Kühn, 2000). Thus the probability amplitude of the electron is negligible after some time at the "site" (quantum well) with the higher level, and if it started its trajectory there we can state that it has effectively been transferred. May and Kühn (2000) choose a working definition of charge transfer in terms of a spontaneous charge redistribution which can be described as a tunneling process. This is a satisfactory working definition for the present review, interpreted here in terms of the result of a core-level measurement upon excitation of an electron in the small system. Because core-level techniques are quite local in nature due to the involvement of the localized core electrons,[1] this is equivalent to a snapshot of the electron distribution on the small system which includes a probe of the excited electron, and a negative result signifies charge transfer. In Sec. III.C.2 we discuss possible exceptions to the simple, one-way charge-transfer model, e.g., recurrences (Kyrölä and Eberly, 1985; May and Kühn, 2000) as they apply to the core-level techniques.

This review is organized as follows: Section II is intended primarily for those inexperienced in the measurement techniques and defines terms used throughout the paper. Section III introduces concepts needed to understand the particulars of the charge-transfer measurements as well as known limitations on the application of these concepts, and some of the foreseeable developments. As may be surmised from a few of the references, most if not all of the concepts presented in Sec. III are well known from optical studies, but have only recently been developed for application to core-level methods. The case studies described in Secs. IV and V were chosen to illustrate the state of the art and the subtleties that have been brought to light thus far. For instance, the size of the small systems studied increases when proceeding through these sections. The effects of the energetics (location of the Fermi level E_F or conduction-band edge relative to the energy levels of the small system) are explored throughout both sections. Electron-electron correlations emerge as a recurrent theme, but expressed in a varying manner from case to case. Several of the studies were aimed at characterizing the method itself (Ar, N_2, CO as the small system), whereas others focused on applications of the method, for which the specifics of the effects of a core hole on the valence charge distribution are crucial to proper handling (Ar, N_2, solid C_{60}), or even constitute the central question being studied (C_{60}, graphite). Rounding off the case studies, the general power of the method for prob-

_____

[1]See, for example, Maciejewski *et al.* (1993) for a discussion and illustration of this property for Auger transitions.

ing the electronic coupling of complex entities is illustrated for the case of CO adsorbed on supported metal particles. The issues involved in utilizing emitted photons instead of electrons, which have been relatively infrequent thus far, are addressed in Sec. VI. Finally, a look at future prospects of the method is presented in Sec. VII.

II. BASIC PRINCIPLES OF CORE-LEVEL RESONANT ELECTRON SPECTROSCOPY

Paramount for an excitation-decay, just as for a conventional pump-probe measurement, is the ability to select defined (core-)excited states, and study the development of the decay spectra. This requires accurate control of the excitation step, which can be thought of in terms of the excitation energy bandpass. Depending on the system, i.e., on the specific levels involved, the requirement on the bandpass varies substantially. It is typically moderate for core levels, $\lesssim 0.5$ eV, roughly the typical resonance width in the soft-x-ray range [e.g., C $1s$, N $1s$, O $1s$ (Coville and Thomas, 1991; Prince *et al.*, 1999; Campbell and Papp, 2001)]. This and higher levels of resolution have been routinely achieved in recent years (Vondrácek *et al.*, 1999). Motivations for this requirement, as well as aspects of the history of the study of the electron spectra following resonant core excitation, have been reviewed recently by several authors (Eberhardt, 1995; Keller *et al.*, 1998a; Gel'mukhanov and Ågren, 1999; Piancastelli, 2000), whereas the fluorescence channel has received somewhat less attention (Rubensson, 2000). The added benefits of resolution well below the resonance width have recently been explored, which enables us to include an assessment of them in what follows.

Figure 1 shows a schematic of different electronic excitation and deexcitation channels of interest here, with and without resonant excitation. Figure 1(a) depicts excitation of a valence electron in standard valence-band photoelectron spectroscopy (PES), creating a vacancy and a $+1$ charge state on an isolated system such as a molecule. Figure 1(b) shows a similar excitation of a core electron to an unbound final state. After such excitation,[2] a vast majority of the decay processes annihilating the core hole will be as shown in Fig. 1(c),[3] Auger transitions leaving the system in a $+2$ charge state. Via the Coulomb interaction, one electron makes a transition to fill the core hole, and a second electron, which takes up the excess energy, is ejected. This produces a

---

[2] In using the concept "after," we ignore here coherence in the excitation-deexcitation process, a topic to which we return later.

[3] Auger decay of core-excited states predominates for core holes with binding energies less than about 1000 eV. For higher binding energies, radiative transitions account for an increasing share of the total core-hole annihilation channels. See, for example, Keski-Rahkonen and Krause (1974) and Walters and Bhalla (1971).
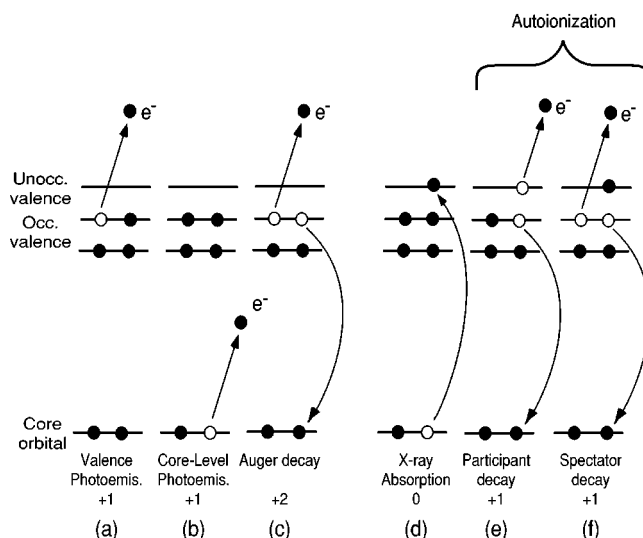

FIG. 1. Schematic molecular-orbital (MO) diagram of the indicated electronic excitation-deexcitation processes. This type of diagram is often used in a model description of spectroscopic processes when no reference to any particular type of system is made. The Fermi level (E_F) would in an extended system be located between the lowest unoccupied and the highest occupied orbital, with the exact position depending on the type of system. The final charge states shown are those for an isolated system, i.e., ignoring coupling that would allow charge transfer to or from the surrounding medium.

double vacancy in the valence bands, as illustrated. The remaining small percentage of the primary decay processes (see Sec. VI) will consist of radiative transitions or soft-x-ray emission. On the other hand, if a core electron is photoexcited to a resonant bound state, a process which we here label x-ray-absorption spectroscopy (XAS), the system remains charge neutral until deexcitation [Fig. 1(d)], and again Auger-like transitions will dominate for the core levels under consideration here. As shown in Figs. 1(e) and 1(f), this leads to two new possibilities for the electron spectra. One channel is characterized by the involvement of the excited electron in the Auger process [Fig. 1(e)], thus taking its name as the *participant channel*, which leaves the system with a single valence vacancy and a charge of $+1$. This final state is energetically the equivalent of valence PES, but the core-hole-assisted path generally has a much larger cross section for the core levels of interest here [see, e.g., Mårtensson *et al.* (1997) and Weinelt *et al.* (1997) for a recent detailed discussion of relative cross sections and interference between these channels in Ni metal]. This channel is often given the name *resonant PES* (RPES) or *participant autoionization spectroscopy*. A second possibility is also shown, Fig. 1(f), in which an electron remains in the normally unoccupied levels in the final state, and two valence electrons have been removed in an Auger-like transition. This channel, often called *resonant Auger* or *spectator autoionization*, also leaves the system in a $+1$ charge state, but is a valence-excited
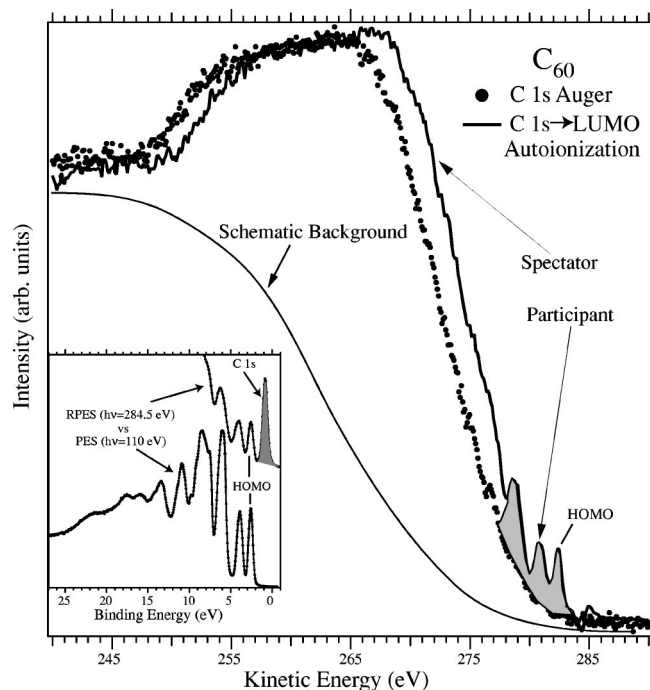
FIG. 2. Data for solid C_{60} corresponding to cases of Fig. 1: points, case (b); solid lines, cases (e) and (f). See Figs. 28 and 29 for XAS data showing the lowest unoccupied molecular orbital (LUMO) and other resonances for C_{60}. Because C_{60} is a van der Waals–bonded molecular solid, the data represent isolated molecules to a good approximation, with kinetic energies (here uncalibrated) modified by the solid-state screening. The difference in kinetic energy between the spectator and Auger spectra, which are nearly identical in shape for this large molecule, is due to the difference in the charge configurations, often denoted the "spectator shift," which is discussed by, for example, Eberhardt (1995). The more easily identifiable participant channels are indicated by shading, and the overall inelastic-scattering background is sketched. Inset: Comparison of photoelectron spectroscopy (PES) to resonant photoelectron spectroscopy (RPES) for excitation at the LUMO resonance. Here the C $1s$ line excited by second-order light (shaded peak) has not been subtracted, i.e, raw data are shown.

state reminiscent of shakeup in PES,[4] i.e., a two-hole–one-electron state.

A comparison of these processes is given in Fig. 2 using data of solid C_{60}. This many-atom system shows a great similarity between Auger and spectator autoionization, which could be expected based on the small perturbation to the system played by a single valence electron. Also seen is the weak relative cross section for participant compared to spectator autoionization. This figure also hints at a fundamental limitation on the usefulness of dividing the spectrum into participant and spectator contributions, since for larger systems these often overlap. For example, due to the fact that solid C_{60}

---

[4]See Sec. IV.A.3 in Sandell *et al.* (1994) for a recent discussion of the relationship between spectator autoionization and PES shakeup.

has a 2-eV band gap, only the band derived from the highest occupied molecular orbital (HOMO) at 282.5 eV has undebatably pure participant origin, whereas the band below may contain slight contributions from other transitions, and the next band at 279 eV is degenerate with a noticeable background of spectator contributions. Indeed, as the transitions in PES become less separated from one another at higher binding energy (see inset in Fig. 2), it becomes virtually impossible to distinguish them in the resonantly excited data. Considering that broadening at higher binding energies in PES is generally an indication of correlation effects mixing the single-hole PES final states with electron-hole states [see Golod *et al.* (1999) for a recent discussion] the submergence of the participant signal into the "Auger background" may be partially explained as an effect of the blurred distinction between participant and spectator channels due to correlations. Another important point relevant to the particular case of C_{60} is that the bands have increasing σ character for increasing binding energy, and relatively little π character for those not observed in the resonant spectrum (the fourth and deeper PES structures; Martins *et al.*, 1991). Since the lowest unoccupied molecular orbital (LUMO) is predominantly of π^* character, Auger-like transitions involving the LUMO and σ-like states can be expected to be reduced in intensity relative to those involving π-like states. A similar result has been observed in solid benzene, for which the LUMO has π^* character and the π HOMO participant is strongly enhanced (Menzel *et al.*, 1992) compared to other levels, all of which have negligible π, or in one case mixed, character (Hüfner, 1996, p. 168).

Thus, in general, if there is significant mixing of the participant and spectator channels, the distinction is less meaningful. As suggested in Sec. III, such mixing may in principle be enhanced via coupling of the excited state to the substrate. Strategies developed thus far for minimizing the impact of these issues emerge in Secs. III, IV, and V and can be divided roughly along the following lines: (1) to make no distinction between participant and spectator, and use the entire resonant spectrum in the determination of charge-transfer times; (2) to isolate the verifiable participant lines and utilize them exclusively.

III. CONDITIONS FOR THE OBSERVATION OF DYNAMIC CHARGE TRANSFER

A. Coupling of a core resonance to a continuum

To introduce the concept of measuring charge-transfer dynamics via core excitation, we present Fig. 3 for the case in which the excited state of the probed small system is coupled to a second large system, and imagine removing the excited core electron "before" the core hole decays. In this case, the two resonant channels, Figs. 1(e) and 1(f), converge to Auger decay instead, leading to a 2+ final local charge configuration. Thus any process that entails the effective removal of the excited electron from the vicinity of the core hole (cou-
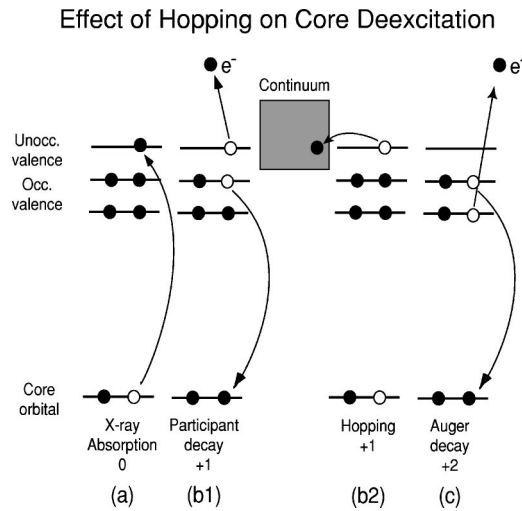
FIG. 3. Schematic of the two main pathways for deexcitation of a system that is loosely coupled to a (substrate) continuum. After excitation via XAS (a), autoionization may occur as usual (b1) [where we include only the participant channel (e) of Fig. 1 to emphasize the role of the excited electron]. Alternatively, the excited electron may tunnel into the continuum (b2), opening an Auger channel (c).
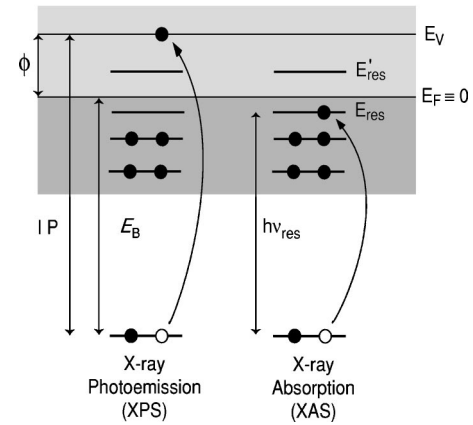

FIG. 4. Schematic of the two main pathways for core excitation of a small system, whose energy levels are assumed to be discrete, loosely coupled to a metallic continuum (occupied states in dark grey, unoccupied in lighter grey). ϕ is the work function of the total system, E_V the vacuum level, E_F the Fermi level, IP the core-level ionization potential of the small system, E_B the binding energy referred to E_F, and $h\nu_{res}$ the photon energy corresponding to the core-level XAS resonance. E_{res}, the energy of the XAS resonance relative to E_F, is thus defined by $h\nu_{res} - E_B$, as shown, and is degenerate with the occupied states of the large system. E'_{res} represents a similar resonance degenerate with unoccupied *traveling states*. Hence $E_{res} < 0$ and $E'_{res} > 0$. Since binding energies for a grounded metal sample are typically measured with respect to E_F of the electron spectrometer, and thus E_F of the sample for a grounded metallic sample, E_B, rather than E_V, is often the most convenient reference. See the discussion in Sec. III.A for details.

pling to the greater environment) corresponds to a quenching of the resonant channels in the decay of the intermediate state.

1. Energetics

A necessary condition for detecting the illustrated change in local charge configuration is that it be allowed energetically. Figure 4 is an illustration of this for a metallic (substrate) continuum. It is perhaps best to begin with a review of standard energy terms in photoelectron spectroscopy (Hüfner, 1996, p. 193). The ionization potential of a particular energy level is formally defined as the difference in energy between the system with the given electron removed to infinity and all others relaxed, and the ground state, $IP = E_{ion} - E_{ground}$. For an electron at E_F removed from a semi-infinite metal into vacuum, $IP = \phi$, the work function. The binding energy E_B can then be defined as the difference in IP between a given state and E_F. We require new terms to relate the XAS spectrum, which is measured in terms of photon energies, to the photoelectron energy scale. The core-level IP connects the two scales, since it is also the photon energy required to eject the core electron at E_V. By subtracting this IP point by point for the x-ray-absorption spectrum, we obtain effectively the (negative) IP for each point, and hence all the XAS resonances under scrutiny. The conversion from an IP to an E_B scale is accomplished similarly, by adding ϕ, as for the PES states. The result of this is illustrated in Fig. 4. With these points in mind, it is simple to establish that the energetics of electron transfer after XAS excitation using photon energy $h\nu_{res}$ are determined by the relative positions of the XAS resonance energies, E_{res}, and E_F. Thus we define here, as a short-hand notation for this

resonance energy, $E_{res} = h\nu_{res} - E_B$, which is a direct measure of the excess energy relative to E_F (available as kinetic energy in the continuum) of the valence electrons in the XAS final state. Another way of understanding this is to perform a thought experiment, in which one removes the core electron to rest at infinity in one step (costing ionization potential), and then returns it to E_F, which yields the work function ϕ, or to the XAS resonance, which yields $IP - h\nu_{res}$. The energy difference between these operations is just E_{res}. The discussion above hopefully illustrates that the energetics are robustly defined, i.e., not dependent on the use of E_F-referenced quantities, or the coupling strength between probe site and continuum. Hence for a metallic substrate the binding energy E_B and ionization potential IP are equally useful starting points for understanding the energetics.

A further clarification of the role of the core-level E_B is perhaps useful at this point. For a metallic large system this energy can routinely be precisely and accurately determined. This is because the core-level E_B represents the energy to create the locally screened state in which the positive core hole is compensated by the presence of an extra charge at the same site in the conduction levels at E_F (Johansson and Mårtensson, 1980; Hüfner, 1996, p.

41). This is a state that generally has a relatively large cross section, and since a metal most often presents a simple steplike structure at E_F, comparison between the two is simple and accurately yields E_B. X-ray absorption for a metallic system has its onset at E_B, which is by definition the lowest energy for the core-excited state (Mele and Ritsko, 1979; Nilsson *et al.*, 1992). For the small system in the weakly coupled case this "adiabatically screened" state is not necessarily observable. In this case the core-level E_B represents the energy of the state that is screened on the excitation time scale. Although the charge flow between the small and large systems is too slow to give the kind of metallic screening described above, the continuum will generally screen the excited state of the small system practically instantaneously via polarization or image screening, and the E_B represents a well-defined reference. It is because of the relatively slow charge-transfer screening of interest here that unstable states can be reached in core-level excitations, often giving rise to effects on the fs time scale amenable to study by the technique. As implied by Fig. 4, we are interested in two primary cases of E_{res}. $E_{res} < 0$ indicates that the XAS final state is more stable than the x-ray photoemission (XPS) final state, in which case charge transfer may occur from a metallic large system's conduction bands to the small system's core resonance level in the x-ray photoemission (or even x-ray absorption) final state. $E_{res} > 0$ favors charge transfer in the opposite sense. Both cases are taken up in detail in Sec. IV.

If the large system is characterized by a fundamental gap (semiconductor or insulator), the core resonance of interest may lie within this gap, thus in general forbidding charge transfer in either direction, as suggested in Fig. 5, although charge transfer to interface states in the gap is a distinct possibility (Zangwill, 1988, p. 63; Huber *et al.*, 2000) (see examples in Sec. V). As noted in the figure caption, the choice of reference energy in defining the sign of E_{res} is usually a matter of convenience for a given case. We avoid the use of E_F for insulators, because there is in general no spectroscopic structure associated with the chemical potential near the surface of an insulator. Referencing to E_F of a metallic support is often used in the literature for insulating samples, but requires understanding the magnitude of the interface dipole and polarization effects (Chiang *et al.*, 1986; Maxwell *et al.*, 1996; Koller *et al.*, 2000) if the reference is to be accurate. In addition, charging-induced shifts (Cazaux, 2000) cause difficulties in determining an accurate E_F, whereas IP can routinely be measured even in the presence of such shifts (Maxwell *et al.*, 1996).

An interesting analog to the insulator large system is that of excitation to relatively localized, *unbound* resonances. In this case, the vacuum level E_V plays the same role as the lower conduction-band edge E_{cond} of Fig. 5, and the relevant continuum is that of free electrons in vacuum, or nearly free electrons in the conduction band. The energetics pictured in Fig. 5 can in such cases therefore be applied to free atoms or molecules, metallic systems with umklapp-induced gaps, and solid surfaces, an example of which is given in Rubensson *et al.* (1997).
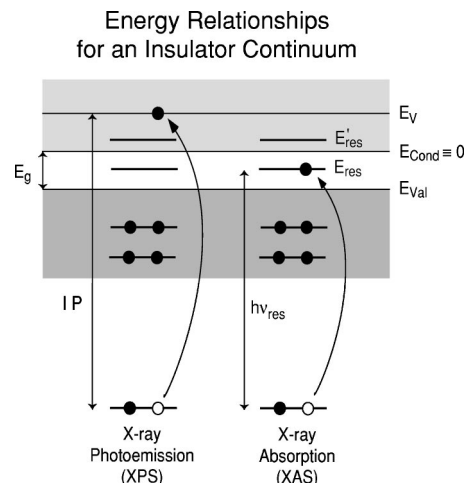

FIG. 5. Schematic of the two main pathways for core excitation of a small system that is loosely coupled to an insulator continuum (valence states in dark grey, conduction in lighter grey, and gap region in white). As in Fig. 4, E_V is the vacuum level, IP the core-level ionization potential of the small system, and $h\nu_{res}$ the photon energy corresponding to the core-level XAS resonance. For the insulator continuum we also define E_{val} to be the upper valence-band edge, E_{cond} the lower conduction-band edge, and E_g the fundamental electron transport gap. The latter quantity often differs from the threshold measured in optical absorption, which is generally a measure of exciton energies (Fulde, 1991; Lof *et al.*, 1992; Hüfner, 1996, p. 193). We define $E_{res} = h\nu_{res} - E_{cond}$. Hence here $E'_{res} > 0$ and $E_{res} < 0$ in analogy to Fig. 4, so that E'_{res} is degenerate with traveling states of the large system for the illustrated case of resonant excitation. If one were interested in describing a system in which charge transfer to an acceptor state of the small system were occurring, then E_{val} would perhaps be a more convenient reference energy, also in keeping with Fig. 4. Binding energies measured with respect to E_F of the electron spectrometer might still be used, but certain energy relationships must be considered. See the discussion in Sec. V for details.

An important practical aspect of the energetics in the measurements described here is that they represent the case of a lone entity, e.g., a single core-excited molecule embedded in a layer of neighbors essentially in their ground states. For the systems considered, E_B can thus have several contributions (image screening, polarization of the remaining adsorbate layer, chemical bonding effects in the core-excited state), which must be considered if a full understanding of the energetics of an isolated individual is desired (see Secs. IV.A.2, IV.B.2, IV.D, IV.E, and V.A) but which are irrelevant if only the sign of E_{res} is of interest (see Secs. IV.A.1, IV.B.1, IV.C, and V.B).

2. Coupling strength

When considering the coupling strength for the hopping processes of interest, it is perhaps helpful *a priori* to construe a continuum of environments for a given core-excited small system in which this type of tunneling process is least (isolated limit) or most (strongly chemically bound limit) likely. This external coupling has two fun-

damental aspects—a probability amplitude given by the transfer-matrix element, and a weighting factor given by the density of states (DOS). One often expresses the product of these two as the net coupling. We are interested here in how this net external coupling will affect the resonant excitations of the small system, since it is these spectral changes which are our source of information on the combined system.

As we discuss below in Sec. III.B.1, the coupling is easily accounted for in terms of the characteristic time required for the excited core electron to tunnel to the large system, which we shall call the *charge-transfer time* τ_{CT}. This time is given in relation to a standard time, in this case the lifetime of the core-excited state τ_C. Via the energy-time variant of the uncertainty relation, the hopping time is then easily reexpressed as an energy $\Gamma_{CT} = \hbar/\tau_{CT}$, corresponding to a distribution of accessible states, i.e., a hopping bandwidth. Hence the coupling to the large system contributes a broadening to the XAS linewidth of the small system, beyond the core lifetime broadening and any vibration-induced broadening. In principle, therefore, at least some of the information sought via dynamic charge transfer is available in the x-ray absorption line profile, as the hopping time is reflected as a perturbation of the XAS final-state wave function [a state (j) in Eq. (14)]. This subject is discussed in some detail for particular cases in Secs. IV.D.1 and V.A.1, and has been expressed formally (Ohno, 1994; Gortel and Menzel, 2001). It can also be reflected in the vibrational line spacing in XAS in a favorable case, exemplified in Sec. IV.B.2. Analysis of only the x-ray-absorption spectrum is, however, generally of limited value, due in part to a lack of access to quantitative theoretical estimates of the vibrational contribution in complex situations. In addition, energy-dependent variations in the measured hopping times (see Sec. III.D) are generally not apparent in the XAS line profile. Thus the utility of determining the coupling strength in terms of dynamic charge-transfer times lies in the possibility to extract the bonding contributions to the x-ray absorption line shape.

B. Revealing the charge-transfer time

1. Exponential charge-transfer rates

If one considers the removal of the excited electron as a tunneling process with exponential probability as a function of time [see Smith and Nozik (1999) for a recent analysis], then a direct comparison with the core-hole decay rate [also exponential (Almbladh, 1977; Mahan, 1977; Almbladh *et al.*, 1989)] becomes a relatively simple matter to understand. Implicit in the description of the two processes as exponential is the assumption that they are independent. This is often the case, and conditions for exceptions to this assumption are discussed in Sec. III.C.2.

In general, an exponential decay law derives from the assumption that the decay rate is proportional to the number of identical systems available in the initial, unstable state, i.e., the decay rate dN/dt is given by

$$\frac{dN(t)}{dt} = -\frac{\Gamma}{\hbar} N(t), \tag{1}$$

where $\hbar/\Gamma \equiv \tau$ is the characteristic time for the decay. The quantity Γ in Eq. (1) is generally given the interpretation of the imaginary part of a complex energy often denoted the self-energy (Ohno, 1994). It is apparent that Γ itself is proportional to the decay rate. For a particular core-excited state this quantity is also proportional to the total intensity in the measured spectrum. A solution of Eq. (1) is given by

$$N(t) = N_0 e^{-t/\tau} = N_0 \exp\left(-\frac{\Gamma}{\hbar} \cdot t\right), \tag{2}$$

where N_0 is the number of "systems" prepared in the decaying state at some (arbitrarily) chosen time zero and $N(t)$ is the number of systems left in the excited state at time t. We can use Eq. (1) to derive time-dependent probabilities by dividing by N_0 and integrating to some time T to determine the likelihood of no decay event for times smaller than or equal to that time. This yields

$$P(T) = 1 - \int_0^T \frac{\Gamma}{\hbar} \exp\left(-\frac{\Gamma}{\hbar} t\right) dt, \tag{3}$$

where $P(T)$ is the probability that no decay has taken place up to time T. By identifying $\hbar/\Gamma$ with the characteristic times for charge transfer ($\tau_{CT} \equiv \hbar/\Gamma_{CT}$) and core-hole lifetime ($\tau_C \equiv \hbar/\Gamma_C$),[5] respectively, we may write the relations corresponding to Eq. (3) for the processes in which we are interested here. This is done below, where we derive a useful relationship between the characteristic times and the intensities found in the decay spectrum.

As stated above in connection to Eq. (3), we may write the probability for no charge-transfer event to occur before time T as

$$P_{\text{No CT}}(T) = 1 - \int_0^T \frac{\Gamma_{CT}}{\hbar} \exp\left(-\frac{\Gamma_{CT}}{\hbar} \cdot t\right) dt. \tag{4}$$

The same form holds for the probability relation $P_C(T)$ that the excited state of an isolated small system has decayed before a given time T after excitation of the core electron,

$$P_C(T) = \int_0^T \frac{\Gamma_C}{\hbar} \exp\left(-\frac{\Gamma_C}{\hbar} \cdot t\right) dt. \tag{5}$$

Note the difference in sign between Eqs. (4) and (5). This reflects the fact that we are considering the situation "nothing happened" (i.e., no charge transfer) in Eq. (4), while we are considering the probability for "something happened"—a core-hole decay in this case—in Eq. (5).

---

[5]See, for example, Coville and Thomas, 1991; Prince *et al.*, 1999; Campbell and Papp, 2001 for values of this quantity for many different core levels.
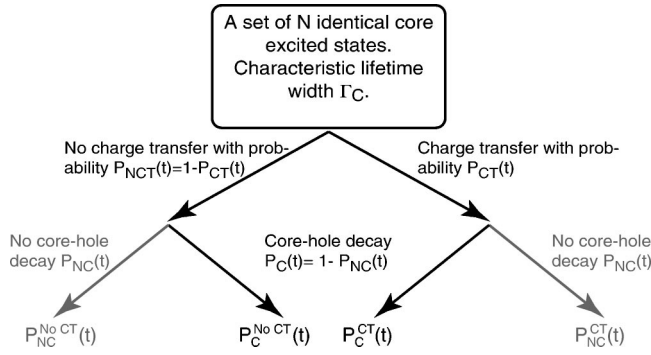
FIG. 6. Illustration of the core-hole decay and charge-transfer process as two independent mechanisms governed by exponential decay laws. Within the time interval $[t, t+dt]$ the system may or may not undergo charge transfer. Both cases may or may not decay during this time interval. When we are calculating the probabilities for any of the routes, we need to consider the *conditional probability* for the sequence. This is done in Eq. (6) for the route in which *no charge transfer occurs before core-hole decay*. In the spectrum we are only observing the situation "at time infinity" for the two central decaying channels, i.e., when all systems have decayed. This fact is reflected in the figure by the heavier color of the decay channels.

If we would like to consider both channels simultaneously, with independent rates, we have to consider the conditional probability for the combined events. The branching of the events is indicated in Fig. 6. Let us first consider the sequence: *A core-excited system decays before or at some time T, with no charge transfer during this time.* This is given by

$$P_C^{No\ CT}(T) = \int_0^T \frac{\Gamma_C}{\hbar} \exp\left(-\frac{\Gamma_C}{\hbar} \cdot t_1 \right)$$

$$\times \left[1 - \int_0^{t_1} \frac{\Gamma_{CT}}{\hbar} \exp\left(-\frac{\Gamma_{CT}}{\hbar} \cdot t_2 \right) dt_2 \right] dt_1$$

$$= \frac{\Gamma_C}{\Gamma_C + \Gamma_{CT}} [1 - e^{-(\Gamma_C + \Gamma_{CT}/\hbar) \cdot T}]. \quad (6)$$

Measuring a spectrum corresponds to $T \to \infty$ in Eq. (6), when the excited systems have definitely decayed, and we obtain

$$P_C^{No\ CT} = \frac{\Gamma_C}{\Gamma_C + \Gamma_{CT}}. \quad (7)$$

Equation (7) tells us that a fraction $\Gamma_C/(\Gamma_C + \Gamma_{CT})$ of the spectral intensity stems from decays where no charge transfer has occurred before core-hole decay. The remaining fractional intensity in the spectrum is given analogously by

$$P_C^{CT} = \frac{\Gamma_{CT}}{\Gamma_C + \Gamma_{CT}}. \quad (8)$$

These equations show that, while Γ_C is proportional to the Auger transition rate which defines the absolute intensity of the entire spectrum (resonant and nonreso-

nant) if this is available,[6] its magnitude relative to Γ_{CT} emerges in the intensity ratios. This can also be confirmed by taking certain limits, such as $\Gamma_{CT} \to \infty$ and $\Gamma_{CT} \to 0$. Since we did not need to specify which core-excited state was originally produced, the expressions above apply, within the stated approximations, to all cases of dynamic charge transfer to be considered. These cases, and their spectral signatures, are given schematically in Fig. 7.

We can now apply the relationships above to obtain expressions relating the measured spectral intensities I to the corresponding quantities Γ. The intensities are defined in Fig. 7, with further discussion given in association with Figs. 2 and 11. For the case of resonant excitation corresponding to Fig. 7(a), in which the core-excited small system transfers charge to the large system, the total intensity in the spectrum corresponds to the core lifetime broadening (transition rate) Γ_C, whereas the Auger fraction corresponds to the tunneling bandwidth Γ_{CT}. Hence the relationship we seek is

$$\frac{\Gamma_{CT}}{\Gamma_C + \Gamma_{CT}} = \frac{I_{Aug}}{I_{res} + I_{Aug}}, \quad (9)$$

for which I_{Aug} represents the intensity of the Auger component in the spectrum, and I_{res} that of the resonant Auger, or spectator component. Figure 7(a) is also relevant for nonresonant excitation followed by charge transfer from the large to the small system, yielding

$$\frac{\Gamma_{CT}}{\Gamma_C + \Gamma_{CT}} = \frac{I_{res}}{I_{Aug} + I_{res}}. \quad (10)$$

In this case, the "resonant" portion of the spectrum is not necessarily equivalent to what one would obtain for truly resonant excitation (Björneholm *et al.*, 1992a), but may be identified by the so-called spectator shift in kinetic energy due to the screening effect of the transferred electron and a general similarity to a truly resonant spectrum.

Since the total Auger-like spectrum is not considered in Figs. 7(b) and 7(c), approximations are required in order to make use of these variations on the method. The principle behind Fig. 7(b) is that the occupied-unoccupied spatial overlap which enters the Auger matrix element for the participator intensity is either weakly dependent on or independent of the coupling of the systems. In that case, one takes the intensity of the participant channel I_{iso} for the isolated small system as proportional to the entire resonant spectral intensity in the spirit of Eqs. (7) and (8), and thus $\Gamma_C + \Gamma_{CT}$. One then assumes that a decrease in intensity of that feature $I_{iso} - I_{coup}$ corresponds to the charge-transfer rate, or tunneling bandwidth Γ_{CT} (Brühwiler, Maxwell, Rudolf, *et al.*, 1993), for which I_{coup} is the participator intensity

---

[6]Absolute intensities are generally not reported due to questions regarding mean-free-path effects and/or excitation volumes, as well as due to the difficulties in calibrating the incident photon flux.
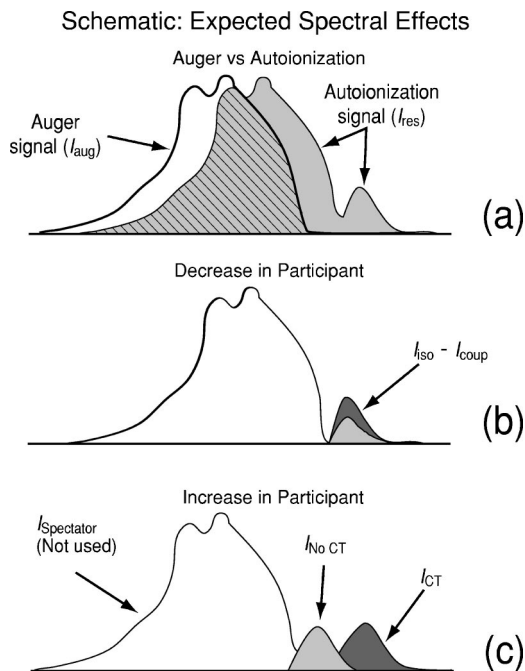
Schematic: Expected Spectral Effects

FIG. 7. Schematic of the three main characteristic measurement approaches for deexcitation of the small system which is loosely coupled to a continuum: (a) A spectrum is analyzed for its primary components, Auger and autoionization, here shown as overlapping components, instead of as the total spectrum. See Secs. III.D, IV.A.2, IV.C, and Fig. 11 for applications of this approach, which can be used for cases corresponding to either sign of E_{res} [see Figs. 4 and 5 and Eqs. (9) and (10)]. (b) A spectrum at resonance is measured for the isolated system and compared to the case of the coupled system. Changes in the participant intensity are used to monitor the overall change in the autoionization intensity associated with dynamic charge transfer from the system of interest (e.g., adsorbed molecule) to the continuum. This approach is adopted, for example, when the kinetic energies of Auger and autoionization are similar, and thus the spectra are too difficult to resolve. The method is applied using Eq. (11). (c) Similar to (b), but with the difference that an increase in participant intensity (a new channel) is observed, corresponding to charge transfer in the opposite direction. This is allowed for $E_{res} \leqslant 0$, and thus is expected to be associated with nonresonant excitation in most cases, although a case of $E_{res} \approx 0$ has been identified, as explained in Sec. IV.B.2. The spectrum can be considered to consist of two spectra, a typical resonant spectrum as in (a), with a second, similar, upwardly shifted spectrum associated with the extra charge in the unoccupied levels (presumably the LUMO in most cases). Thus this is a kind of spectator shift, which now applies to the entire spectrum instead of merely the Auger-like portion. This approach is preferred when only the participant portions of the two components are resolvable, and is applied using Eq. (12).

for the coupled small-large systems. For this approximation to be quantitatively valid, the participator matrix element must be the same for the isolated and coupled small systems. A second issue is the intensity calibration, which must correspond in the ideal case to an intensity per unit small system. The latter issue was solved for the case of solid C_{60} (see Sec. V.A) in a novel manner, and

the question of the matrix elements was also resolved for that system to a high accuracy by studying a state in the gap, for which the charge-transfer rate was taken to be zero. With these considerations in mind, one can write

$$\frac{\Gamma_{CT}}{\Gamma_C + \Gamma_{CT}} = \frac{I_{iso} - I_{coup}}{I_{iso}}. \tag{11}$$

Alternatively, the participant intensity may increase upon charge transfer from a large to small system (via the opening of a new channel). The new channel will then have a different (presumably higher) kinetic energy due to the screening effect of a second electron in the unoccupied levels, i.e., a new type of spectator shift.[7] As illustrated in Fig. 7(c), this approach is quite similar to that in Fig. 7(a). Indeed, that approach could be taken instead if the different contributions in the spectator region were resolvable; the motivation for choosing the participator channels lies in the fact that they may be more easily separated and analyzed in certain cases. For this approach one must make the assumption that the participator matrix elements are not very different for neighboring channels (Brühwiler *et al.*, 1995; Puglia, Bennich, *et al.*, 1998; Puglia, Brühwiler, *et al.*, 1998). Now it is the participator intensity I_{CT} due to the new channel which corresponds to the charge-transfer rate Γ_{CT}, whereas the intensity of the overall participator spectrum $I_{No\ CT} + I_{CT}$ corresponds to the total intensity $\Gamma_C + \Gamma_{CT}$, giving

$$\frac{\Gamma_{CT}}{\Gamma_C + \Gamma_{CT}} = \frac{I_{CT}}{I_{No\ CT} + I_{CT}}. \tag{12}$$

Thus this approach has similarities with that of Fig. 7(a) and is illustrated by the case study in Sec. IV.B.2.

It is worth pointing out that Γ_C need not be independent of charge state, though it has been found in at least one case of a small molecule to be relatively insensitive to situations in which the Auger effect occurs from a core-*ionized* state, as in Fig. 1(c), or from a core-*excited* intermediate state, as in Figs. 1(e) and 1(f) (Osborne *et al.*, 1995). Indeed, the C 1*s* levels of small molecules were the basis of a case study by Coville and Thomas, (1991), who showed that variations of 20% depending on the molecular composition are to be expected. On the other hand, the case of graphite indicates possible pitfalls in relying exclusively on experimental data. After an initial report of an unusually large value of over 0.2 eV for Γ_C of graphite (Sette *et al.*, 1990), the present conservative upper limit of 0.16 eV, established using better resolution and a judicious choice of photon energies (Prince *et al.*, 2000; Balasubramanian *et al.*, 2001), suggests that the difference in Γ_C between macroscopic and molecular carbon may also be of the order of 20% or less. This is the working hypothesis thus far for all work of which we are aware, and it remains to be seen whether there are cases for which this assumption will require a reevaluation.

———

[7]The "spectator shift" is illustrated in Fig. 2.

2. Nonexponential charge-transfer rates

Nonexponential charge-transfer rates are more difficult to treat numerically. This issue emerges, for example, in "core-hole clock" studies of dissociation, for which a step function was used in place of the t_2 integral of Eq. (6) to approximate the decoupling of atoms (Naves de Brito *et al.*, 1997) from small molecules. For very strong coupling, $\Gamma_{CT} \gg \Gamma_C$, the form of the t_2 integral is not important, since the electron (or hole) is transferred or delocalized for all measured events. As noted above, for cases in which $\Gamma_{CT} \sim \Gamma_C$ the exponential form is expected to be a good approximation (Ohno, 1994; Gortel and Menzel, 2001). Exceptions to this ansatz have been characterized in cases of sparse continua, or if other degrees of freedom such as vibrations are coupled to the excited state, and this is discussed in detail in Sec. III.C.2.

C. The effects of coherence

We have already suggested in Sec. III.A that the quenching of the resonant excitation-deexcitation channel is a primary signature of dynamic charge transfer.[8] Studies of molecules in the gas phase show that isolated (small) systems exhibit many effects of coherence for such resonant excitation-deexcitation. We attempt now to illustrate in more detail how coherence plays a fundamental role in core-level measurements of dynamic charge transfer and to make some connection to the many studies using valence excitation to induce charge transfer (Lanzafame *et al.*, 1994; Miller *et al.*, 1995; Ramakrishna and Willig, 2000).

1. Basic aspects

The most general description of the measurements must include the possibility of coupled core excitation-decay processes (Gunnarsson and Schönhammer, 1980). We must also include terms that do not involve core excitation, such as direct photoemission, in a quantum-mechanical description of the spectra. We shall express the resonant processes in terms of an inelastic x-ray scattering process, using the Kramers-Heisenberg formalism to expose the presence or absence of interference. To second order we consider scattering processes of the type

$$\hbar\omega + \mathcal{S} \rightarrow \mathcal{S}^{++} + e + e_{\text{Auger}} \tag{13a}$$

$$(\rightarrow \mathcal{S}^+ + e + \hbar\omega'), \tag{13b}$$

where $\mathcal{S}$ represents the system of interest. Equation (13a) corresponds to Auger (resonant) Raman scattering, which is our focus here, while Eq. (13b) represents inelastic x-ray scattering. Expressed in this general form, the transitions are implicitly resonant, since we ignore

details of the intermediate state. Near threshold, we typically find the small system ($\mathcal{S}^{++,+} + e$) in a bound (autoionizing), excited state. As already pointed out, in cases of dynamic charge transfer, the excited electron e will typically have a finite probability of delocalizing into the large system within the core-hole lifetime, quenching the resonant deexcitation channel, and activating the nonresonant channel. We described this as an exponentially evolving branching in the previous section. Here, we would merely like to note that in the most general sense the apparent resonant and nonresonant (i.e., normal Auger) decay processes should *both* formally be considered as autoionizing channels of the coupled small-large system (Gunnarsson and Schönhammer, 1980; Kassühlke *et al.*, 1998).[9]

The intensity of the Auger Raman-scattering spectrum is given by the following type of expression (Almbladh and Hedin, 1983):

$$w_{f0} = 2\pi \sum_f \left| \langle f|V_r|0 \rangle + \sum_j \frac{\langle f|V_A|j \rangle \langle j|V_r|0 \rangle}{E_0 - E_j + \dfrac{i\Gamma_j}{2}} \right|^2$$

$$\cdot \delta(E_f - E_0). \tag{14}$$

The first part of the matrix element represents direct photoemission. The second part represents core excitation-deexcitation channels. The initial-state (0) and final-state (f) wave functions contain the incoming photon and the outgoing electron, respectively. (j) denotes the intermediate core-excited states. V_r and V_A denote the radiative and Coulomb operators, respectively. Γ_j is the core-level lifetime-induced width of state (j), often assumed to be independent of (j). As usual, the δ function ensures energy conservation. The amplitudes for the direct and core-resonant processes in Eq. (14) contribute to the intensity for each separate final state symbolically as

$$w_{f0} = \left| \text{direct} + \frac{\text{core}}{\text{resonant}} \right|^2, \tag{15}$$

which is often rewritten to emphasize the role of the quantum phases of the different channels,

$$w_{f0} = |\text{direct}|^2 + \left| \frac{\text{core}}{\text{resonant}} \right|^2 + \text{interference terms}. \tag{16}$$

If the two processes lead to inequivalent final states, the intensity will be given by the sum of the intensities of the uncoupled processes, i.e., Eq. (16) without the interference terms. Strong interference leads to Fano-type profiles in the photon energy-dependent cross section (Fano, 1961; Weinelt *et al.*, 1997). This type of excitation-channel interference is not important for the cases discussed here.

---

[8]With XAS excitation. Note that autoionization channels emerge in the Auger spectrum for nonresonant (XPS) excitation in the case of dynamic charge transfer from the large to the small system (Björneholm *et al.*, 1992a).

[9]In the following, we ignore any interaction between the two particles $e + e_{\text{Auger}}$ or $e + \hbar\omega'$ present in the final state. That is, we neglect post-collision interactions (Kassühlke *et al.*, 1998).

2. The core-hole clock and detuning

To see in detail how coherence might be manifested in the measurements described later, it is useful to assess what is known from gas-phase work. A number of studies of core-level excited molecular vibrational and/or dissociation dynamics have recently been published which make use of the fs sensitivity that we take up here (Gel'mukhanov and Ågren, 1994; Björneholm *et al.*, 2000; Feifel *et al.*, 2000). In those studies vibrational dynamics, including dissociation, are at issue, and the fs time scale is exploited in a manner analogous to the approach for dynamic charge transfer (Naves de Brito *et al.*, 1997). There are two aspects of the physics of these applications of core decay dynamics which we would like to consider. First, the gas-phase works constitute studies of small systems, for which a more or less complete quantum-mechanical description is possible, and thus constitute benchmarks for many studies of interest here. Second, the so-called "detuning effect" demonstrated for such systems is often described in terms of selecting a time for the deexcitation portion of the resonant transition, and should therefore be examined in detail for possible application to the case of dynamic charge transfer. In this subsection we compare and contrast the cases of atomic/molecular (small) and extended/solid-state (large) systems at a rather simple, general level. We shall focus on two aspects of coherence, which we label "energy coherence" and "phase coherence," a pragmatic choice to facilitate the discussion that follows.[10]

When considering core-level autoionization of an atomic/molecular system, we expressed the matrix element [Eq. (14)] in terms of eigenstates of the intermediate state $|j\rangle$ using the appropriate Hamiltonian, including both the electronic and vibrational degrees of freedom. We can say that the system S in the intermediate state is described by a total wave function

$$|\Psi\rangle = \sum_j c_j |j\rangle, \tag{17}$$

given by a linear combination of the eigenstates $|j\rangle$. We shall now consider the role of these eigenstates in the observed spectral trends.

a. Energy coherence

Energy coherence is simply the law of energy conservation. We consider first the case of an intermediate state in which a *single* eigenstate dominates, due, for example, to a large cross section or to a large energy separation to the next available states. Exciting to this state with highly monochromatic radiation, which has an energy spread comparable to or less than the core-level lifetime broadening, leads to qualitatively interesting be-

---

[10]This is because both aspects are not necessarily reflected in a given measurement. For example, a detectable phase coherence is generally accompanied by energy coherence (conservation), but the opposite is not always true.
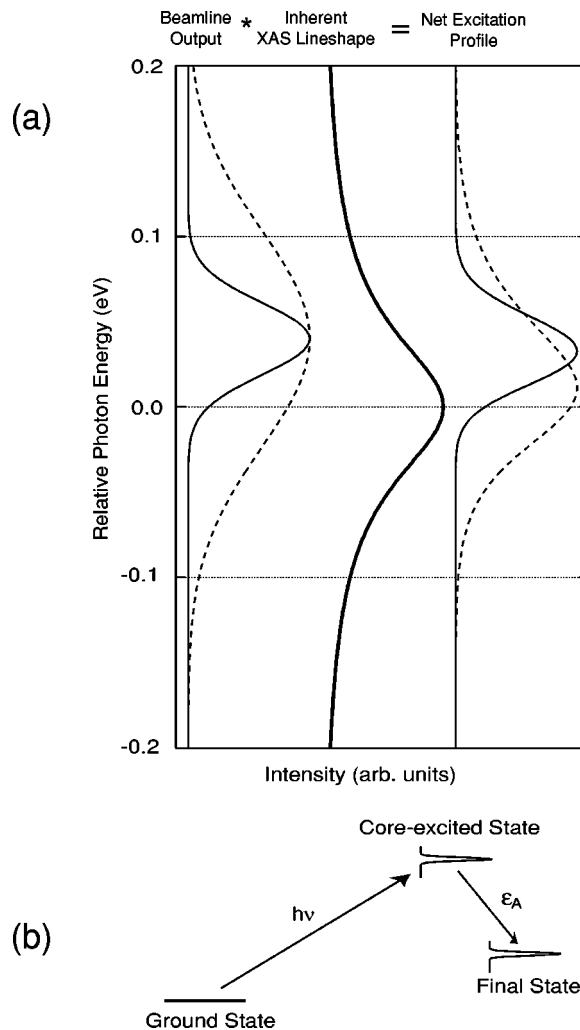

FIG. 8. The Auger resonant Raman (ARR) effect: (a) Schematic of the excitation step. The beamline output is assumed to be Gaussian in profile, though this is not always the case (Kivimäki *et al.*, 1993; Aksela *et al.*, 1995). The inherent line shape is assumed to be Lorentzian. The net profile is the product of these two as indicated. If the electron measured in deexcitation is the only channel for energy release from the core-excited system, narrow-band excitation defines a narrow input energy range, and thus an equally narrow band of output energy for each final state via energy conservation. Also indicated is a case of broad-band excitation, in which the intrinsic line profile determines to a great extent the effective excitation and, again via energy conservation, the deexcitation profile. This schematic is incomplete if direct photoemission has a large cross section; see Sec. III.C. (b) Schematic of the evolution of an electron spectrum under ARR conditions. The net excitation profile is transferred via energy conservation to the electron energy distribution for each Auger-like final state.

havior, sketched in Fig. 8. Here we show that the XAS excitation step at high resolution (solid line) creates states of well-defined energy "within" the resonance of Fig. 1(d). Energy conservation in this case demands, for an isolated system such as a free atom or molecule, that the resonant channels disperse linearly with the photon energy in this excitation interval. For such a case one can state that there is energy coherence between the
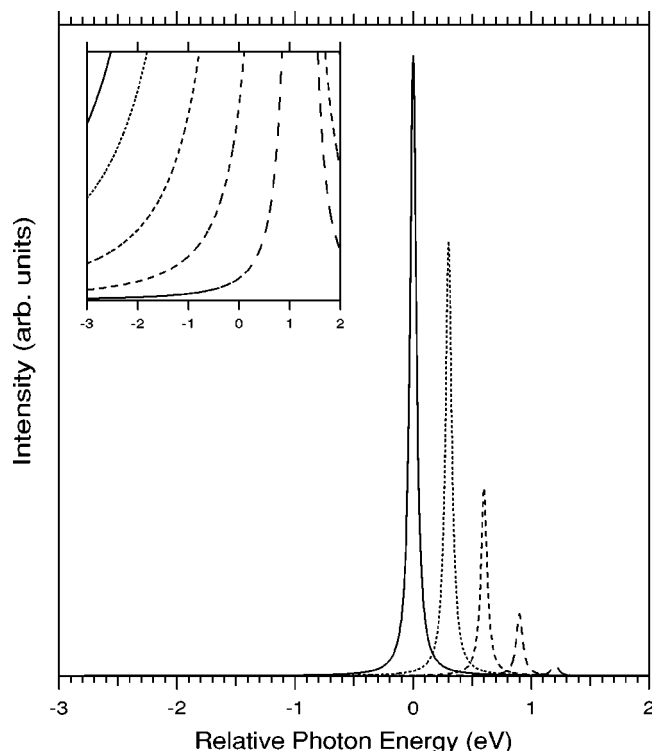
FIG. 9. Schematic of the XAS spectrum of a simple molecule such as N_2, showing the different vibrational states. Inset: closeup of the Lorentzian tails of the different vibrational states for excitation energies below the resonance (so-called negative detuning), indicating the greater relative contribution of the entire space of available vibrational eigenstates to the excitation, compared to excitation on a particular state.

excitation and deexcitation steps (Kivimäki *et al.*, 1993; Eberhardt, 1995; Kukk *et al.*, 1996; Gel'mukhanov and Ågren, 1999; Piancastelli, 2000). This is sometimes called the Auger resonant Raman (ARR) condition. For increasingly broad-band excitation the resonant channels will have an input energy uncertainty given by the XAS resonance width to an increasing extent, seen by comparing the net excitation profiles to the inherent line shape in Fig. 8.

b. Phase coherence

The situation becomes somewhat more complex when several eigenstates are simultaneously accessible (Köppel *et al.*, 1997). Figure 9 offers some pictorial insight into this point. This figure represents a typical x-ray-absorption spectrum of a given electronic excitation for a molecular system, with several relatively well-separated vibrational states (or close-lying electronic states)—thus each peak corresponds to a separate eigenstate $|j\rangle$. High-resolution excitation on a particular vibrational resonance places the system $\mathcal{S}$ predominantly in that eigenstate $|j\rangle$. Exciting midway between two such vibrational resonances, on the other hand, places the system in a linear superposition of the two corresponding eigenstates (plus small components of all the others), brought about by the lifetime broadening of the core hole. A time-dependent description of such a superposi-

tion state displays quantum beat phenomena, modified by the damping effects of the core-hole decay (Gortel *et al.*, 1998; Gel'mukhanov and Ågren, 1999; Malinovskaya and Cederbaum, 2000; see, e.g., Höfer, 1999, for an illustration of this for valence excitations in the time domain). Excitation in such situations can give rise to strong intensity redistributions among the final vibrational states (Neeb *et al.*, 1994; Gel'mukhanov and Ågren, 1999), often denoted "lifetime-vibrational interference." Dissociation events can also be described along these lines (Feifel *et al.*, 2000).

Within this description, it is clear that the presence of interference effects in the spectra is a natural consequence of the coherent superposition of different states $|j\rangle$ of the small system, plus any effects of interference with direct photoemission [Eq. (14)]. The relative phases, and therefore amplitudes, of the different $|j\rangle$ will vary during the (unitary) evolution of the intermediate superposition state (Gel'mukhanov and Ågren, 1999; Gortel *et al.*, 1999), but the eigenstates of the core-excited small system are always sufficient to describe the total state. We maintain that the state of the system is well defined.

In its interaction with the large system, the excited core electron of the small system will spatially overlap electronic levels of that system. This leads to level mixing. To understand the consequence of this coupling to the large system, we must examine the role of the accompanying delocalization of the excited electron. One approach would be to use linear combinations of the states $|j\rangle$ of the small system and relevant states $|k\rangle$ of the large system in a type of tight-binding description of the wave function of the intermediate state. This is generally not practical at present (Ramakrishna and Willig, 2000), although the effects of increasing size of the large system can be appreciated from model calculations; compare, for example, Fig. 3 of Smith and Nozik (1999) to Fig. 3 of Lanzafame *et al.* (1994). The general effect of such mixing is understandable in terms of the excited electron, once it has been transferred, traveling through the combined system (coherently), thus spending most of its time in the large system and occasionally revisiting the small system (Lanzafame *et al.*, 1994). To the extent that the electron is located elsewhere, the charge state of the small system has changed, and the resonant channel is quenched. Thus one can say that the entropy of the excited state for the combined system is much larger than that of the electron localized on the small system. This alone is enough for macroscopic large systems to correspond to virtually perfect charge sinks on the fs time scale. However, it is also generally true that excited carriers in bulk solid-state continua relax on times scales of tens of fs or less for the energies of interest here (Halas and Bokor, 1989; Schmuttenmaer *et al.*, 1994; Xu *et al.*, 1996; Bauer *et al.*, 1998). This places an upper limit on the time scale for coherent exchange of the excited electron back to the small from the large system, if there should be a significant amplitude for this event, hence

the generalization that charge transfer is equivalent to a change in charge state for the small system (Lanzafame *et al.*, 1994).

With these points in mind, we can take up the question of detuning, which refers to excitation away from resonance, with the measure of detuning being the difference in energy referred to the peak or centroid of the resonance.[11] The fact that energy and phase information are dissipated via the coupling into the large system (out of the measurement) will have interesting consequences for the concept of detuning applied to a spectrum of the small system. The effects of detuning have been demonstrated experimentally and theoretically for simple molecules in the gas phase by several authors (Skytt *et al.*, 1996; Sundin *et al.*, 1997; Gortel *et al.*, 1998; Gel'mukhanov and Ågren, 1999). We consider here the case of excitations below the first resonance in a group (negative detuning). This is illustrated in the inset of Fig. 9. We shall discuss the phenomenon first in a time-independent picture, which we feel is easier to visualize in terms of XAS resonance widths (Ohno, 1994) and the role of multiple resonances, and then in terms of a time-dependent picture, which is strongly advocated by some workers (Gortel and Menzel, 2001).

Taking the time-independent perspective, from Fig. 9 we see that detuning causes a wider range of the vibrational and/or electronic intermediate states to be more equally and coherently selected, thus not specifying any particular state as strongly.[12] Using Eq. (14), we can understand the consequence of this more equal weighting of the intermediate eigenstates contributing in Eq. (14), due to the slow variation of the denominator when the detuning is large. The sum over intermediate states is then approximately equal to a closure relation (Merzbacher, 1970), i.e.,

$$\sum_j \frac{|j\rangle \langle j|}{(E_j - E_0 - \hbar\omega - i\Gamma_j/2)} \approx \frac{1}{\text{const}}. \tag{18}$$

That is, when Eq. (18) can be assumed to be valid, a more direct representation of the ground state transformed by the dipole matrix element is obtained in the final state, and vibrational coupling via the intermediate state is effectively quenched.

In terms of the time dependence of the excitation, the result of detuning is to create (to a greater extent) a wave packet that is confined by interference effects to the ground-state configuration, so that at the time of deexcitation the vibrational coupling proceeds as if the excitation were directly from the ground state (Gortel *et al.*, 1998; Gel'mukhanov and Ågren, 1999). This has

led to the concept of an "effective duration time" of the excitation-deexcitation process, which is shorter for greater detuning, corresponding to the spectra increasingly approaching the direct transition from ground to final state. That is, with increasing detuning the intermediate core-excited state can be considered to be probed at earlier times, disallowing a well-defined core-excited state to develop (short evolution of the intermediate state), i.e., a faster *effective* decay process. The relationship between the detuning energy and the effective duration time is the same within both the time-independent (Gel'mukhanov and Ågren, 1999) and time-dependent (Gortel *et al.*, 1998) pictures, as one would expect for consistent descriptions.

From the discussion above, it is clear that the detuning effects of interest here would be those which alter the probability, for example, that an excited electron tunnels to the large system. The framework derived for simple molecules (see, for example, Glans, Gunnelin, *et al.*, 1996; Sundin *et al.*, 1997; Gortel *et al.*, 1998, 1999; Sałek *et al.*, 1999) can be applied to coupled systems, if one exchanges the dissociated state for such cases with the charge-transfer state of interest here. It is crucial for observing effects of such vibrational detuning that the degree of intersystem vibrational excitation be comparable to Γ_C, placing constraints on the change in small-large bond distance and the variation in potential energy as a function of distance as well. Depending on the particulars of this variation, and the direction of the changes in bonding if detuning changes the intersystem wave-packet evolution, one could imagine that both increases and decreases of small-large coupling could occur.[13] At the same time, detuning would still be expected to have an impact on the internal (measurable) degrees of freedom and to affect the resonant part of the deexcitation spectrum in terms of vibrational profiles, as for free molecules. For most systems, we expect the concept of "effective duration time" to lose its meaning with regard to the charge-transfer process, because the relatively large masses of interesting small systems will tend to minimize intersystem vibrational relaxation upon core excitation on the fs time scale. In practice, for example, faster charge-transfer times were found for the case of Ar/Pt upon detuning, which is most easily explained in terms of a greater contribution of states $|k\rangle$ of the large system to the intermediate state, rather than as an effect of Ar-Pt vibrations, and thus a higher nonresonant contribution (see Sec. III.D). Smaller atoms are found to be ejected in dissociation on the relevant fs time scale (Naves de Brito *et al.*, 1997; Björneholm *et al.*, 2000; Feifel *et al.*, 2000), whereas larger atoms require longer time scales in experiments performed thus far (Magnuson *et al.*, 1999). These results and others (Gortel and Menzel, 2001) suggest that detuning will not be

---

[11]The detuning energy "origin" is not precisely defined for a general case, but for small systems the effects are well understood.

[12]Using poorer resolution in the excitation step, as taken up in Fig. 8, does not induce coherent excitation of, for example, several vibrational states, but rather a sampling of different states according to the photon energy distribution (Gel'mukhanov and Ågren, 1999).

---

[13]Some effects of the intersystem distance may be appreciated from the discussion in Sec. IV.A.2, e.g., in Fig. 15 below.

effective in varying the charge-transfer dynamics in most cases of interest, and give a flavor of the relevant parameters.

On the other hand, there are known model examples of large systems for which the energetics facilitate coupling to a localized state or states in the continuum, in which charge-transfer events would not dissipate coherence (Kyrölä and Eberly, 1985; Smith and Nozik, 1999). This could allow one to affect the charge-transfer dynamics by varying the excitation energy. For example, d and f levels (Matzdorf *et al.*, 1999) or surface states, would be candidates for observing this possibility. In cases such as these, one could imagine that detuning would either positively or negatively enhance the electronic coupling, depending on the details. This is described in terms of including the localized state in the primary (small) system as opposed to the reservoir (large system) in a recent density-matrix approach (Gortel and Menzel, 2001). More general treatments of this issue, which further illuminate the issue, have been developed to handle intermolecular charge transfer. Kyrölä and Eberly (1985) show that, for a so-called quasicontinuum in which the energy separation of the states is δ, an electron transfer process can display oscillations corresponding to coherent back transfer after a time $T_{QC} = 2\pi/\delta$. A version of this model aimed at adsorbate-substrate vibrations and including band-edge effects has also been illustrated recently (Ramakrishna *et al.*, 2001).

To our knowledge, neither of these types of interference effects have yet been observed in resonant core excitation studies of electron transfer.[14] *Energy coherence*, on the other hand, can be expected to be retained for the resonant part of the deexcitation spectrum. Sections III.D and IV.C contain illustrations of the utility of this property in studying charge-transfer dynamics.

D. Ar physisorption on Pt(111): A model charge-transfer system

Let us now concretize the discussion of the previous subsections using the case of Ar physisorbed on Pt(111) (Karis *et al.*, 1996). Ar adsorbed on various metal and semimetal surfaces constitutes an ideal system to investigate the influence of the intermediate state on the resonant processes (Karis *et al.*, 1996; Sandell, Hjortstam, *et al.*, 1997; Keller *et al.*, 1998a, 1998b). As we review below, a whole range of intermediate states can be

---

[14]Interference effects, exemplified by Fano profiles, have indeed been observed in the case of Ni $2p$ resonant photoemission (Weinelt *et al.*, 1997). In this case, however, the interference was between the photoemission and Auger channels, facilitated by the localization of the core-excited state on the probe atom, and not an effect of coupling to localized modes on, e.g., neighboring sites. Such effects could, in principle, affect dynamic charge-transfer measurements and can be studied by varying the excitation and measurement geometries to vary the cross section for this type of interference.
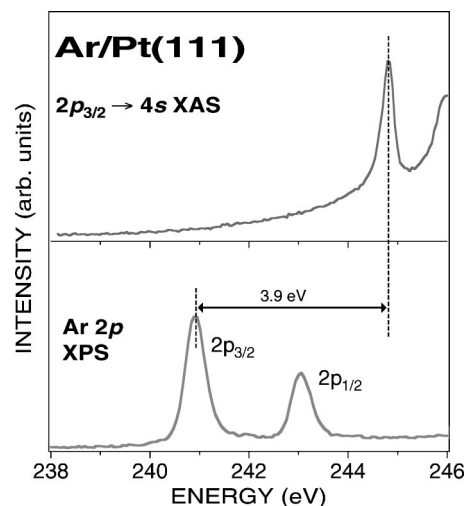
FIG. 10. The Ar $2p_{3/2} \rightarrow 4s$ x-ray-absorption and the Ar $2p$ x-ray photoemission spectra shown on a common energy scale for Ar/Pt(111). For XPS the binding energy E_B is used, as it is for XAS $h\nu$ (see Fig. 4).

reached, with varying degrees of wave-function localization. The autoionization spectra of adsorbed Ar simultaneously contain features that exhibit Auger resonant Raman and normal Auger behavior (Wurth *et al.*, 1993; Karis *et al.*, 1996; Keller *et al.*, 1998a, 1998b). The shift between these ("spectator shift," due to screening by the $4s$ spectator electron) is large (Aksela *et al.*, 1998a; Wurth *et al.*, 1992), which results in well-separated spectral features for the two decay channels.

In Fig. 10, the Ar $2p_{3/2} \rightarrow 4s$ x-ray-absorption and $2p$ x-ray photoemission spectra are shown on a common energy scale for Ar/Pt(111). The energy of the ionic photoemission final state is 3.9 eV lower than that of the neutral x-ray absorption final state. Thus $E_{res} = +3.9$ eV. The resonance in the absorption spectrum is due to excitations to the $4s$ level of Ar. However, it is evident from the spectral shape that this is not simply an atomic level, but is modified by the interaction with the substrate (Karis *et al.*, 1996). The atomic peak has been broadened and has a tail extending all the way to the energy of the Ar $2p_{3/2}$ binding energy E_B.

The $4s$ interaction with the substrate is also manifest in the decay spectra. We may view the $4s$-derived states as quasilocalized atomic states which can delocalize into the substrate via charge transfer. This can also be described as a transition to the energetically most favored core-excited state within the core-hole lifetime, i.e., the core-ionized photoemission final state in this case. The decay of this state gives rise to Auger-like features in the resonant decay spectrum (Wurth *et al.*, 1993; Karis *et al.*, 1996; Keller *et al.*, 1998a; Sandell *et al.*, 1999). The charge-transfer time τ_{CT} will depend on the charge-transfer (hopping) matrix element for the intermediate core-hole state.

Figure 11 shows the Ar/Pt(111) autoionization spectrum recorded at the maximum of the XAS resonance. The spectrum reveals two sets of spectral features, which
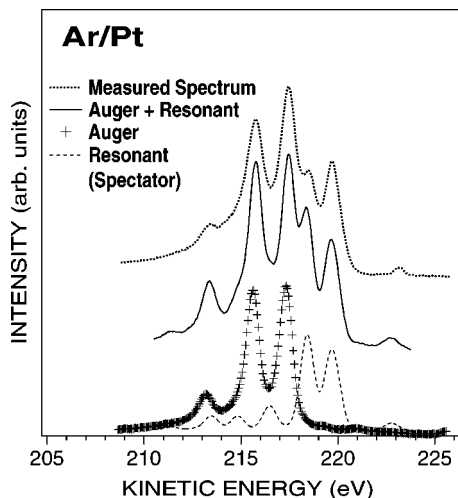
FIG. 11. Application of the analysis depicted in Fig. 7(a) to Ar/Pt(111). The upper curve is the spectrum measured at $h\nu = 244.8$ eV, which is the XAS resonance maximum in Fig. 10. The Ar/Pt(111) $2p_{3/2}^{-1}4s^1$ autoionization spectrum may be decomposed into two parts. One part corresponds to decay to a spectator $2p^44s^1$ configuration, while the other part is found to correspond to Auger-type $2p^4$ final states. See the caption of Fig. 14 for details.

may be identified as demonstrated in the lower part of the figure in the spirit of Fig. 7. The Auger spectrum (crosses) corresponds to a $2p_{3/2}$ off-resonance-excited Auger spectrum for the Ar/Pt sample $h\nu \gg 245$ eV. The different peaks in the spectrum are due to multiplets of the $3p^4$ configuration. The gas-phase autoionization spectrum (dashed line) is from the $2p^44s^1$ spectator configuration. It is convoluted with a 0.3-eV Gaussian and shifted to coincide with the spectator features in the top autoionization spectrum. By summing the Auger and gas-phase spectator autoionization spectra with appropriate weight factors, we obtain the model spectrum given by the solid line. This curve mimics almost all features of the experimental Ar/Pt autoionization spectrum.

The Ar autoionization spectrum may thus be thought of as consisting of two parts consistent with Fig. 7(a), one with Auger-like $3p^4$ final states and one with $3p^44s^1$ spectatorlike final states (Wurth *et al.*, 1993). One set of final states contains an extra electron in the $4s$ shell of Ar, yielding a polarization-screened $3p^44s^1$, atomiclike, configuration. This is the only parent configuration that would be produced if the $4s$ level were not mixed with continuum states. This configuration gives rise to a set of features at constant binding energy, and we may view it as a resonantly enhanced photoemissionlike final state. This implies conservation of energy according to the usual photoemission condition $E_{\text{kin}} = \hbar\omega - E_{\text{B}}(3p^44s)$.

In the second category of final states, the spectator electron is instead decoupled from the core-hole site. The appearance of this configuration is a direct consequence of the mixing between the $4s$ and substrate orbitals. The time evolution of the intermediate states will largely be determined by the charge-transfer (hopping)
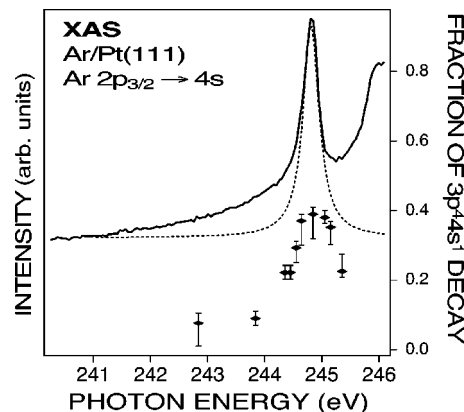

FIG. 12. Summary of the relationship between x-ray absorption and resonant photoemission for Ar/Pt(111). Top: Solid line, the Ar $2p_{3/2} \rightarrow 4s$ x-ray-absorption spectrum (same spectrum as in Fig. 10); dashed line, a Lorentzian, to illustrate the deviation from the behavior expected from a pure resonance model (Newns, 1969; Zangwill, 1988, pp. 212–216). The absorption line shape reflects the detailed interaction between the adsorbate level of the small system and the large system. Bottom: The variation of the fraction of photoemissionlike (coherent) final states over the Ar/Pt(111) $4s$ absorption profile, derived for the corresponding photon energies according to an analysis like that of Fig. 11. The fraction of coherent signal is largest at the $4s$ absorption maximum, corresponding to the longest charge-transfer time.

matrix element. A strong overlap (hybridization) in the intermediate state results in a faster delocalization into the substrate of the excited electron. By tuning the exciting radiation over the absorption resonance, we probe the variation of the branching between the two types of final states. This variation may be interpreted as a variation of the charge-transfer time. For each photon energy we analyze the spectrum according to Fig. 11 and Eq. (9). The results are displayed in Fig. 12. We find that the charge-transfer time is longest at the absorption maximum, corresponding to the intermediate-state wave function with the largest Ar $4s$ character there.

This result is largely consistent with what one would expect from a simple resonance model of the adsorbate-substrate interaction. Depending on the detailed structure of the substrate DOS, deviations from this behavior could be expected. We also note that, as worked out in Sec. III.C.2, the variation of the fraction of decay from coherent spectatorlike intermediate states is *not* as we would expect from a simplistic application of the molecular detuning picture of the deexcitation process. For such a case, in which the vibrational dynamics determine the time evolution of the system,[15] one would expect that the intermediate-state wave function would evolve less in its potential as the excitation energy is moved below the absorption maximum. This, in turn, would give a larger fraction of spectatorlike decays when the

----

[15]One should keep in mind that other quasiparticles, such as low-energy electronic excitations, could play a similar role.

excitation energy is off resonance,[16] contrary to what is observed. The observations are supported by model calculations as well, explicitly considering core-level excitations (Gortel and Menzel, 2001) or not (Lanzafame *et al.*, 1994). Changes in the hopping rates due to variations in the substrate density of states are in principle accessible in the energy dependence, but the smooth variation displayed in Fig. 12 suggests that this is not important for Ar/Pt(111). Coupling to localized states (see the end of Sec. III.C.2.b for more discussion) could induce coherent back transfer of the electron, in principle, also on a time scale longer than that of the core hole, thus making this process difficult to characterize. On the other hand, such states show up in terms of sharp variations in the density of states, which we have already ruled out for this case. While this idea could certainly be tested for the present method in calculations of model systems, we surmise that detuning as a means of controlling the intermediate-state wave packet is not practically applicable for known cases of intersystem coupling, a deduction which is supported by Gortel and Menzel (2001).

IV. CASE STUDIES: METAL CONTINUA

In this section we present examples of the study of charge-transfer dynamics for coupling to metallic continua. We begin with cases using XAS/autoionization vs Auger deexcitation to study the coupling of core-excited Ar to metal substrates, and then move on to increasingly large and/or complex systems. Insulating continua are discussed in Sec. V. Precise charge-transfer times are increasingly difficult to obtain as the complexity of the small system increases, and the tunability of the parameters (bonding configuration, structure) decreases. Nevertheless, detailed pictures of the relevant physics and chemistry of the core-excited state can be obtained even for relatively large and heterogeneous systems, and the results for the smaller "test case" systems are used to good effect.

A. Ar

1. Variable transfer-matrix element

It is clear from the discussion in Sec. III.A.2 and from theoretical modeling (Smith and Nozik, 1999) that tunneling times can be expected to vary with the effective bond, or coupling, between the excited system and the continuum. Keller *et al.* (1998a, 1998b) have studied this aspect using autoionization/Auger in an interesting series of experiments (see also Wurth, 1997; Menzel and Wurth, 2000; Wurth and Menzel, 2000). They studied the case of Ar/Ru(0001), which is directly analogous to that

---

[16]Detuning in both directions is expected to give similar results (Gel'mukhanov and Ågren, 1999), but has not yet been reported to do so, presumably at least partially because of the contributions of higher excitations as one detunes to higher energy.

TABLE I. Charge-transfer times for Ar monolayers with and without selected spacer layers on Ru(0001), taken from Keller *et al.* (1998a); Menzel and Wurth (2000); Wurth and Menzel (2000). The asterisk (*) indicates which layer is being probed.

Sample	Charge-transfer time (fs)
Ar*/Ru(0001)	1–2
Ar*/O/Ru(0001)	3–4
Ar*/CO/Ru(0001)	8
Ar*/Xe/Ru(0001)	12
Ar/Ar*/Xe/Ru(0001)	8
Ar*/Ar/Xe/Ru(0001)	>50

of Ar/Pt(111) (Karis *et al.*, 1996; see Sec. III.D), with $E_{res} > 0$ in all cases. For Ar adsorbed directly on Ru(0001) they obtained a tunneling time of 1–2 fs (Keller *et al.*, 1998a). To tune the coupling strength, they used spacer layers consisting of monolayers of O and CO, and of Xe alone and in combination with an extra layer of Ar. Their results, obtained using the method of Fig. 7(a) augmented by measuring with ARR conditions to more easily identify the resonant component, are summarized in Table I. There one sees that an increasing spacer-layer thickness leads to a decreasing coupling between core-excited Ar and the metallic substrate, as expected within a simple picture. The increase in charge-transfer time found when going from CO to Xe has an unexpected inverse correlation with the expected distance between the excited Ar atom and the surface. At the same time, E_{res} increases by about 1 eV for adsorption on O and CO layers due to the interface dipole formed for those layers (Wurth and Menzel, 2000), and one can expect a higher tunneling probability to correlate with the size of E_{res}. The slight enhancement of the coupling when Ar is encased in two other rare-gas layers—as opposed to merely being adsorbed on Xe—is also most likely due to the enhanced tunneling probability expected for higher energies. In this case, the Ar $2p \rightarrow 4s$ resonance is pushed up in energy by the effect of confinement, raising the value of E_{res} as defined in Fig. 4, and lowering the effective tunneling barrier. Of course, the simple interpretations of the spacer layers given here can be applied because there are no states in the relevant energy region for Xe or Ar in the ground state (see, for example, Sonntag 1977).

2. Variable continuum density of states: Core-excited Ar = "K" on graphite

Another method of varying the coupling which is less transparent can be achieved in two ways—by effectively varying the value of E_{res} with selective excitation within the resonance at high resolution (see Figs. 8 and 12), or by varying the physical structure or chemical content of the substrate so that other (chemical bonding) factors play an important role. The first approach has already been discussed in Sec. III.D and was also studied for Ar/Ru(0001) (Keller *et al.*, 1998a; Menzel and Wurth,

2000; Wurth and Menzel, 2000). Here we shall discuss the role of the substrate for the case of Ar as adsorbate.

For a quantitative understanding of the coupling of the core-excited state of the probe system to the continuum, it is advantageous to use ground-state calculations to the extent possible, since these are quite sophisticated, whereas calculations of the resonant processes employed have not reached the same level of reliability. This turns out to be quite within reach, due to the similarity of the electronic structure of the core-excited species to the same species with the core-excited atom exchanged for the $Z+1$ element, reflecting the higher charge near the nucleus represented by a core hole. This approximation has been tested many times by comparing model calculations with experimental energies and line shapes (Johansson and Mårtensson, 1980; Hüfner, 1996, p. 41; Föhlisch *et al.*, 1998), and it is also possible to explicitly calculate the electronic structure of a core-excited species, which tends to give similar results. The exceptions that do occur (see, for example, Aldén *et al.*, 1994) can be associated with unusually large changes of the electronic density in the core region, due, for example, to the population of a new electronic (sub)shell in the $Z+1$ species. Core-excited Ar can then be expected to have a chemical configuration similar to that of K, and this expectation has been tested and found to be quite accurate for the case we now explore, Ar/graphite.

In the $Z+1$ model, each core excitation of Ar can be considered as a measurement on a K atom placed at the Ar position, in the middle of an Ar overlayer. This is consistent with the usual Franck-Condon approximation (Hüfner, 1996, p. 148). We neglect to a good approximation the chemical interaction of Ar and K, and thus expect the data to reflect the bonding of atomic K to the substrate, graphite, with a slightly larger bonding distance. One piece of information obtained directly in XAS is the value of E_{res}, which, as seen in Fig. 13(a), is positive. This suggests that transfer of the electron is allowed from the $4s$ resonance of "K," as we denote core-excited Ar, to the substrate. This in itself is confirmation of the generally held picture of the bonding of isolated K atoms to graphite as predominantly ionic, with a largely empty $4s$ resonance. The width of the $4s$ resonance reflects the value of the total hopping probability convoluted with the core-hole lifetime broadening (Brühwiler, Maxwell, Rudolf, *et al.*, 1993; Ohno, 1994; Sandell, Hjortstam, *et al.*, 1997; Keller *et al.*, 1998a) and the experimental resolution function, plus possible extrinsic contributions such as vibrational broadening.

An autoionization determination of the net hopping-matrix element is summarized in Fig. 14(a). The area of the Auger spectrum as fitted to the raw data and compared to the total spectral area gives the ratio $\Gamma_{CT}/(\Gamma_C + \Gamma_{CT})$ as given in Eq. (9). This yields $\Gamma_{CT} \approx 0.05$ eV, so that $\hbar/\Gamma_{CT} = \tau_{CT} = 1.3 \times 10^{-14}$ s, as indicated. The theoretical side of this test case consists of calculating the electronic structure of "K" at the Ar distance in a supercell approximation (Sandell, Hjortstam, *et al.*, 1997;
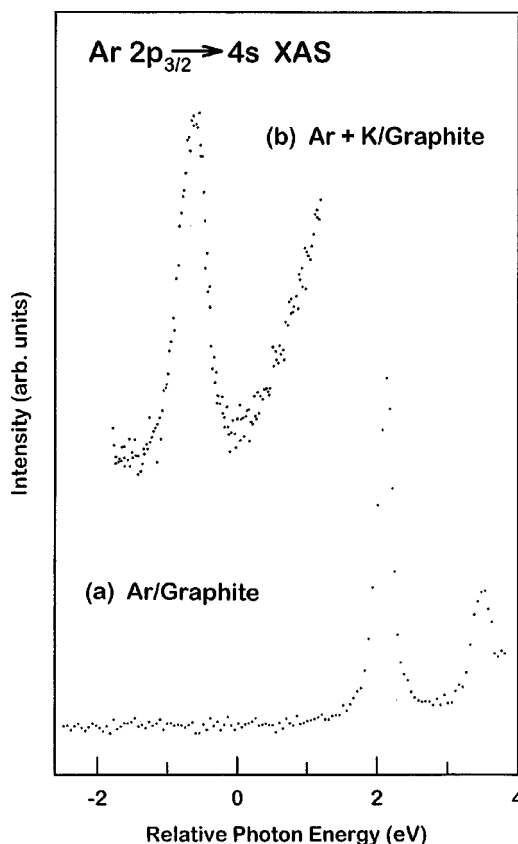

FIG. 13. Ar $2p \rightarrow 4s$ XAS spectra: (a) a monolayer of Ar on graphite; (b) Ar in nearest-neighbor configuration with isolated K atoms on graphite. The Ar $2p$ binding energy E_B has been subtracted from the photon energy scale, thus placing all structures on an E_{res} scale analogous to Fig. 4, i.e., with E_F at the origin. From Sandell *et al.*, 1999; Sandell, Hjortstam, *et al.*, 1997.

Hjortstam *et al.*, 1998). This is shown in Fig. 15. Calculations using Ar with a core hole and using K give the same result, confirming a high degree of validity for the $Z+1$ model of this system. The energy found in the calculations is quite close to the (corrected) experimental energy, and the width of the "K"-derived DOS is quite close to the value of Γ_{CT} of 0.05 eV, indicating that the theoretical approximations are accurate. A similar calculation at the proper distance for K in the ground state indicates the role of covalent effects on the position and width of the K $4s$ level. The high degree of agreement between theory and experiment gives one confidence in the resulting picture of the bonding of isolated K atoms to graphite.

A further confirmation of the general picture can be seen in Fig. 13(b), in which Ar atoms adsorbed in nearest-neighbor proximity to isolated K atoms on graphite are studied. $E_{res} < 0$ for this system. Examination of the raw data (Sandell, 1993) shows that this is mainly due to a change in the Ar $2p$ binding energy E_B, and so can be attributed to a change in (electrostatic) core-hole screening in one picture. However, one can also employ a chemical interpretation, that the "K" $4s$ resonance now lies below E_F due to the proximity of a second K atom. This is consistent with the observation
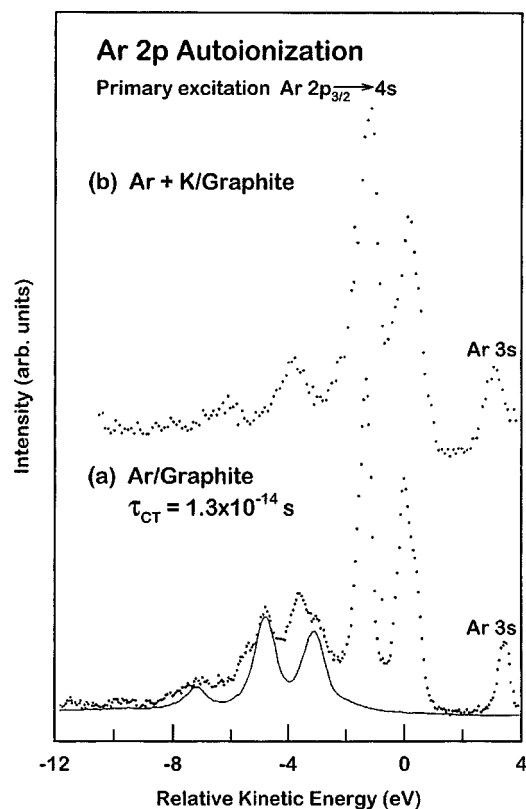
FIG. 14. Ar $2p_{3/2} \rightarrow 4s$ decay spectra corresponding to the data of Fig. 13. The kinetic-energy scale has been arbitrarily shifted in both cases. The dots represent the raw data, and the solid line in (a) represents the $2p_{3/2}$ Auger spectrum, scaled to match the intensity of the Auger-derived features in the raw data analogously to the analysis of Fig. 11. Spectrum (b) is identified as being composed purely of autoionization decay and can be understood in the following manner: Aside from a direct photoemission contribution from the Ar 3s level, the first three peaks, at about 0 eV, -1.5 eV, and -4 eV, are due to different final-state multiplets of the $3p^4 4s^1$ type, whereas those at about -6.5 eV and -8 eV (quite weak) are due to multiplets of the $3p^4 5s^1$ type (Aksela et al., 1988b; Carlson et al., 1989). While τ_{CT} is to be associated with a bond giving the 4s resonance width in (a), in (b) the lack of an Auger component implies that $\tau_{CT} \gg \tau_C$, which merely reflects the minimum-energetic cost of charge transfer to create the positive ionic "K" configuration, and thus an absence of any Auger signal. See the discussion in the text for details.

that isolated K atoms undergo a transition to metallic islands above a critical concentration (Li et al., 1991; Bennich et al., 1999) and suggests further that a metallic state sets in already with the formation of dimers (Sandell et al., 1999). The result presented in Fig. 14(b), in which zero dynamic charge transfer (and thus $\tau_{CT} \gg \tau_C$) is observed, is consistent with this picture.

One could also note that, for excitation at high (non-resonant) energies, certain spectral responses are expected. For the case represented in Fig. 13(a), a lone "K" adsorbate, we expect this to lead to an Auger spectrum without autoionizationlike contributions, which is what is observed (confirmed via comparison to gas-phase Auger data), and it is the pure Auger spectrum
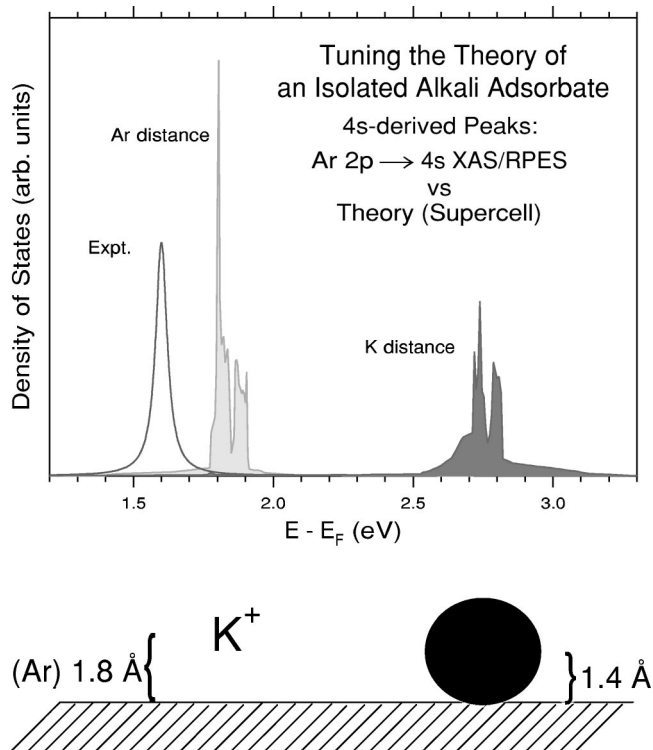

FIG. 15. Theoretical results for the 4s-derived density of states (DOS) of isolated 2p-excited Ar atoms on graphite in the indicated geometries, from Hjortstam et al. (1998); Sandell, Hjortstam et al. (1997). The curve denoted "Expt." is a Lorentzian with a full width at half maximum of 0.05 eV corresponding to Γ_{CT}, located at an energy given by that of the data in Fig. 13, and corrected for electron confinement effects on XAS, and polarization effects on the XPS binding energy (Sandell, Hjortstam, et al., 1997). A schematic of the geometries used in the calculations is also shown.

that is displayed in Fig. 14(a). Conversely, high-energy excitation for the case represented in Fig. 13(b), which can be thought of as a quasidimer ("K"-K), could lead to an Auger spectrum with autoionizationlike contributions, which is indeed observed (Sandell, 1993) [suggesting that the charge-transfer time is similar to that determined in Fig. 14(a)]. Thus energy scales such as those in Figs. 4 and 13 are on solid footing and allow one to speak confidently of the location of E_F in x-ray-absorption spectra, as is already common for metals. Note that it is not clear how the result in Fig. 14(b) is connected to the 4s resonance width, since Auger emission is required to gain this information. This is because of possible contributions from, for example, vibrations (see Sec. IV.E for a dramatic example of this). Such effects cannot be ruled out at the given energy resolution.

One could speculate a priori that a second electron might be energetically allowed to populate the "K" 4s resonance shown in Fig. 13(b), but this is not observed. With reference to the above discussion of the electronic structure of condensed K adsorbed on graphite, this is a reasonable result. One would expect a metallic K dimer to be the favored species based on that work, with rela-

tively neutral K atoms. In other words, one would not expect a largely polarized K dimer ("K"$^-$-K$^+$) to be energetically favored to exist on graphite, also due to the symmetry of the system. The case of N_2 in Sec. IV.B.2 illustrates how this can, in principle, be understood in terms of electronic correlation energies, which strongly rearrange the electronic structure as the number of electrons on a given species is altered.

Ar as a means of studying atomic K has also been studied on a series of metallic substrates (Sandell *et al.*, 1999). There the basic ideas developed for isolated alkali atoms as ionic species when adsorbed on metals were confirmed as correct. Furthermore, a dependence on the surface work function was found, albeit for different metals. For the surface with the lowest work function in that series, Ag(001), the Ar $2p$ x-ray-absorption spectrum shows a noticeable edge at the $2p$ binding energy E_B, as expected for a metallic system, indicating a strong mixing of the $4s$ resonance and the substrate s band, which was also reflected in the short $\tau_{CT} = 1 \times 10^{-15}$ s at resonance. Thus this approach can easily be extended to other systems. Other techniques, such as inverse photoemission, can, in principle, also be applied to the problem of isolated alkali atoms. However, inverse photoemission spectroscopy in particular has suffered from difficulties in separating out the weak adsorbate signal from the strong substrate signal, as well as from generally poorer resolution. Thus the strength of this approach compared to other experimental techniques is that it is possible to characterize a single adsorbate problem using a complete monolayer of a nonreactive species, and it is indeed applicable to cases other than alkali adsorbates, as can be seen in the following case study.

B. N_2

1. Physisorbed, isolated: N_2/Xe/Ru(0001)

A closed-shell homonuclear dimer represents perhaps the smallest increase in complexity relative to Ar, which motivates the relatively large number of resonant core excitation studies carried out on N_2 both adsorbed and in the gas phase. N_2 has recently been shown to exhibit vibrational interference phenomena, including detuning effects, when adsorbed on a Xe spacer layer on Ru(0001) (Keller *et al.*, 1999). This is consistent with the observation that $E_{res} < 0$ for the first $1s \rightarrow 1\pi_g$ resonance (Keller *et al.*, 1999) and that the x-ray-absorption spectrum is virtually identical in all respects to gas-phase data, indicating a negligible bonding interaction, so that no dynamic charge transfer is expected or observed. The detuning effects so well understood for the $(1\pi_u)^{-1}$ participator transition (Gortel *et al.*, 1998) are, however, modified somewhat by the presence of the surface, albeit in a straightforward manner. This is deduced to be a final-state effect. In particular, the vibrational potential of the $(1\pi_u)^{-1}$ final state is found to reflect a higher vibrational energy, and thus a stronger bond, than in the gas phase, consistent with the ionic final state's being
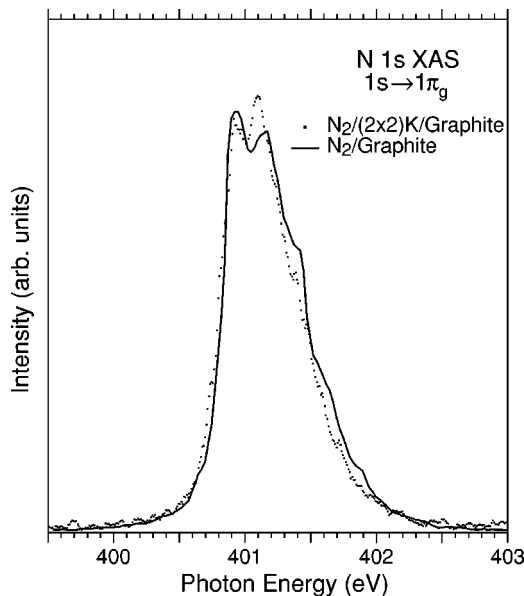

FIG. 16. N $1s \rightarrow 1\pi_g$ spectra for the indicated samples, from Puglia *et al.* (1998a, 1998b). E_{res} (see Fig. 4) is negative with a magnitude of several eV for both cases, as discussed in the text.

stabilized (the effective molecular charge reduced) by image and polarization effects in the substrate and Xe spacer layer, respectively (Keller *et al.*, 1999).

2. Core-excited $N_2 = N"O"$ on metallic K

The case of N_2 on graphite was the first to show strong effects of dynamic charge transfer (Björneholm *et al.*, 1992a). Just as in the previous two cases of N_2/Xe/Ru(0001) and Ar+K/graphite, $E_{res} < 0$ for excitation of the first $1s \rightarrow \pi_g$ resonance. Thus charge-transfer dynamics from the large to the small system are observed by exciting nonresonantly, corresponding to Fig. 7 and Eq. (10), and as discussed above for the case in Fig. 13(b). $\tau_{CT} = 9 \times 10^{-15}$ s for ionized N_2/graphite (Björneholm *et al.*, 1992a). An interesting possibility that was not observed at that time was the transfer of *two* electrons to core-ionized N_2 to produce a negatively charged adsorbate. This charge state was observed, however, for the first time for N_2/(2×2)K/graphite (Puglia *et al.*, 1998a, 1998b) in resonant excitation.

This can be appreciated already in the N $1s$ x-ray-absorption spectrum, compared to that of N_2/graphite in Fig. 16. Although those vibrationally resolved spectra are quite similar in photon energy and line shape, there is a noticeable difference in the vibrational spacing between the two cases. Curve fitting using a Poisson distribution yields a spacing of close to 0.23 eV for N_2/graphite, and 0.20 eV for N_2/(2×2)K/graphite (Puglia *et al.*, 1998a, 1998b). The former value is quite close to that of NO in the ground state, consistent with a quite accurate representation by the $Z+1$ approximation applied to core-excited N_2 ($=N"O"$), as already established for the gas phase (Chen *et al.*, 1989). The observed vibrational energy of 0.20 eV suggests a
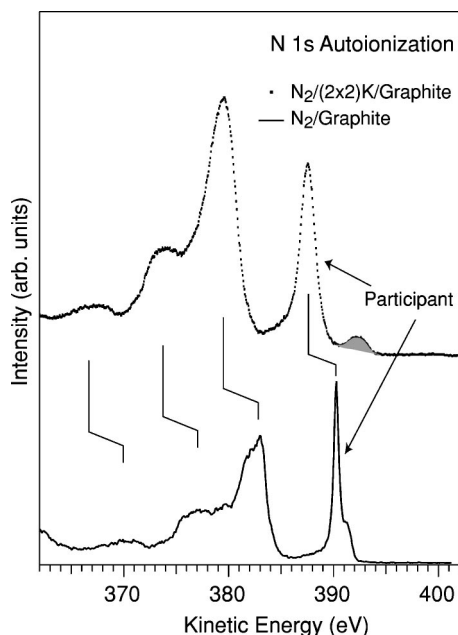
FIG. 17. N $1s \rightarrow 1\pi_g$ autoionization spectra for the indicated samples, from Puglia *et al.* (1998a, 1998b). The participant contributions, representing both $(3\sigma_g)^{-1}$ and $(1\pi_u)^{-1}$ final states, are indicated, and the spectator contributions lie at lower kinetic energy. An overall, slightly nonuniform energy shift is also indicated. The lone structure in the spectrum for $N_2/(2 \times 2)K$/graphite at 392.2 eV (shaded) is a new type of participant transition involving transitions to $(3\sigma_g)^{-1}1\pi_g$ and $(1\pi_u)^{-1}1\pi_g$ final states, as discussed in the text.

weaker bond when adsorbed on a metallic K layer, consistent with charge transfer to the antibonding $1\pi_g$ level, but less than unit electronic charge based on the value of 0.15 eV for NO^- (Schulz, 1973). In a single-particle picture of the molecular orbitals, a charge transfer of this type could be allowed *a priori*, based on the value of E_{res} for this system: $E_{res} = h\nu_{res} - E_B = 400.9$ eV $- 406.8$ eV $= -5.9$ eV. However, $E_B = 403.9$ eV (Puglia *et al.*, 1998a) for N_2/graphite also entails a negative E_{res} $= -3.0$ eV, with no apparent resulting dynamic charge transfer based on XAS. The autoionization data help to clarify the difference between these two cases in terms of electronic correlation effects.

Autoionization data for the two samples shown in Fig. 16 are presented in Fig. 17. We find similar N $1s \rightarrow 1\pi_g$ autoionization spectra, with the primary exception of a noticeable energy shift. This is consistent with ultraviolet photoelectron spectra of the N_2 valence states (Puglia *et al.*, 1998a), which show no differences except for a change in E_B similar to (but not equal to) that of the $1s$ level, as well as extra broadening for $N_2/(2 \times 2)K$/graphite. The shift is primarily due to the change in work function of the substrate, consistent with a weak (primarily van der Waals) bond. A similar extra broadening is observed in autoionization. However, a new feature appears for the K-adsorbed case at high kinetic energy. From the fact that this state has a higher energy than the $1\pi_u$ participant it is clear that it represents transitions from a higher-energy level of the mol-

ecule, and one that is not observed in photoelectron spectroscopy (PES). This suggests an explanation in terms of dynamic charge transfer. This peak is explained as participantlike transitions, but with an "extra" electron in the $1\pi_g$ level of the excited molecule (Puglia *et al.*, 1998a, 1998b), based on comparison to such neutral final states measured for XES in the gas phase (Glans, Skytt, *et al.*, 1996). Thus this case corresponds to Fig. 7(c).

The ratio of the "new" to the "main" participator line in the autoionization data is consistent with a partial electron transfer from the substrate to N"O," consistent with the analysis of the reduced vibrational splitting in XAS. (We make the assumption that the Auger transition probability for this transition is the same as that for the participant transition.) Hence one can conclude from the data of Figs. 16 and 17 that the affinity level overlaps E_F. Though the vibrational potentials reflect this, the negligible difference in $h\nu_{res}$ for N_2 on the two substrates and the fact that the vibrational sublevels are not hybridization broadened into a continuous line in XAS are both consistent with a slow charge transfer. Thus the data describe a situation in which the molecule would be neutral a significant fraction of the time in a hopping picture of the bond to the surface. Analysis according to Eq. (12) could easily be carried out with the assumption that the transition rate of the new channel is close to that of the neighboring participator line, and would give a lower limit on the charge-transfer bandwidth. The upper limit would be more difficult to derive at this point, beyond noting the width of the spectral features in XAS and RPES. Vibrationally resolved RPES would be interesting to further elucidate this case, as would changing the work function of the surface, e.g., by choosing a heavier alkali metal.

The picture of the energetics of this system which emerges from this analysis is clearer than that of the charge-transfer time. To begin with, we note that the first ionization potential of NO at 9.26 eV (Collin and Natalis, 1968) involves removing the lone 2π electron, corresponding to the $1\pi_g$ of N_2. This can be contrasted with the gain of adding a single electron to the same single-particle level of virtually 0 eV (Alle *et al.*, 1996; Randell *et al.*, 1996), for a difference of over 9 eV, which can be identified as the electron-electron correlation energy U (Hüfner, 1996, p. 178) for this orbital. A primary source of external screening to describe the stabilization of the so-called "affinity level" to E_F, where we observe it via autoionization, is the substrate image charge. The image screening is estimated for N_2/graphite by the shift in the ionization potential (IP) between gas phase and adsorbate, and one would expect a similar value for $N_2/(2\times 2)K$/graphite. This could explain only about 50% of the charge stabilization of the required magnitude of 2.9 eV required to shift the N"O" affinity level from E_V to E_F (Puglia *et al.*, 1998a). This means that the observed dynamic charge-transfer screening requires an additional bonding or chemical interaction between NO and the metallic (Li *et al.*, 1991; Bennich *et al.*, 1999) alkali overlayer as a source of electronic stabilization.
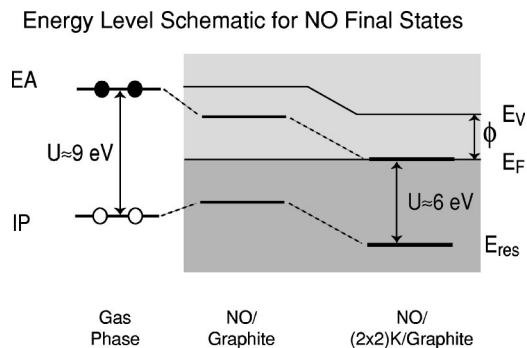
Energy Level Schematic for NO Final States

FIG. 18. Schematic of the energetics of the NO electron removal and electron addition states derived from the XAS/autoionization data of N_2 on the indicated substrates. The states shown are total states of the molecule, rather than the one-electron states shown in previous figures, and are characterized pictorially by the number of electrons in the 2π level. EA denotes the electron affinity, IP the ionization potential in each case, and U their difference, which corresponds to the correlation energy of electrons in the 2π valence shell. All quantities are derived from measurements (see the text for details), except for the EA of NO/graphite, which is estimated from the gas-phase result by subtracting the image screening observed in N 1s PES data of N_2 from the work function of graphite. E_{res} is equated with the ionization potential of the adsorbates, and electron affinity for adsorption on (2×2)K/graphite is derived from the data in Figs. 16 and 17. For adsorption on pristine graphite the position of EA is an estimate according to Puglia et al. (1998a). See the discussion in the text for details.

With the molecular states placed as shown in Fig. 18, U is reduced by roughly the same amount for adsorption on both substrates. This explains the lack of dynamic charge transfer for the case of pristine graphite, for which the work function ϕ is too large (Puglia et al., 1998a).

Another interesting aspect of these results is that it should be possible to observe a second qualitatively new peak in the autoionization spectrum. This peak would be due to an Auger-like process in which the excited electron and the substrate-donated electron were active, and hence *none* of the valence electrons of N_2. Thus one could hope to observe a peak corresponding to the electronic *ground state* of the molecule in the final state (with, of course, a hole near E_F in the substrate). This peak could be estimated to lie at an energy above the "charge-transfer participant" of approximately the N_2 first excitation energy of 6–8 eV (Schulz, 1973), or at around 398–400 eV. Such a peak is not clearly observed. An estimate of the intensity of the predicted peak along the lines of the simple method given by Brühwiler et al. (1995) and Ahuja et al. (1996) indicates that its intensity is expected to be within the noise of the available measurement (Puglia et al., 1998a), leaving observation of this type of transition to future work.

In addition to producing novel ideas, such as an expected peak corresponding to the ground state of the small system, the 1s excitation of $N_2/(2\times2)$K/graphite has implications for the chemistry of NO (Puglia et al.,

1998b). NO is known to pick up electrons when scattering from alkali-covered surfaces (Böttcher et al., 1993) and to thereby induce the substrate to emit electrons in a type of Auger process. With a substrate work function of several eV, strong screening is necessary to explain this phenomenon, which requires that the affinity level of NO be shifted from E_V to a position several eV below E_F as the molecule approaches the surface. The results of Puglia et al. (1998a, 1998b) suggest that a covalent bonding interaction is likely to be important in this process. In addition, since the affinity level is found to straddle E_F, (all-valence) interatomic Auger emission for the particular configuration of N"O" studied is not energetically allowed, since it requires the affinity level to lie below E_F with an energy equivalent to the work function. This suggests that such processes occur at molecular surface separations significantly different from the typical bond distance of N_2, at which the dynamic charge transfer was measured.

C. CO: Fast charge transfer

CO is a molecule that has also been studied intensively, both in the gas phase and as a primary model adsorbate. It was also the subject of many early studies with the aim of elucidating the charge-transfer dynamics as discussed here. Many researchers, for example, have pointed out the similarity between Auger and resonantly excited spectra for CO adsorbed on transition-metal surfaces (Chen et al., 1985; Wurth et al., 1987, 1988; Murphy et al., 1989; Porwol et al., 1994), but without a clear quantitative analysis of the hopping rate for many years (Wurth and Menzel, 1995), with the exception of those deriving a lower limit on the hopping bandwidth from a line-shape analysis (Murphy et al., 1989). Small changes can be observed in highly resolved spectra which suggest that electronically excited states on the adsorbate survive with a significant probability until the core hole decays (Porwol et al., 1994; Sandell et al., 1994). In contrast, for CO adsorbed on oxide surfaces, the general pattern is that Auger and resonantly excited spectra differ dramatically, with autoionization showing a strong resemblance to the equivalent gas-phase data (Klinkmann et al., 1996).

Quite recently, high-resolution studies by Keller et al. (1998b) have shown that it is possible to identify a participant contribution to the spectra for CO adsorbed on a metal surface using ARR conditions and the accompanying linear dispersion of the resonant portion of the spectrum, shown in Fig. 19. The authors then estimated the spectator contribution using spectra of physisorbed CO as calibration. The fraction of resonant decay processes [determined in the spirit of Fig. 7(a)] was of the order of 10% for CO/Ru(001), giving $\tau_{CT}\approx0.6$ fs. Since the spectral intensity associated with charge transfer is given as shown in Eq. (9) by $\Gamma_{CT}/(\Gamma_C+\Gamma_{CT})$, where the denominator represents the total spectral area, the ultimate limit on the measurability of the ratio will be given by signal noise, assuming one has the energy resolution to enable ARR conditions. The data in Fig. 19 have ex-
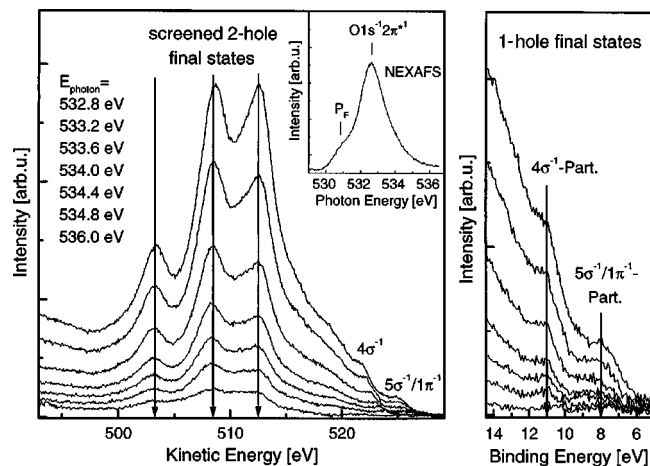
FIG. 19. O $1s$ resonant Auger spectra (after subtraction of the direct photoemission background) at the O $1s \rightarrow 2\pi^*$ resonance for a saturated CO monolayer on a Ru(001) surface (Keller *et al.*, 1998b). The photon energy (narrow-band excitation) varies across the resonance as given. Left-hand panel: plot against kinetic energy, emphasizing the Auger channels; right-hand panel, plot against binding energy, emphasizing the resonant channels; inset, O $1s \rightarrow 2\pi^*$ photoabsorption of the same sample (P_F indicates the photon energy corresponding to E_F).

cellent statistics, and the work of Keller *et al.* (1998b) suggests that the ultimate lower limit on the times that can be probed accurately is of the order of 0.1 fs, using the core levels discussed here with lifetimes τ_C of the order of 5 fs.

D. C_{60}: Placing and characterizing the core-excited state

The experiments described above have been aimed at a quantitative study of charge-transfer times using resonant core spectra. This is possible for small systems, in which an excitation of a core level at one atomic site results in perturbed valence levels on the entire entity. To understand this core-hole effect in general, more complex cases must be investigated. For increasing size, it is possible to envision the perturbation's being localized to a particular part of the small system, which is what studies of aromatic carbon systems such as C_{60} and graphite have shown, and which we take up here. Larger systems are taken up in Sec. V.

1. X-ray absorption spectroscopy

C_{60} is a highly symmetric molecule, making it an ideal stepping stone from the atomic to the mesoscopic scale. The large size, compared to the systems treated in the previous sections, gives one a chance to study length scales corresponding to more than a few bond lengths, and the high symmetry means that there are well-defined and highly degenerate bands in PES which change significantly in response to structural or bonding changes (Maxwell *et al.*, 1998; Rudolf *et al.*, 1999), i.e., lowering of the molecular symmetry. To be able to use RPES to study the coupling of the core-excited state to
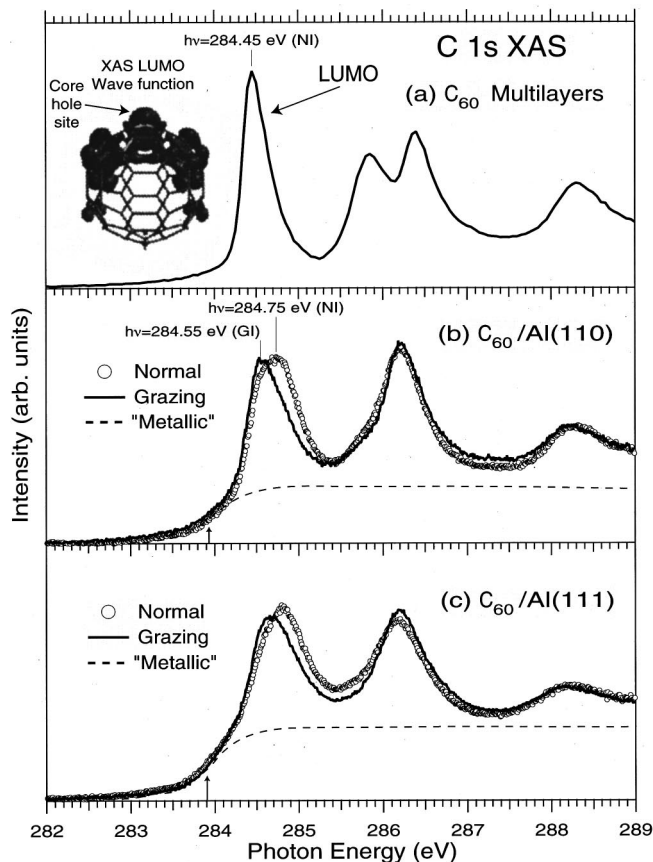

FIG. 20. C $1s \rightarrow$ LUMO x-ray-absorption spectra for the indicated samples, at a resolution of 0.16 eV (Maxwell *et al.*, 1997, 1998). The inset is a $Z+1$ calculation (Enkvist *et al.*, 1993; Lunell *et al.*, 1994) of the LUMO wave function, which should be applicable to XAS (Wästberg *et al.*, 1994; Nyberg *et al.*, 1999). The angle of incidence of the light is indicated for the monolayer systems, whereas no angle dependence has been observed for thick films. The schematic "metallic" background signal is explained in the text. The arrows just below 284 eV for the overlayer spectra indicate the C $1s$ binding energy E_B for the given sample, corresponding to E_F (see Fig. 4).

the greater environment, one may consider the x-ray-absorption spectrum of solid C_{60} shown in Fig. 20, which is quite similar to that of the gas phase (Brühwiler, Maxwell, Rudolf, *et al.*, 1993; Krummacher *et al.*, 1993; Rudolf *et al.*, 1999). The peaks represent different molecular orbitals, whose high degeneracies (threefold, for the first three peaks) are split by the effect of the core hole (Enkvist *et al.*, 1993; Wästberg *et al.*, 1994; Nyberg *et al.*, 1999). Beyond this effect, only one component of the trio of orbitals has significant weight in the spectra (Wästberg *et al.*, 1994). One generally invokes the $Z+1$ model to explain this degeneracy breaking, which is intuitively appealing in that a C atom replaced by a N atom would certainly cause this. However, to a good approximation—virtually exact in the gas phase and well satisfied even for the solid phase—all C atoms are equivalent, and thus a $1s$ hole can be considered to be distributed among all atoms according to the appropriate molecular-orbital probability density [see, for example, Kempgens *et al.* (1997) for an experimental study

of the magnitude of this effect]. Nevertheless, core-hole localization via nontotally symmetric vibrational modes, which couple to the electronic state and invalidate the Born-Oppenheimer principle, is well understood, and well demonstrated for small molecules (Gadea *et al.*, 1991; Schulte and Cederbaum, 1995; Skytt *et al.*, 1996; Köppel *et al.*, 1997). C_{60} has a multitude of Jahn-Teller active modes (Lannoo *et al.*, 1991), which could and should fill this role, as has been observed rather directly in PES in the gas phase (Gunnarsson *et al.*, 1995; Brühwiler *et al.*, 1997). Ungerade modes are also involved in the C 1s excitations of C_{60} (Käämbre, 2002). Thus the already low tunneling bandwidth of the core hole will be greatly reduced by vibronic coupling, effectively localizing it.[17]

Hence $Z+1$ and vibronic coupling pictures of the core-hole perturbation have a localization aspect in common. The fact that a $Z+1$ description captures the essential aspects of the 1s XAS data (Wästberg *et al.*, 1994; Nyberg *et al.*, 1999) strongly suggests that this description is accurate in its main details. Calculations of similar quality within a Jahn-Teller picture have not been carried out at this time, presumably due to computational difficulties, but one surmises that the results, for example, of the LUMO probability distribution in the core-excited state should be similar in its major details to that found in a $Z+1$ model (Bagus and Schaeffer, 1972; Domcke and Cederbaum, 1977; Ågren *et al.*, 1981; Enkvist *et al.*, 1993; Gel'mukhanov and Ågren, 1994, 1999; Lunell *et al.*, 1994).

The wave function shown as an inset in Fig. 20 reflects the $Z+1$ electronic structure, and, as we now discuss, the XAS data as a function of angle probe for the spatial extent of this wave function. Participant autoionization was used in this study as a digital ("on" or "off") monitor of dynamic charge transfer.

The excitation probability of the LUMO level in 1s XAS is independent of angle for solid C_{60}, and this should be a good approximation for adsorbed C_{60}, since the molecular structure is largely, though not perfectly (Maxwell *et al.*, 1998), preserved. The LUMO has a predominantly π^* character (Wästberg and Rosén, 1991), so that it is made up in the ground state primarily of combinations of p orbitals oriented perpendicularly to the quasispherical molecular surface. Thus the excitation probability as a function of atomic site in the dipole approximation is given pictorially by Fig. 21. We note that the C 1s XPS line is quite narrow for adsorption on Al [0.43 eV on Al(110), 0.55 eV on Al(111)], which is almost as narrow as the vibronically broadened solid C_{60} 1s line (~ 0.35 eV; Rotenberg *et al.*, 1996). The LUMO
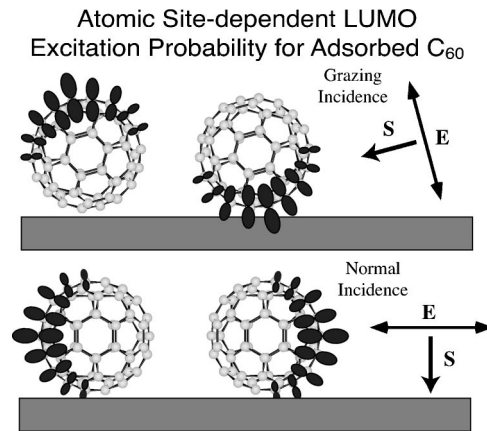
---

[17]The core hole could well be completely localized for excitation at the (0,0) vibronic line if one could neglect core-lifetime-induced vibronic mixing, since vibrational excitation is needed to take the system out of a local minimum in the vibrational potential. It is this core-lifetime-induced mixing which is responsible for detuning and other coherence effects in resonant core spectra of isolated molecules.

Rev. Mod. Phys., Vol. 74, No. 3, July 2002

Atomic Site-dependent LUMO Excitation Probability for Adsorbed C_{60}

FIG. 21. Qualitative atomic site-resolved transition probability for C 1s→LUMO excitation (Maxwell *et al.*, 1997), as well as excitation of other π^*-like levels. The size of the local π^* $-2p$ orbital drawn is proportional to the excitation probability and represents the projection of the corresponding 1s orbital onto it via the photon **E** vector. Grazing incidence corresponds here to 75° from the crystal surface normal for the Poynting vector **S**. It is clear that, in the geometry shown above, there will be a much higher cross section for the core hole to be located on the sides (top and bottom) of the molecule in normal (grazing) incidence.

resonance is approximately 60% larger [0.70 eV on Al(110), 0.80 eV on Al(111)]. This discrepancy between XPS and XAS suggests that we cannot explain the angle dependence of the LUMO x-ray absorption spectrum as being trivially due to a site-dependent core level E_B (Maxwell *et al.*, 1998). Indeed, a naive analysis might suggest a double-peaked structure for grazing incidence if that were the case, corresponding to different E_B's at and away from the interface. Hence the angle dependence is due to the interaction of the LUMO wave function with the surface.

As indicated in Fig. 21, this interaction will be expressed as a weighted average over the two sides of the molecule being excited, and as a peaked function of atomic site. A rough picture of this averaging process is given in Fig. 22. Thus we expect two signals in the case of grazing incidence excitation, and a more homogenous signal for normal incidence. Since C_{60} establishes a reasonably strong covalent bond to these free-electron substrates (Maxwell *et al.*, 1998), it is clear that x-ray absorption to the metallic continuum above E_F is expected, as has long been construed for adsorption of smaller aromatic molecules on metallic substrates (Stöhr, 1992). The dashed "metallic" curves in Fig. 20 show an estimate of the magnitude and location of this contribution. The low-energy portions are assigned based on the fact that the main line of the C 1s photoemission spectrum is centered on a broad steplike onset in both cases, indicated by the arrows, which is consistent with onset of absorption in free-electron-like metals [see, for example, Michiels *et al.* (1992) and the discussion in Sec. III.A.1], and with earlier practice (Stöhr, 1992). The observation that the fullerene-substrate bonding is stronger on Al(111) than Al(110) (Maxwell

C_{60} Core-excited LUMO at a Surface

Grazing-Incidence Excitation

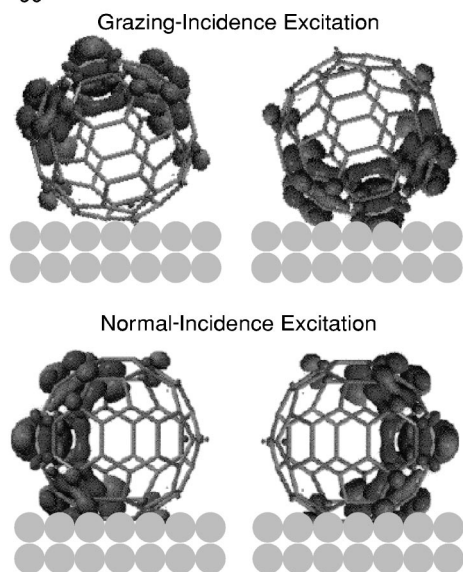### Normal-Incidence Excitation

FIG. 22. Depiction of the LUMO resonance wave-function distribution for the atomic sites with maximal excitation probability shown in Fig. 21.

et al., 1998) correlates well with the size of this metal-like onset and its total contribution to the spectrum.

We identify the *peaks* in the spectrum with molecular-orbital-like contributions, as already suggested by the good correlation with the data of pure C_{60}. These peaks show an angle dependence that rapidly decreases for higher states, which are also increasingly delocalized in space (Martins *et al.*, 1991). Indeed, the second peak in the pure C_{60} spectrum becomes quite broad upon adsorption on virtually all metal surfaces (Tsuei *et al.*, 1997; Maxwell *et al.*, 1998, 1994), an observation which is quite well understood as an effect of overlap with substrate states for molecular orbitals and Rydberg states of smaller molecules (Björneholm *et al.*, 1992b; Nilsson *et al.*, 1992). Hence the sharpness of a peak, the localization of the corresponding orbital, and the angle dependence of the peak are all correlated in the XAS of C_{60}. This already points to a particularly strong localized character for the LUMO wave function on general arguments, and we attempt now to analyze the angle and energy dependencies.

It is obvious from the C $1s$ binding energy E_B for the monolayers that $E_{res}>0$ for all of the XAS resonances. We note next that the LUMO resonance energy is an increasing function of the bond strength on Al, seen from the substrate dependence (Fig. 20 and Maxwell *et al.*, 1998). This we attribute to the covalent character of the bonding, which is different from cases of charge-transfer bonding (Chen *et al.*, 1991; Maxwell *et al.*, 1995, 1998), for which a rigid shift of the molecular orbitals is observed. Thus the angle dependence of the LUMO resonance suggests that, for grazing incidence, LUMO states with very little interaction/bonding with the substrate are probed, whereas normal-incidence excitation probes LUMO states with a greater interaction. This view is corroborated by the fact that the LUMO reso-

nance in grazing incidence for Al(110) has an energy and width close to that of pure C_{60}, and that the stronger interaction with Al(111) has reduced this similarity. Viewing Figs. 21 and 22 in light of these arguments gives a consistent picture, in that the LUMO resonance wave function can be totally isolated from the surface for grazing-incidence excitation. At normal incidence it will generally have a significant weight on those atoms involved in the [sp^3-like (Maxwell *et al.*, 1998)] covalent bond to the substrate. It is obvious that 50% of the excitation probability involves atoms quite close to or directly involved in the interface bond for grazing incidence, and a comparable number for normal incidence as well. We speculate that it is these atoms which contribute to the strong "metallic" background, and atoms far from the interface which give rise to sharp features and even isolated-C_{60}-like features.

2. Resonant photoemission: Digital charge-transfer dynamics

To test these speculations, we use C $1s$ resonant photoemission, shown in Fig. 23 for the Al(110) substrate. Because $E_{res}>0$ in all cases of interest, charge transfer out of the core-excited state is always allowed, and we expect changes (if any) in the resonant photoemission spectrum corresponding to Fig. 7(b). One observes clearly that the intensity is reduced at both angles of interest from that for pure C_{60}, and that it is stronger for excitation in grazing than in normal incidence. This is summarized quantitatively in Table II. Considering that in both geometries virtually all atoms are excited, but that the primary weight of the LUMO resonance wave function will be distributed as shown in Fig. 22, we conclude that the resonant photoemission intensity loss compared to pure C_{60} in each case is roughly proportional to the overlap of the LUMO resonance wave function with the atoms at the interface. This suggests that this overlap is equivalent to a very rapid (on the 1-fs time scale) transfer of the excited electron into the Al conduction band, which gives a "digital" character to the RPES cross section. This can further be taken as a strong confirmation of the analysis of the x-ray-absorption spectra given above. Finally, it is a semiquantitative measure of the extent of the LUMO resonance wave function, in agreement with that shown in Fig. 20. With the recent availability of macroscopic quantities of $C_{59}N$ (Hummelen *et al.*, 1995), XAS/RPES of C_{60} in various configurations is interesting as a means for studying the bonding properties of this prototypical heterofullerene.

E. Graphite: Core-excited states localized in a continuum

Graphite has much in common with C_{60} regarding structure and electronic states, in that both are based on sp^2 bonding configurations. An ideal sheet of graphite (graphene) can be considered as the largest fullerene. However, graphite is a semimetal due to the very weak interlayer interaction, which effectively converts a given
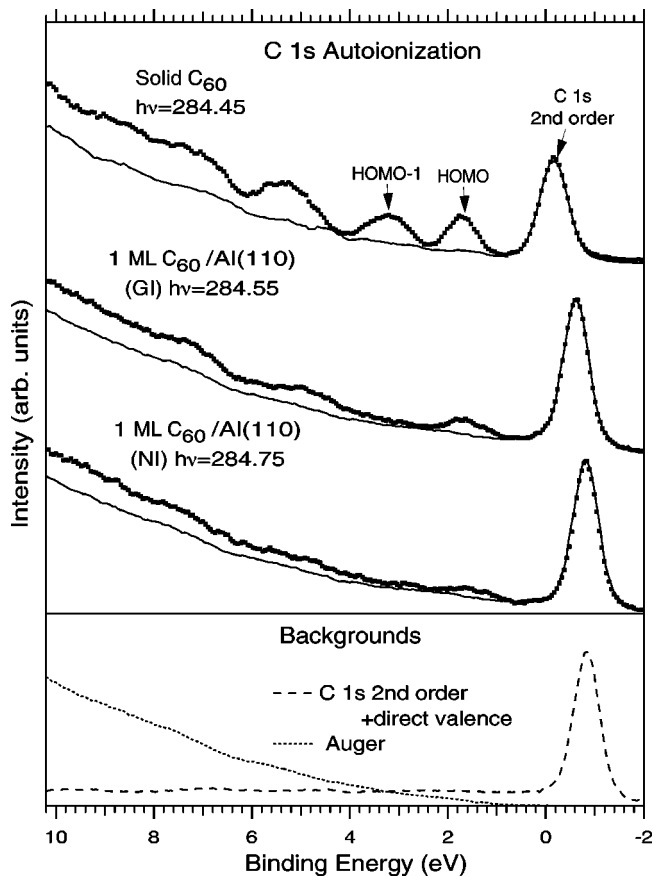
FIG. 23. C $1s\rightarrow$LUMO-excited resonant photoemission spectroscopy (RPES) spectra for solid C_{60}, and for 1-monolayer (ML) C_{60}/Al(110) in grazing incidence (GI) and normal incidence (NI) (symbols), shown with the estimated background contribution (lines). The RPES data were acquired at a photon resolution of 0.16 eV and electron resolution of 0.3 eV. The bottom panel illustrates the components of the background due to Auger emission and direct photoemission (Maxwell *et al.*, 1997).

graphene layer from a zero-gap semiconductor into an anisotropic metal, with nonzero conductivity in the plane that increases as a function of temperature. The electronic structure can be described as having two components, a set of σ bands with a band gap of $\sim$7 eV, and largely within that gap a set of π bands, roughly centered on E_F (Ahuja *et al.*, 1995). Thus graphite is to a certain extent intermediate between a metal and a typical planar aromatic molecule. The fact that carbon nanotubes have much in common with graphite electronically, but may be doped by atomic impurities, or may be closed by a fullerene cap (Dresselhaus *et al.*, 1996), suggests that it is worthwhile to understand the transition from graphite to fullerenes in more detail. XAS in particular will be quite useful when implemented in transmission electron microscopy, which enables one to gain unprecedented detail on the atomic scale, and at the same time measure XAS-like electron-energy-loss spectra. Thus it is becoming increasingly important to understand the x-ray-absorption spectra of the full fullerene-graphene size variation.

TABLE II. The expected variation in XAS cross section for 1 ML C_{60}/Al(110) as measured by resonant photoelectron spectroscopy (RPES) resulting purely from the variation in incidence angle of the x rays (see Fig. 21), compared to the measured HOMO RPES intensity when the maximum of the LUMO resonance is excited. The positive correlation between columns B and C, and negative correlation between A and C, strongly support the thesis developed in the text. The fact that the HOMO RPES intensity is close to 50% is consistent with the conclusion in the text that half of the atoms (those nearest to the interface) contribute much less. Results for monolayers on Al(111) show even lower RPES intensities, also consistent with the arguments in the text, due to the strong bonding to the substrate observed in that case.

Incidence angle	A Cross section for 30 atoms near equator (% of total)	B Cross section for 30 atoms at top/bottom (% of total)	C HOMO RPES intensity ($h\nu=$LUMO$_{max}$) (% of thick film)
Grazing	43	57	62
Normal	68	32	36

1. X-ray absorption spectroscopy

The first x-ray-absorption spectrum of graphite accompanied by theoretical estimates was published by Mele and Ritsko (1979). Their results indicated the existence of a localized state in the lower part of the π^* continuum. Later, a structure in electron-excited x-ray emission spectroscopy (XES) was interpreted as due to a localized (excitonic) state at the lower σ^* edge, also embedded in the π^* continuum (Mansour *et al.*, 1985); this state was resolved directly in XAS for the first time almost a decade later (Batson, 1993; Ma *et al.*, 1993). However, by then newer theoretical work had appeared which suggested a ground-state picture of the XAS data (Weng *et al.*, 1989), conflicting with most of the results above. It was with this in mind that a dynamic charge-transfer study of the strong $1s$ XAS features in graphite was undertaken, which gave impetus to theoretical work that makes a strong connection to the results for C_{60} in Sec. IV.D and lays out an experimental basis for understanding the entire fullerene structural series, from benzene to graphite.

C $1s$ XAS data for graphite are shown in Fig. 24. The π^* and σ^* characters of the different structures are easily determined from the angle dependence as indicated, and correspond in terms of symmetry vs energy quite well to expectations from the ground-state electronic structure (Ahuja *et al.*, 1995). The large π_1^* structure was originally identified as being excitonic, that is, corresponding to an electron localized by the core hole to the vicinity of the excited atom (Mele and Ritsko, 1979). σ_1^* is also a feature felt to be excitonic (Mansour *et al.*, 1985; Ma *et al.*, 1993), with strong similarities to the edge excitation x-ray-absorption spectrum in diamond (Ma *et al.*, 1993). Batson (1993) studied all three features marked in Fig. 24, and employed the ground-state calculations of Weng *et al.* (1989) to describe his data.
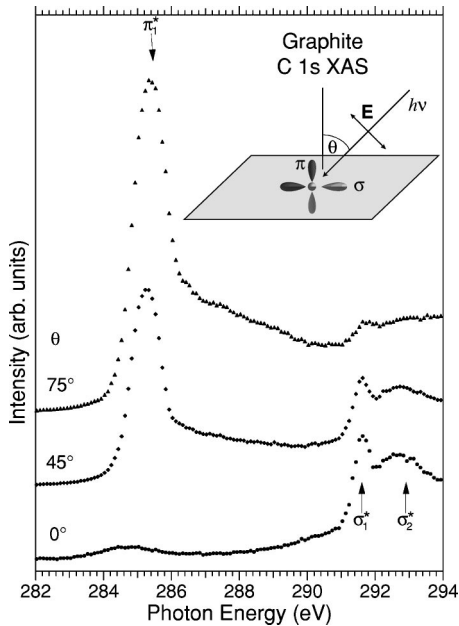
FIG. 24. Angle-dependent C 1s XAS data for highly oriented pyrolytic graphite, acquired at a photon resolution of 0.13 eV (Brühwiler *et al.*, 1995).

The width of the σ_1^* state is the lowest of the three features, and, considering the discussion of Secs. IV.A.2 and IV.D.1, is a strong candidate for a localized state, with an unexplained width of at most ~0.2 eV (Ahuja *et al.*, 1996), giving credence *a priori* to exciton descriptions. σ_2^* is ~1 eV wide, suggesting a much more delocalized state (Batson, 1993), but without information on the effects of phonon coupling for this excitation it is impossible to confirm this speculation. π_1^* is over 1 eV wide, which would correspond to a well-delocalized resonance if the width were entirely due to electronic contributions, as indeed was the model of Mele and Ritsko (1979). It is these uncertainties about the role of vibronic coupling that make RPES study of the dynamic charge transfer particularly useful in studying the coupling of the labeled XAS structures to the continuum of the extended system.

2. Resonant photoemission: Proof of localization

RPES data for the graphite σ^* excitations are shown in Fig. 25. One can note directly that excitation at σ_2^* is almost equivalent to high-energy continuum (photoemission) excitation, via the similarity of the σ_2^* decay spectrum to the Auger spectrum. At σ_1^*, on the other hand, participant contributions to the spectrum are observed. This is shown in detail in the inset of Fig. 25, which compares the highest structure beginning at 290 eV (now on a binding-energy scale) to the nonresonant photoelectron spectrum. The agreement between the two spectra is excellent, confirming the interpretation of the resonant spectrum as a participant transition. An overall kinetic-energy shift of 0.5 eV between RPES and PES corresponds very well to the vibronic relaxation of the σ_1^* state before core-hole decay determined from
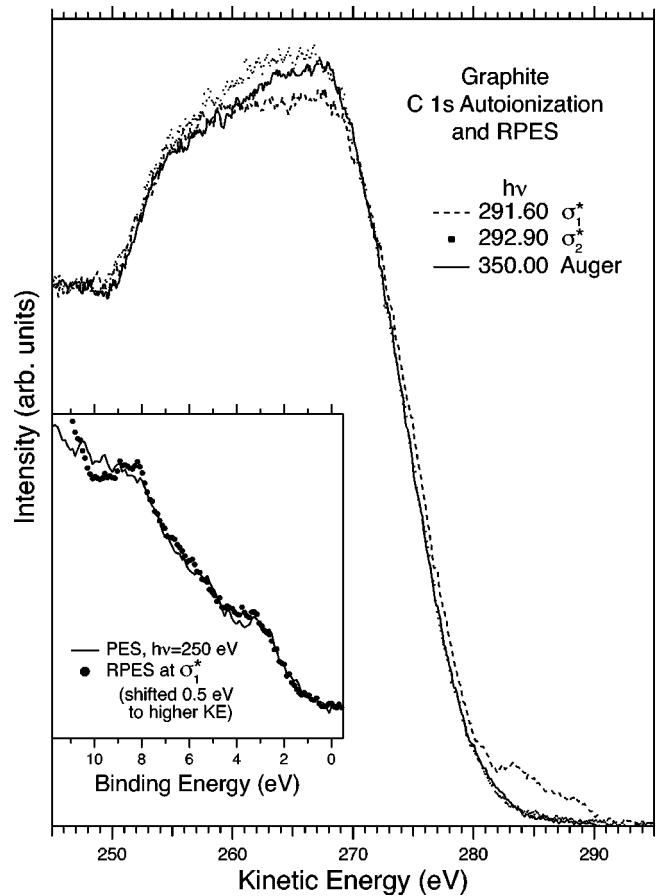

FIG. 25. $1s \rightarrow \sigma^*$-excited resonant photoemission spectra at the indicated photon energies, excited at normal incidence as shown in Fig. 24. The RPES data were acquired at a photon resolution of 0.3 eV and electron resolution of 0.6 eV (Brühwiler *et al.*, 1995). Note the great similarity between the spectra at $h\nu=292.90$ eV and $h\nu=350.00$ eV, which differ noticeably only for kinetic energies below about 270 eV. Inset: High-kinetic-energy RPES (participant) at σ_1^* compared to PES at the same emission angle.

XES (Ma *et al.*, 1993). The contrast between the σ_1^* and σ_2^* cases is a confirmation both of the utility of RPES for this study and of the completely different electronic character of the two XAS final states (Brühwiler *et al.*, 1995). The excitonic character of σ_1^* was confirmed in supercell calculations of the core-excited state (Ahuja *et al.*, 1996), showing it to be isolated in the π^* continuum, as previously speculated, and giving quite good agreement with experiment for E_{res}. The total quenching of the resonant part of the spectrum observed at the σ_2^* excitation, in the spirit of Fig. 7(b), suggests that its width would have to be due largely to electronic coupling. Interestingly, this excitation is not reproduced at all in the graphene calculations (Ahuja *et al.*, 1996), which could be an indication that it is due to transitions to an interlayer band, as suggested by Batson (1993) and McCulloch and Brydson (1996).

At π_1^* (see Fig. 26), a significant difference between autoionization and Auger emission is observed. Once again, the high-kinetic-energy portion of the spectrum
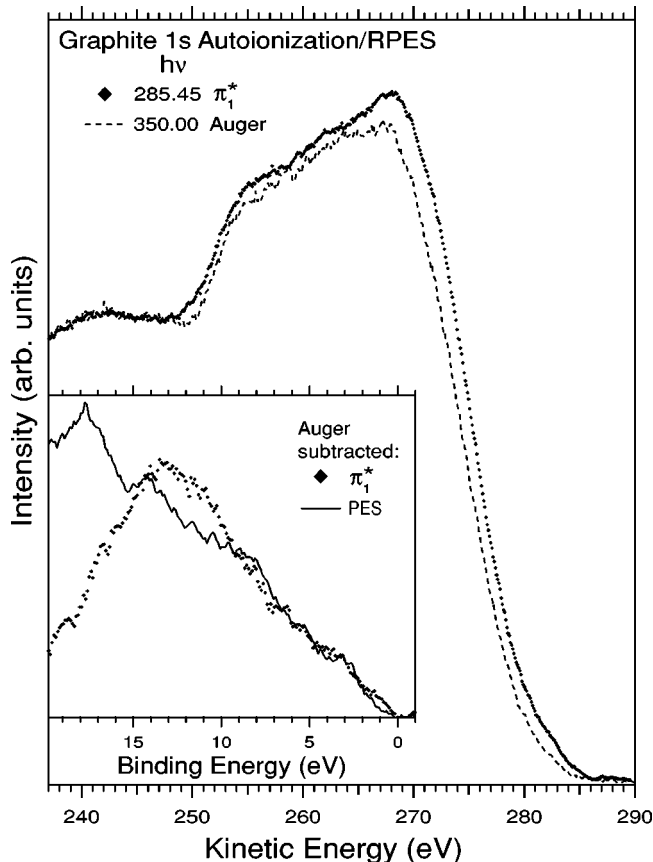
FIG. 26. $1s \rightarrow \pi_1^*$-excited resonant photoemission spectrum, excited at grazing incidence as shown in Fig. 24. The RPES data were acquired at a photon resolution of 0.3 eV and electron resolution of 0.6 eV (Brühwiler *et al.*, 1995). Inset: High-kinetic-energy RPES (participant+spectator) at π_1^* compared to PES at the same emission angle.

FIG. 27. Theoretical results for the $2p$-derived DOS at a core-excited C atom in a layer of graphene, from a supercell calculation (Ahuja *et al.*, 1996). The solid curve is the core-excited DOS directly from the calculation, which is then broadened by a 0.1-eV Lorentzian (to represent the core-hole lifetime) and a 0.6-eV Gaussian (for resolution and additional, presumed to be vibronic, broadening). The energy scale is given by subtracting the C $1s$ binding energy E_B from the photon energy, making it consistent with the definition of E_{res} of Sec. III.A.

agrees well with PES, suggesting a strong participant contribution. Thus, in spite of the large width of the π_1^* peak, which is comparable to that of the σ_2^* excitation, the excited electron is localized to the core hole. First-principles calculations of the core-excited state along the lines of Sec. IV.A.2, and Hjortstam *et al.* (1998) and Sandell, Hjortstam, *et al.* (1997) again give good agreement with the experimental value of E_{res}, and furthermore show a sharp double structure for the DOS associated with this excitation (Ahuja *et al.*, 1996). The overall width could thus be described as a combination of the effect of this double structure and a reasonable level of vibronic coupling-induced broadening (0.6 eV). A model following this argument indeed reproduces the data at a satisfactory level (Ahuja *et al.*, 1996), as shown in Fig. 27.

In analogy to the study of C_{60} in Sec. IV.D, this is once again a "digital" application of RPES to dynamic charge transfer, to differentiate between electronic coupling (band or resonance widths) on the eV vs tenth-of-an-eV scale. The success of the supercell approach within the full-potential linear muffin-tin-orbitals method used for this study of graphite (Ahuja *et al.*, 1996) and the study of K/graphite (Sandell, Hjortstam, *et al.*, 1997; Hjortstam
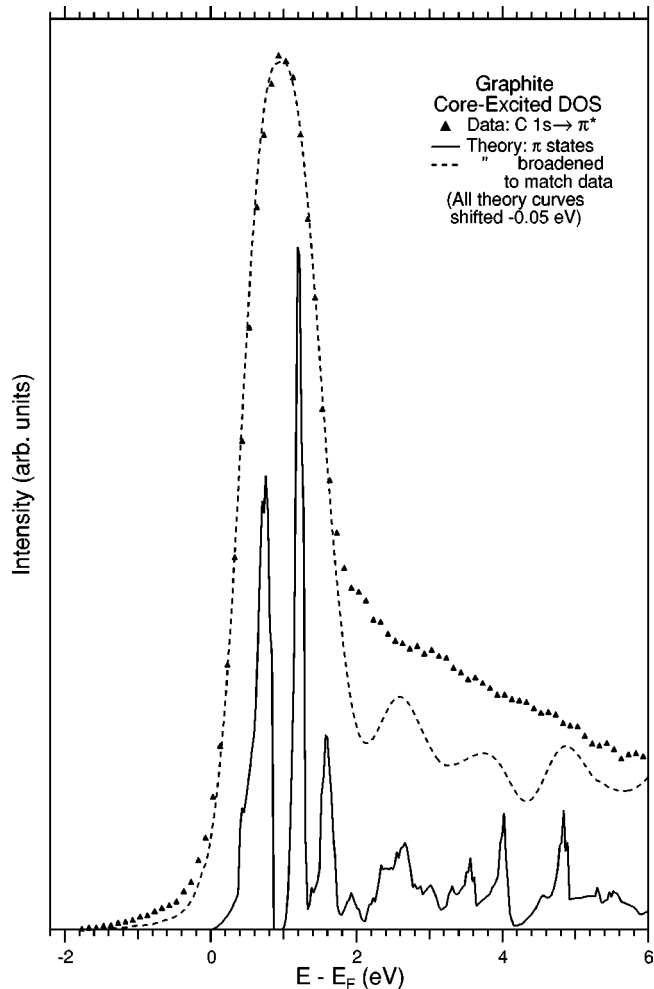
et al., 1998) shows that the DOS of the core-excited state is well described, and that a single-site approximation in XAS is adequate to a good first approximation. The calculations for graphite also reproduce the occupied states observed in x-ray emission from double-core-hole-excited graphite, as expected according to the final-state rule (Mansour *et al.*, 1985).

An apparent weakness of the theoretical curve in Fig. 27 is the presence of several small gaps or near-gaps in the DOS, e.g., between the double peak, and above E_F $+2$ eV and E_F+4 eV, although the overall weight of this portion of the excited-state DOS matches experiment reasonably well. This could be an effect of the use of a supercell approach or due to the fact that interlayer interactions were neglected. In any case, smaller supercells gave quantitatively quite similar π_1^* resonance widths, suggesting that the overall shape of the spectrum

and the derived coupling of the π_1^* resonance to the underlying π^* continuum is not an artifact of the calculation (Ahuja *et al.*, 1996). In contrast, Mele and Ritsko (1979) *forced* the width of their calculated π_1^* resonance to match the data by varying two parameters. More recent calculations (van Veenendal and Carra, 1997; Shirley, 1998, 2000) also model the entire width of the π_1^* resonance of more than 1 eV as due to electronic coupling to the π^* continuum. $\Gamma_C < 0.16$ eV for the $1s$ level of graphite (Prince *et al.*, 1999; Balasubramanian *et al.*, 2001; Brühwiler, 2001), which is a conservative upper limit, placing it more in line with what is found for C $1s$ levels of relatively small molecules. Thus the models of Mele and Ritsko (1979); van Veenendal and Carra (1997); Shirley (1998, 2000) imply, in turn, that the relative intensity of the resonant portion of the spectrum derived from Eq. (9) would be less than 10%, which does not seem motivated considering that the Auger-like profile is modified over the entire kinetic-energy range from 250 eV to threshold.[18] Based on the results for C_{60} [see Fig. 2 and Brühwiler *et al.* (1992)] and smaller molecules (Menzel *et al.*, 1992), the difference between the resonant and nonresonant spectra in Fig. 26 should correspond to a very minor (participant-dominated) portion of the total resonant contribution. Thus the available data are more consistent with the picture of Ahuja *et al.* (1996) than with models including only electronic contributions (Mele and Ritsko, 1979; van Veenendal and Carra, 1997; Shirley, 1998, 2000) to the width of the π_1^* resonance.

It is noteworthy that core excitation of C_{60} (see Sec. IV.D) gives evidence of a similar spatial extent for the core-hole perturbation. This suggests that the localization of core-excited charge distributions will be similar for fullerenelike structures for sizes between that of C_{60} and graphite (Ahuja *et al.*, 1996). These results could not have been placed on such a strong footing without the combination of XAS and RPES dynamic charge transfer.

V. CASE STUDIES: INSULATOR CONTINUA

As already noted in Sec. III.A.1, the case of coupling to a continuum in an insulator has many similarities with that of coupling to a metallic continuum, but the qualitative differences due to the existence of one or more band gaps can give qualitatively different dynamic charge-transfer coupling and energetics, as we shall attempt to demonstrate in this section. Resonant photoemission has long been employed to analyze the character and energetic placement relative to the gap of

core-excited states in insulators, used, for example, in the techniques of constant final-state or constant initial-state spectroscopy. Examples of excitations studied in this manner include the characterization (Ichikawa *et al.*, 1992) and evolution with coupling strength (Elango *et al.*, 1996) of excitons in alkali halides and related systems, and the identification (O'Brien *et al.*, 1991a) of excitons (or lack thereof) in simple metal oxides or at surfaces (Wang *et al.*, 1994). The σ^* states of graphite fall into this category as well. For these cases excitonic effects are expected at the absorption edges, and it is more the lack of such effects which is surprising (O'Brien *et al.*, 1991a). In addition, the energies E_{res} of core excitons are generally determined by curve fitting (O'Brien *et al.*, 1991b), which is a method that in principle can suffer from model dependence for its quantitative (or even qualitative) accuracy.

Here we shall discuss cases of increasing complexity and attempt to bring out the relevant aspects discussed in Sec. IV for metallic continua. Thus the energy scales and coupling strengths will be analyzed in each case to the extent possible. These cases have perhaps a greater potential for applications to problems of more general interest, since many technologies involve excitation and dynamic transfer of electrons from, for example, molecules to semiconductors (Miller *et al.*, 1995).

One experimental difficulty common to all insulating samples is that of energy referencing and sample charging (Cazaux, 2000). Sample charging occurs as a matter of course in electron spectroscopy, and the hindered charge rearrangement inherent in insulating solids means that a macroscopic charge can build up during a given measurement. If the charge state varies with time, as can be the case for thick insulating samples, strong measures are common, such as using an electron flood gun or illuminating the sample with light to excite carriers. Another variation on this problem which is less severe can occur with thinner samples supported by conducting substrates. One example of this which has been studied in some detail is several-nm-thick films of C_{60} on metal substrates. These samples show E_B shifts due to charging, which, however, are constant over long-time periods, yielding high-quality spectra but with a E_B scale that is shifted an unknown amount from the correct scale (Maxwell *et al.*, 1994, 1996). However, by taking appropriate measures, reproducible ionization potentials can be obtained in such cases, and it is this approach which was used in Sec. V.A below (Maxwell *et al.*, 1996).

A related question is the relative calibration of XAS and PES. The core-level ionization potential IP locates E_V for the x-ray-absorption spectrum. If one then subtracts the IP from the photon energy scale in the absorption spectrum, one obtains XAS on an IP scale, such that the energy to remove the excited core electron from the given excited state is read directly from the energy scale. An example of this is given below in Fig. 28. However, the correct *relative* alignment of PES to XAS to give the placement of the x-ray-absorption spectrum relative to E_{val} (see Fig. 5) may be achieved even without the correct IP scale, if the difference between the

---

[18]One should keep in mind that a large secondary background should be removed, in the sense of Fig. 2, and that the resonant portion of the spectrum I_{res} includes the spectator contribution, whose strength cannot be judged unambiguously, but whose form can be assumed to resemble that of nonresonant Auger emission based on the results at the σ_2^* excitation shown in Fig. 25.

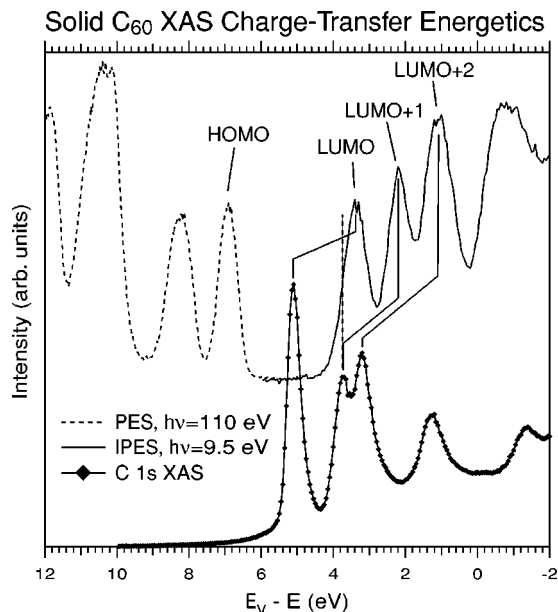## Solid C_{60} XAS Charge-Transfer Energetics

FIG. 28. Photoemission spectroscopy (PES; Brühwiler, Maxwell, Nilsson, *et al.*, 1993), inverse photoemission spectroscopy (IPES; Pedio *et al.*, 1995; Rudolf *et al.*, 1999), and C 1*s* x-ray-absorption spectroscopy (XAS; Brühwiler, Maxwell, Rudolf, *et al.*, 1993) data for C_{60} multilayer films, placed on an absolute (IP, $E_V = 0$) energy scale (Maxwell *et al.*, 1996). The effect of the core hole in XAS on the measured unoccupied state energies is indicated for the first three transitions, as is the relative placement of the LUMO in IPES and the LUMO+1 in XAS (dashed line). See the text for details.

binding energies of the valence and the relevant core line is known. This can be seen by noting that any error in the core level IP, which causes an unknown shift of the x-ray-absorption spectrum on the IP scale, will be compensated by the equivalent shift of the PES data on the IP scale.[19] As an example, if the C 1*s* ionization potential were $+1$ eV from the correct value in Fig. 28, the LUMO resonance would appear at an "effective" ionization potential 1 eV further below E_V, or $+1$ eV on the indicated scale. The photoelectron spectrum would also be shifted $+1$ eV on that scale, maintaining the correct relative placement. This approach has been used to study the placement of the absorption spectrum in the band gap of C_{60} (Schwedhelm *et al.*, 1998) and gives virtually identical results to the IP-based analysis (Maxwell *et al.*, 1996; Rudolf *et al.*, 1999), as expected. This makes it possible to study samples for which the position of E_V, and thus the IP, is difficult to measure reliably.

A. Solid C_{60}

Solid C_{60} is in many ways a typical molecular solid. The electronic bands are quite reminiscent of those of the free molecule, and a direct parentage can be identi-

fied for all of the bands near the fundamental gap (Martins *et al.*, 1991), as suggested in Fig. 28. Indeed, there is a debate about the nature of the extended states in solid C_{60}, which suffers from a lack of unambiguous experimental data (Brühwiler *et al.*, 1997; Rudolf *et al.*, 1999). Theoretical work shows that one expects solid-state bandwidths of ~ 1 eV for the levels around the fundamental gap (HOMO and LUMO and their immediate neighbors; Louie and Shirley, 1993; Shirley and Louie, 1993), though it has not yet been possible to include the effects of vibronic coupling on the electronic structure. We adopt the point of view that the theoretical bandwidths represent upper limits on the true quantities.

1. X-ray absorption spectroscopy

The x-ray-absorption spectrum of solid C_{60} has already been shown in Fig. 20. We remind the reader that the peaks that dominate the spectrum represent in each case (in the $Z+1$ picture, see Sec. IV.D.1) one of a trio of unoccupied orbitals which were triply degenerate in the ground state and which are localized to the core-excited atomic site (Wästberg *et al.*, 1994; Nyberg *et al.*, 1999). To understand the energetics of the dynamic charge transfer to be discussed here, we replot the XAS data on an electron removal energy scale, done by subtracting the photon energy scale from the C 1*s* ionization potential (Maxwell *et al.*, 1996; Rudolf *et al.*, 1999) in accordance with Fig. 5. PES (Brühwiler, Maxwell, Nilsson, *et al.*, 1993) and inverse photoemission spectroscopy data [the latter from Pedio *et al.* (1995) and calibrated by Rudolf *et al.* (1999)] are also plotted on this scale, though in inverse photoemission the measurement corresponds to the energy released when an electron is added (Hüfner, 1996, p. 403). PES and inverse photoemission spectroscopy measure (and result in) charge vacancies and additions, respectively, which can move from molecule to molecule in the solid without incurring an energy cost. Hence these data are preferable to most theoretical densities of states for the comparison shown. This is because the charge-charge correlation energy (U) is ~ 1.5 eV in solid C_{60} (Lof *et al.*, 1992; Brühwiler, Maxwell, Rudolf, *et al.*, 1993; Rudolf *et al.*, 1999), causing ground-state calculations to give an incorrect measure of, for example, the HOMO-LUMO gap, although more sophisticated calculations can correct for such correlations (Louie and Shirley, 1993). The shift in the LUMO from inverse photoemission spectroscopy to XAS is a direct measure of the core-valence correlation energy (Brühwiler, Maxwell, Rudolf, *et al.*, 1993), which is about 1.8 eV. This is only about 0.3 eV larger than the typical valence-valence correlation energy of 1.5 eV (Lof *et al.*, 1992; Brühwiler, Maxwell, Nilsson, *et al.*, 1993), which can be explained by the fact that the core-hole charge is screened by the entire valence electron shell of the molecule to redistribute the positive charge over virtually the entire molecule, as for a valence vacancy (Rotenberg *et al.*, 1996). The remaining difference can be considered to be a core-hole effect

---

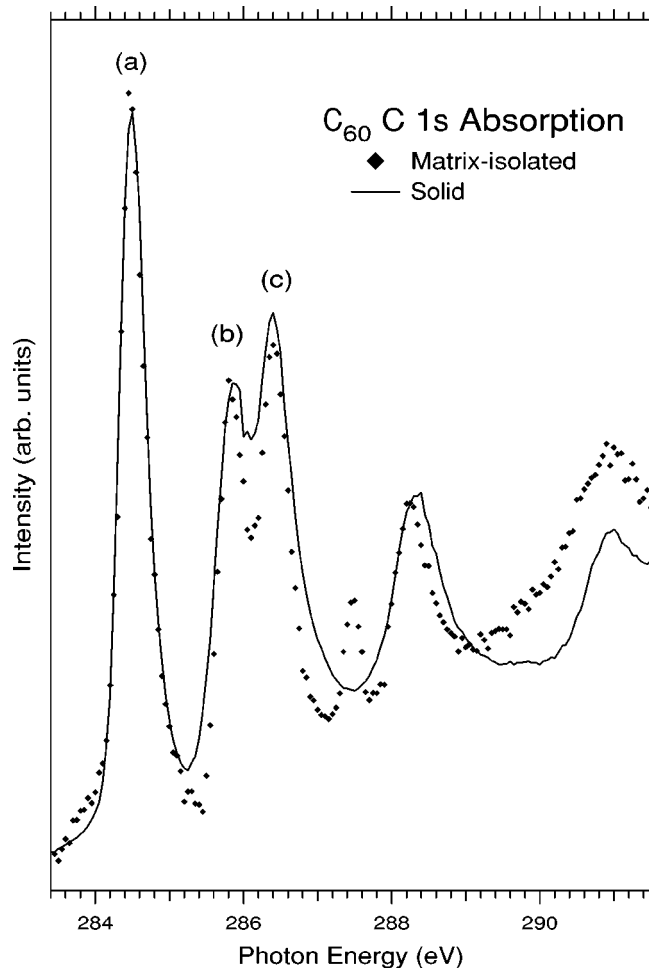[19]We thank Dr. S. Södergren for pointing this out.

FIG. 29. C $1s$ XAS data (Brühwiler, Maxwell, Rudolf, *et al.*, 1993) for C_{60} multilayers, molecularly isolated in a Xe matrix. The excitations probed using RPES (see Fig. 30) are labeled (a)–(c). The peak at ~ 287.4 eV is due to CO condensed from the background gases in the vacuum chamber.
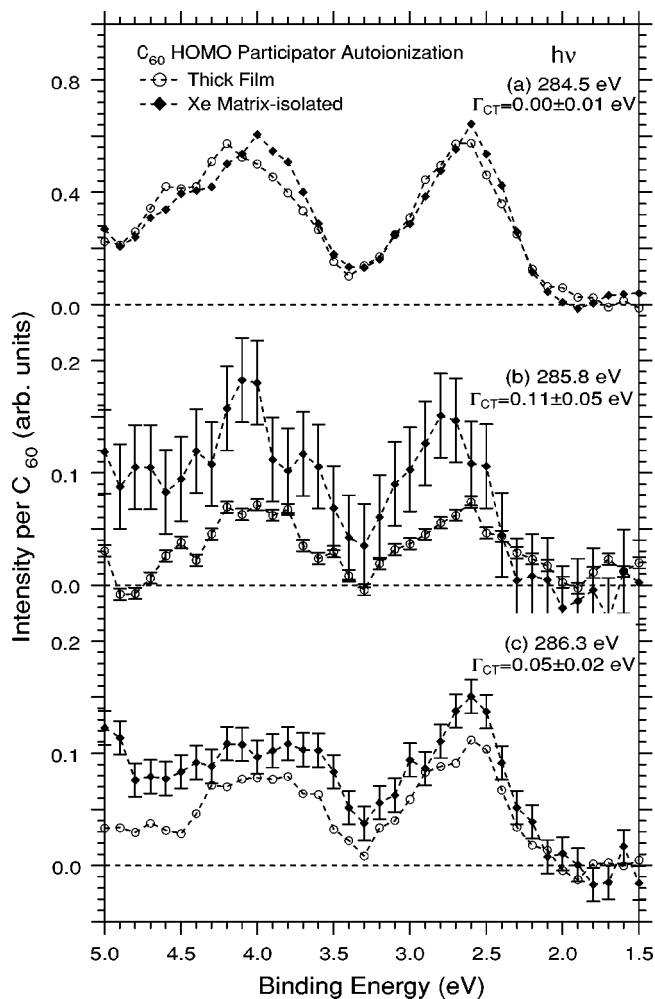

FIG. 30. C $1s$ RPES data (Brühwiler, Maxwell, Rudolf, *et al.*, 1993) for the indicated samples, corresponding to the XAS data and indicated transitions (a)–(c) in Fig. 29. The data are calibrated to an arbitrary intensity per molecule, as described by Brühwiler, Maxwell, Rudolf, *et al.* (1993). The intensities given at the different XAS transitions are calibrated to the same arbitrary scale and thus may be compared. The binding-energy scale is arbitrarily referenced to the spectrometer E_F, with a slight shift to align the solid and matrix-isolated data. The values of Γ_{CT} are derived from the intensity changes according to Eq. (11).

(Brühwiler, Maxwell, Rudolf, *et al.*, 1993; Rudolf *et al.*, 1999), or, equivalently, the effect of vibronic relaxation (Köppel *et al.*, 1997).

With these considerations in mind, Fig. 28 shows directly that the LUMO excited in XAS of solid C_{60} lies in the fundamental gap, as a true exciton. Thus its width gives a direct measure of the vibronic coupling. As the vertical dashed line indicates, the LUMO+1 in XAS is largely misaligned with respect to the LUMO in inverse photoemission spectroscopy, thus suggesting that it, too, may lie at least partly in the gap, depending on the effects of vibronic coupling on the inverse photoemission spectroscopy line shapes. To study this using RPES requires a calibration of the RPES intensities (Brühwiler *et al.*, 1992), provided in this case by data for single molecules isolated in a Xe matrix.

Figure 29 shows the XAS data for solid C_{60} compared to data for a highly dispersed sample in a Xe matrix. The C_{60} concentration was calibrated from monolayer studies and chosen to put an average of three Xe layers be-

tween each pair of molecules, with a control study at an even lower concentration (Brühwiler, Maxwell, Rudolf, *et al.*, 1993). The transition energies are almost unaffected by the difference in environment between the two cases, though a significant broadening, especially of resonances (b) and (c), is noticeable for solid C_{60}. A similar effect was detected when studying second monolayer molecules adsorbed on Au(110) (Maxwell *et al.*, 1994). Just as was the case for the studies of Ar discussed in Sec. IV.A.1, the Xe band gap should greatly reduce or eliminate any electronic coupling between the isolated fullerenes, and the observed change in XAS broadening is indeed consistent with a lower electronic and/or vibrational coupling.

2. Resonant photoemission: Charge transfer as a function of the excited state

The data in Fig. 30 bear detailed consideration. Because the Xe matrix contributes a strong background, which dominates for binding energies just outside the range presented, the determination of charge-transfer times must proceed along the lines of Fig. 7(b). The details of the intensity calibration are given in Brühwiler, Maxwell, Rudolf, *et al.* (1993). As already noted in Sec. V.A.1, for transition (a) in Fig. 29 the resonance energy consistent with Fig. 5 is $E_{res-a} \approx -1.8$ eV peak to peak, using the LUMO in inverse photoemission spectroscopy as the conduction-band reference. Thus, for any model of the inverse photoemission spectroscopy line shape, it is expected that no dynamic charge transfer should occur upon excitation to this transition which lies so deeply in the fundamental gap, as is observed to within experimental uncertainties. The second XAS resonance is characterized by $E_{res-b} \approx -0.35$ eV peak to peak and overlaps part of the LUMO profile. RPES shows that the excited core electron delocalizes with roughly 50% probability during the core lifetime, since $\Gamma_{CT} \approx \Gamma_C \approx 0.1$ eV. This could in principle be explained by correcting E_{res-b} to a value closer to 0 to account for solid-state band dispersion suggested by the inverse photoemission spectroscopy data in Fig. 28, although this is not seen in angle-resolved inverse photoemission spectroscopy of solid C_{60} (Themlin *et al.*, 1992). Vibrational coupling may explain much or all of the broadening in inverse photoemission spectroscopy, as appears plausible for PES (Brühwiler *et al.*, 1997; Kjeldgaard *et al.*, 2001), and in this case the stated value of $E_{res-b} \approx -0.35$ eV may be more appropriate. One aspect of the hopping not yet considered here is the fact that the electron, once transferred to a neighboring molecule in the solid, should still interact with (screen) the core hole, and this energy gain constitutes a correction (V) to E_{res-b} estimated to be about 0.3 eV (Antropov *et al.*, 1992), which would compensate for the observed small excitonic binding of the core-excited LUMO+1 resonance. Thus this is an alternative explanation of the measured hopping. $E_{res-c} \approx 0.15$ eV is very small, and comparable to the core-hole lifetime broadening of ~0.12 eV, thus giving a reasonable explanation for the hopping observed in Fig. 30(c). The correlation energies U and V will in any case be included somehow in a proper description of the hopping process [see, for example, Koch *et al.* (1999)].

These results confirm a picture of solid C_{60} as composed of virtually independent semiconducting nanounits, for which a change in the charge state represents a strong perturbation (Lof *et al.*, 1992). In contrast to the concept of continuous band bending, so well established for the screening of charges in traditional semiconductors (Zangwill, 1988, pp. 221–227), the idea of band bending can be applied for this and presumably many other molecular solids only in a discrete manner, as depicted in Fig. 31. The energies of the given levels at each site represent the case in which the excited electron
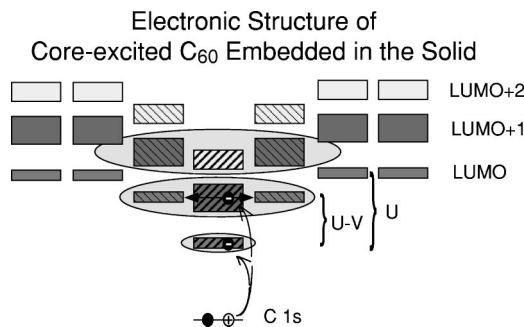

Electronic Structure of Core-excited C_{60} Embedded in the Solid

FIG. 31. Schematic of the unoccupied electronic bands of solid C_{60} with a core excitation at one site, showing the effects of charge-charge correlation as discussed in the text. U represents the energy to remove the electron in the LUMO resonance to a site (molecule) far away, i.e., with a negligible remaining Coulomb interaction. V is the Coulomb interaction of the LUMO electron with the charged molecule when transferred to a nearest-neighbor LUMO orbital.

resides on that molecule, thus showing that screening effects such as those represented by V can allow a type of two-center resonance bond to form, analogous to that discovered for the case of $N_2/(2\times2)K/graphite$ (see Sec. IV.B.2). We make the approximation that screening of the core hole by the electron on a next-nearest neighbor is negligible. Transport of the electron away from the core-excited site is prohibited to different degrees depending on the value of E_{res}. A study in a similar spirit was recently used to characterize the degree of molecular character of the structural units of solid $NaNO_2$ (Vinogradov *et al.*, 1999).

B. A complex substrate: CO adsorbed on oxide-supported metal clusters

In the previous section we considered a somewhat more complex adsorbate on a single-crystal substrate as a first step towards the study of a heterogenous system. Here we examine a prototype adsorbate (CO) on a relatively complex substrate, supported Pd particles—$Pd_N/Al_xO_y/NiAl(110)$. For this system, a thin oxide formed on a metal single crystal in a self-limiting oxidation process serves as the substrate for Pd particles formed by aggregation of monomers evaporated onto the surface (Bäumer and Freund, 1999). These particles are then exposed to CO to examine their chemical properties. One of the issues with this type of model catalyst is the extent to which the very thin (several atomic layers thick) oxide layer represents the surface structure and electronic properties of the "true" oxide.

The observation that core-level binding energies of the metal atoms making up the particles vary strongly as a function of particle size is direct evidence that the particles remain charged by the photoemission process on the time scale observable in direct photoemission, which is of the order of 10^{-17} s. Dynamic charge transfer in this case has been applied to gain insight into processes on the significantly longer fs time scale (Sandell, Libuda, *et al.*, 1997).
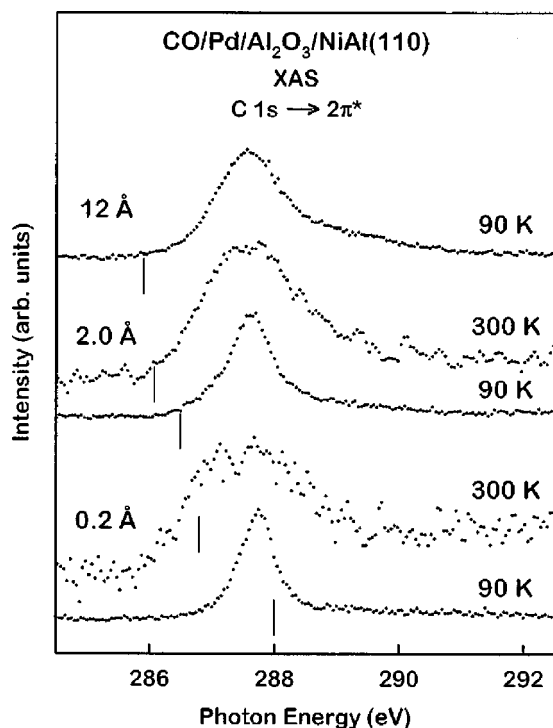
FIG. 32. C 1s x-ray-absorption spectra for the indicated samples. The vertical lines indicate the C 1s binding energy E_B. The specified Pd coverages can be converted to approximate average particle sizes as follows (Sandell, Libuda, *et al.*, 1997): 0.2 Å, 10 atoms; 2.0 Å, 100 atoms; 12 Å, 2000 atoms. The particles were CO saturated at 90 K, studied spectroscopically, warmed to 300 K to drive off a more lightly bound CO species, and studied again.

The XAS data shown in Fig. 32 reflect the position E_{res} (taking into account the C 1s binding energy indicated) and broadening of the core-excited CO π^* resonance, which has been studied previously for CO adsorbed on a number of single-crystal substrates (Jugnet *et al.*, 1984; Björneholm *et al.*, 1992b; Nilsson *et al.*, 1992). E_{res} is greater than 0 for the larger clusters, as it is for single-crystal metal substrates. The smallest clusters, however, show $E_{res} < 0$. Since metal clusters are in general metallic for the larger sizes shown here, it is perhaps not surprising that the physics is the same for these cases. It is also important to note that the CO-Pd bond is relatively strong, based on the temperature needed to desorb the more weakly bound species. In addition, the close similarity between Auger and resonantly excited spectra at the C 1s threshold (see Fig. 33 and the discussion in Sec. IV.C) suggests a bond similar to that observed on single-crystal surfaces (Sandell, Libuda, *et al.*, 1997). These pieces of information suggest that the difference between the smallest particles and the larger sizes is due to electrostatic effects, i.e., the final-state charge in PES is more difficult to screen for the smallest particles and brings about the increasing E_B. That the neutral C 1s x-ray-absorption state is roughly constant in energy supports this assertion. The intermediate case (2.0 Å/100 atoms) appears to be near the border between the others, with a C 1s binding energy E_B that lies
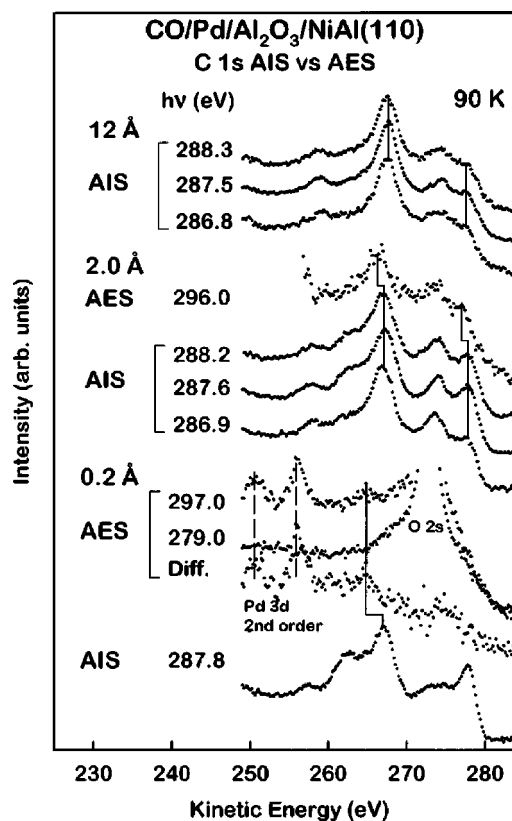

FIG. 33. C 1s autoionization spectra (denoted AIS in the figure) and Auger electron spectra (denoted AES) for the indicated samples. The vertical lines indicate the position of equivalent two-hole states. The dashed line for the 0.2-Å sample indicates Pd PES lines excited by second-order light, as well as a strong O 2s photoemission spectrum. The spectator shift between the single-hole autoionization states and the two-hole Auger states is due to the significant screening provided by the original core-excited electron present for the single-hole autionization final states.

noticeably higher in energy than for the infinite-size limit.

Further support for this picture is derived from resonant Auger data, shown in Fig. 33. Excitation on resonance (autoionization spectra) leads to resonant Auger (two-hole) states, which have significantly higher kinetic energy than Auger emission spectra excited at high energy. This is due to the presence of the spectator electron [see Fig. 1(f)] and confirms that the clusters are electronically isolated from a ready electron reservoir, such that no low-energy screening electrons are available on a fs or faster time scale. This is once again a digital measure of the electronic coupling, in this case of the Pd-cluster-plus-CO-overlayer complex to other clusters and to the NiAl(110) substrate.

VI. X-RAY EMISSION/RESONANT INELASTIC X-RAY SCATTERING

One subject which we have not broached is the potential of resonant inelastic x-ray scattering (RIXS), or resonant x-ray emission spectroscopy (XES) (Rubens-

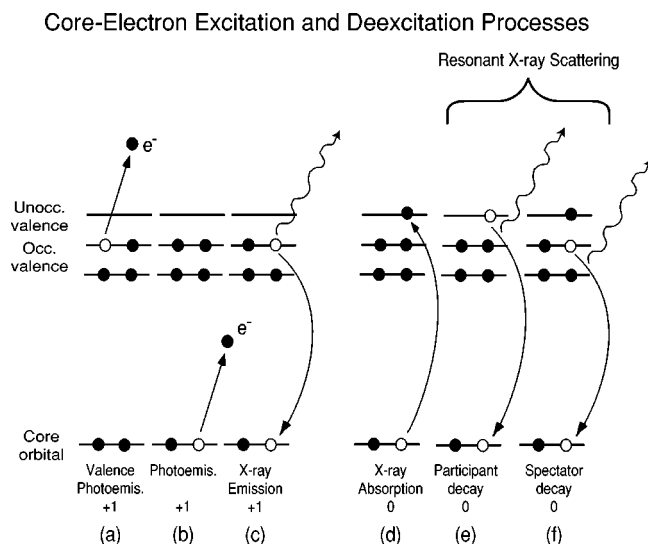## Core-Electron Excitation and Deexcitation Processes

FIG. 34. Schematic of the indicated electronic excitation-deexcitation processes, analogous to Fig. 1, but emphasizing the radiative core decay channels. The final charge states shown are those for an isolated system, i.e., no extrinsic screening is considered.

son, 2000; Shirley, 2000; Kotani and Shin, 2001), for this kind of study. These radiative counterparts to RPES are sketched in Fig. 34. It is apparent that, in principle, RIXS offers a similar potential for observing dynamic charge transfer to that established for RPES/resonant Auger spectroscopy (Rubensson, 2000). For example, even though the cross section for radiative core-hole decay is roughly a factor of 1000 lower than that for Auger-like decay for the core levels accessible via soft x rays, XES/RIXS reflect the same charge-transfer times with the same spectral ratios derived in Sec. III.B.1 (Rubensson, 2000). However, thus far only a few such studies have been published (Rubensson *et al.*, 1997; Magnuson *et al.*, 1999), and they took up the questions of molecular dissociation and coupling of a quasibound state to the ionization continuum, respectively, rather than coupling of a bound state to a continuum, as we have stressed here.

A major challenge in the use of XES/RIXS to study charge-transfer dynamics is the fact that the absolute charge states of the probed species (without external screening) are 0 and $+1$, rather than $+1$ and $+2$ as for the corresponding electron spectra. Thus the local charge-charge correlation energies (U) are significantly less for XES/RIXS, and this makes identification of the resonant vs nonresonant channels more difficult. Raman-like dispersion of the resonant channels brings about an increasing separation which can enable one to employ this approach in favorable cases, e.g., for wider resonances (Rubensson *et al.*, 1997). In principle, the symmetry selection rules relevant for free molecules upon resonant excitation could aid in distinguishing between the two channels (Käämbre, 2002), but vibronic coupling alone is also a cause of relaxation of those rules (Luo *et al.*, 1995; Skytt *et al.*, 1995, 1996), and so the line shape is not a trivially conclusive measure at the present

level of computational power (Triguero *et al.*, 1999). A strength of the technique is that resonant x-ray emission or resonant inelastic x-ray scattering spectra, because they are measured in terms of photon energies, can directly be coupled to x-ray-absorption spectra to give information on the states that lie in the gap. Because these techniques are both able to be used as photon-in, photon-out methods, one can measure samples composed of, for example, fluids and buried interfaces, which suggests that an investment in the understanding of the resonant processes would be repaid itself many times in the amount of information made available for those kinds of interesting and complex systems.

VII. OUTLOOK

The study of dynamic charge transfer with resonant core excitation-deexcitation spectroscopy has a broad potential for applications to currently interesting problems. The technique has a relatively useful placement in terms of time scales due to the difficulty in obtaining similar time resolution using lasers. In addition to providing a detailed understanding of model systems, the method enables one to elucidate electron-electron correlation effects and their role in excited electron dynamics. Even quite complex systems can be studied, such as adsorbed nanoparticles and large molecules adsorbed on surfaces, and the potential for choosing different atoms of the same element in such systems is only beginning to be exploited. There is no prerequisite of translational symmetry in this type of core-level measurement, which means that this approach might also offer important complementary information to photoemission-based laser pump-probe methods for particular cases. In what follows, we attempt to point more explicitly to some of the interesting fields in which the approach might profitably be applied.

(*a*) *Molecule-to-semiconductor charge transfer*. Focusing on the time scales that have thus far been utilized, i.e., roughly 5 fs relevant to N and C $1s$ levels, several areas of electron transfer dynamics would be interesting to explore, and are being explored. Molecular photovoltaics based on semiconductor-supported dyes (Hagfeldt and Grätzel, 2000) involve excitation of an electron in a large molecule or polymer, and subsequent transfer to a substrate or other molecule. In both cases, rapid transfer is desirable to minimize the phase space for deexcitation (or other unfavorable capture/recapture) of the photo-excited electron. Both systems contain components amenable to study using the core levels of choice thus far. Indeed, Schnadt *et al.* (2002) have studied a model system for the "Grätzel cell" (Patthey *et al.*, 1999; Hagfeldt and Grätzel, 2000) using a dense distribution of photon energies as in Figs. 12 and 19, but using the strategy illustrated in Fig. 7(b) to monitor the charge transfer from a large molecule into a semiconductor. The related issue of the transmission of electrons through molecules into a semiconductor substrate as a function of molecular length was studied for the first time using core tech-

niques by Bournel *et al.* (2000), in analogy to studies using lasers (Asbury *et al.*, 2001).

(*b*) *Molecule-to-molecule charge transfer.* A fundamental issue for the future is the role of the size of the large system. This is because, for decreasing size, back transfer to the small system becomes increasingly likely, as discussed in Sec. III.C. Studies of large molecules in contact with smaller molecules would be a natural direction for exploring this issue, as suggested by the enormous success of theoretical models in explaining core-level dynamics of free molecules (Gortel *et al.*, 1998; Gel'mukhanov and Ågren, 1999). For larger molecules such as polymers, it is noteworthy that polymer-fullerene mixtures constitute an alternative and attractive photovoltaic system (Brabec *et al.*, 2001). This is yet another avenue along which core-level dynamics could be used to determine the scale of charge-transfer times involved, as well as "pick out" particular points along a polymer to inject a core electron, for instance. Here the challenge would be to decide which C atom is being excited at which photon energy, and this may require detailed model studies. Otherwise, insertion of foreign atoms could help to "tag" particular portions of the molecule of interest in some cases. Boron, for instance, is interesting in that, upon core excitation, its $Z+1$ analog is carbon, making it ideal as a means to mimic the ground state with an extra electron upon $1s$ excitation. Yet another variety of this type of system is the molecular superconductor, a relatively recent prototype of which is alkali-intercalated C_{60}. Käämbre (2002) may be the first to succeed in utilizing RIXS to access the charge-transfer dynamics in K_3C_{60}, which gives information on the intermolecular charge transfer in the *bulk* of this nanostructured material. A hindrance to previous experimental determinations in the past has been the strong effect of rotational disorder (Louie and Shirley, 1993) and intramolecular vibronic coupling (Brühwiler *et al.*, 1997). As suggested not least by the recent work on molecular superconductors in field-effect-transistor constructions (Schön *et al.*, 2000),[20] this is a rich field for future work, in which the complexity of the system often renders conventional methods of studying the electronic structure difficult or even impossible.

(*c*) *Tuning the time scale: longer times.* Via the choice of different core levels and different elements (see, for example, Fuggle and Alvarado, 1980; Mårtensson and Nyholm, 1981, for a broad sampling of core lifetimes), one can access different dynamics. It would be interesting to compare measurements on the same system by both traditional laser pump-probe methods and those using core-hole dynamics, with core levels having longer lifetimes, such as the S $2p$ level (Prince *et al.*, 1999), if a suitable optical transition could be found which more or less matched that of XAS. Core exciton binding energies do not differ much from valence exciton binding energies in aromatic systems [one can take C_{60} as perhaps the best-studied example (Rudolf *et al.*, 1999)], suggesting that this could be achieved for selected cases.

(*d*) *Tuning the time scale: shorter times.* Taking the opposite approach, dynamics such as those due to electron-electron interactions might become accessible if the time scale could be reduced from the present state of the art. Again, one might choose different core transitions, which should leave the basic description of the process given here unmodified, although the degrees of freedom relevant to the question of coherence could be expected to change, e.g., from vibrations to electronic excitations. A different version of the core-hole clock could be envisioned utilizing soft-x-ray pulses, which can now be obtained in sub-fs lengths. It has already been shown to be possible to measure core electron spectra excited by such pulses, with timing information via the temporal coherence of those pulses with the visible pulses used to generate them as higher harmonics (Hentschel *et al.*, 2001). The soft-x-ray pump and visible probe pulses on Auger spectra are already foreseen or near-future applications. We note that the light fluences presently available are insufficient to produce highly resolved spectra of the standard accepted in synchrotron work; we assume, as well, that the intensities needed for soft-x-ray pump-probe techniques will sorely test the experimentalist's ability to obtain a measurement on solid samples before the spectral consequences of sample damage become apparent. With these factors in mind, we anticipate that this field will be more or less limited to gas-phase studies for the foreseeable future. They will, nevertheless, at the very least provide an alternative route for characterizing the finer details of what is measured using the core-hole clock as described here on well-defined systems, e.g., selected cases of molecule-to-molecule charge transfer.

(*e*) *Electronic phase transitions, nanostructured materials.* A general problem in condensed-matter physics is the issue of the electronic coupling between localized sites, a description which fits both correlated materials and nanostructured materials such as the fullerenes and fullerides, among others. There are several known cases of phase transitions between metallic and insulating phases as a function of temperature and/or composition, often connected with the presence of strong electron-electron correlations [see, for example, Park *et al.* (2000)]. While the presence of satellites in XPS and RIXS data can be used to study the local correlations, and even gain information on the electronic coupling which is important for the transport physics (Hüfner, 1996, Chap. 3), it is clear that the core-level dynamics discussed here give access to a weak coupling that lies beyond the range accessible in those more direct techniques. A recent example related to this takes up the question of how much molecular character is retained in a solid that can be considered to consist of a lattice of molecular units and that uses the core-hole clock to characterize the intermolecular character of the electronic states (Vinogradov *et al.*, 1999). This can be considered a variation on the work on C_{60} solid and on

---

[20]RIXS will perhaps be increasingly important due to the presence of high electric fields in the field-effect-transistor superconductors.

graphite discussed here as case studies. The importance of correlated materials with narrow electronic bands in condensed-matter physics suggests that this could be an increasingly important field for applications of the core-hole clock. The ability to address the underlying physical principles of transitions between a conducting and a nonconducting or semiconducting phase will be important, for example, in the development of novel electronics based on mixtures of organic polymers and inorganic materials. There is already intense scientific activity in this field, where the ability to determine the charge-transfer properties precisely will open the way to tailoring optical and electronic properties. This will have an impact on the development of diverse technologies such as optical interconnects, data storage, sensors, and information-processing systems.

(*f*) *Spintronics*. Finally we speculate on the related future possibilities of addressing problems explicitly involving the electron spin. In resent years we have witnessed a large increase in the combination of electronic transport properties with degrees of freedom related to spin (De Boeck and Borghs, 1999; Das Sarma *et al.*, 2000). This development is the basis for the enormous increase in capacity of magnetic storage media devices in the last decade. Examples include reading heads based on the gigantic magnetoresistive effect and other types of sensor applications. Paramount in this line of research is the wish to integrate electronic, optoelectronic, and magnetoelectronic functionality in a single device. The methods outlined in this article could well be adopted to study charge dynamics in spintronics in, at least, subclasses of relevant problems. In materials based on Mn perovskites the colossal magnetoresistance (CMR) effect is thought to be due to a charge transfer between a Mn^{3+} ion and a Mn^{4+} ion via a double exchange mechanism involving oxygen atoms in the perovskite. Below the Curie temperature T_C, the CMR perovskite is a semiconductor or insulator, while above T_C it behaves as a metal. In these systems one might be able to investigate the charge transfer between the two Mn ions as a function of temperature in order to address relevant parameters in proposed models for the double exchange (Zener, 1951; Anderson and Hasegawa, 1955). This class of experiments could be performed at any synchrotron-radiation facility, since no special characteristics of the source, such as circular polarization, are required. Instead, the experiment would rely on a variable charge transfer dependent on the magnetic state of the material. Spintronics in a ferromagnetic state constitutes the other class of materials. Here we imagine that, by making use of circularly polarized x rays, we could use the spin selectivity present in the excitation process similarly to x-ray magnetic circular dichroism (Carra, Konig, *et al.*, 1993; Carra, Thole, *et al.*, 1993; Arvanitis *et al.*, 1996). This will introduce a spin polarization of the core-excited intermediate state.

In summary, we suggest that the constantly improving experimental resolution and the presently available light intensity at synchrotron facilities, combined with increasing theoretical sophistication, will enable core-level charge-transfer dynamics to be profitably exploited for the foreseeable future. We look forward to following the progress of the field and hope that this review will be useful in expediting it.

REFERENCES

Aeschlimann, M., M. Bauer, S. Pawlik, R. Knorren, G. Bouzerar, and K. H. Bennemann, 2000, Appl. Phys. A: Mater. Sci. Process. **71**, 485.

Ågren, H., P. S. Bagus, and B. O. Roos, 1981, Chem. Phys. Lett. **82**, 505.

Ahuja, R., S. Auluck, J. Trygg, J. M. Wills, O. Eriksson, and B. Johansson, 1995, Phys. Rev. B **51**, 4813.

Ahuja, R., P. A. Brühwiler, J. M. Wills, B. Johansson, N. Mårtensson, and O. Eriksson, 1996, Phys. Rev. B **54**, 14 396.

Aksela, H., S. Aksela, H. Pulkkinen, G. M. Bancroft, and K. H. Tan, 1988a, Phys. Rev. A **37**, 1798.

Aksela, H., O. P. Saimnen, S. Aksela, G. M. Bancroft, and K. H. Tan, 1988b, Phys. Rev. A **37**, 1798.

Aksela, S., E. Kukk, H. Aksela, and S. Svensson, 1995, Phys. Rev. Lett. **74**, 2917.

Aldén, M., H. L. Skriver, and B. Johansson, 1994, Phys. Rev. B **50**, 12 118.

Alle, D. T., M. J. Brennan, and S. J. Buckman, 1996, J. Phys. B **29**, L277.

Almbladh, C.-O., 1977, Phys. Rev. B **16**, 4343.

Almbladh, C.-O., and L. Hedin, 1983, in *Handbook on Synchrotron Radiation*, edited by E. E. Koch (North-Holland, Amsterdam), Vol. 1, p. 607, and references therein.

Almbladh, C.-O., A. L. Morales, and G. Grossmann, 1989, Phys. Rev. B **39**, 3489.

Anderson, P. W., and H. Hasegawa, 1955, Phys. Rev. **100**, 675.

Antropov, V. P., O. Gunnarsson, and O. Jepsen, 1992, Phys. Rev. B **46**, 13 647.

Arvanitis, D., M. Tischer, J. Hunter Dunn, F. May, N. Mårtensson, and K. Baberschke, 1996, in *Spin Orbit Influenced Spectroscopies of Magnetic Solids*, edited by H. Ebert and G. Schütz (Springer Verlag, Berlin), p. 145.

Asbury, J. B., E. Hao, Y. Wang, H. N. Ghosh, and T. Lian, 2001, J. Phys. Chem. B **105**, 4545.

Bagus, P. S., and F. Schaeffer, 1972, J. Chem. Phys. **56**, 224.

Balasubramanian, T., J. N. Andersen, and L. Walldén, 2001, Phys. Rev. B **64**, 205420.

Batson, P. E., 1993, Phys. Rev. B **48**, 2608.

Bauer, M., S. Pawlik, and M. Aeschlimann, 1998, Proc. SPIE **3272**, 201.

Bäumer, M., and H.-J. Freund, 1999, Prog. Surf. Sci. **61**, 127.

Bennich, P., C. Puglia, P. A. Brühwiler, A. Nilsson, A. J. Maxwell, A. Sandell, N. Mårtensson, and P. Rudolf, 1999, Phys. Rev. B **59**, 8292.

Björneholm, O., M. Bässler, A. Ausmees, I. Hjelte, R. Feifel, H. Wang, C. Miron, M. N. Piancastelli, S. Svensson, S. L. Sorensen, F. Gel'mukhanov, and H. Åren, 2000, Phys. Rev. Lett. **84**, 2826.

Björneholm, O., A. Nilsson, A. Sandell, B. Hernnäs, and N. Mårtensson, 1992a, Phys. Rev. Lett. **68**, 1892.

Björneholm, O., A. Nilsson, E. O. F. Zdansky, A. Sandell, B. Hernnäs, H. Tillborg, J. N. Andersen, and N. Mårtensson, 1992b, Phys. Rev. B **46**, 10 353.

Böttcher, A., R. Grobecker, T. Greber, and G. Ertl, 1993, Chem. Phys. Lett. **208**, 404.

Bournel, F., F. Jolly, F. Rochet, G. Dufour, F. Sirotti, and P. Torelli, 2000, Phys. Rev. B **62**, 7645.

Brabec, C. J., A. Cravino, G. Zerza, N. S. Sariciftci, R. Kiebooms, D. Vanderzande, and J. C. Hummelen, 2001, J. Phys. Chem. B **105**, 1528.

Brühwiler, P. A., 2001, J. Phys.: Condens. Matter **13**, 11 229.

Brühwiler, P. A., A. J. Maxwell, P. Baltzer, S. Andersson, D. Arvanitis, L. Karlsson, and N. Mårtensson, 1997, Chem. Phys. Lett. **279**, 85.

Brühwiler, P. A., A. J. Maxwell, A. Nilsson, N. Mårtensson, and O. Gunnarsson, 1993, Phys. Rev. B **48**, 18 296.

Brühwiler, P. A., A. J. Maxwell, A. Nilsson, R. L. Whetten, and N. Mårtensson, 1992, Chem. Phys. Lett. **193**, 311.

Brühwiler, P. A., A. J. Maxwell, C. Puglia, A. Nilsson, S. Andersson, and N. Mårtensson, 1995, Phys. Rev. Lett. **74**, 614.

Brühwiler, P. A., A. J. Maxwell, P. Rudolf, C. D. Gutleben, B. Wästberg, and N. Mårtensson, 1993, Phys. Rev. Lett. **71**, 3721.

Campbell, J. L., and T. Papp, 2001, At. Data Nucl. Data Tables **77**, 156.

Carlson, T. A., D. R. Mullins, C. E. Beall, B. W. Yates, J. W. Taylor, D. W. Lindle, and F. A. Grimm, 1989, Phys. Rev. A **39**, 1170.

Carra, P., H. Konig, B. T. Thole, and M. Altarelli, 1993, Physica B **192**, 1.

Carra, P., B. T. Thole, M. Altarelli, and W. Xindong, 1993, Phys. Rev. Lett. **70**, 694.

Cazaux, J., 2000, J. Electron Spectrosc. Relat. Phenom. **113**, 15.

Chen, C. T., R. A. DiDio, W. K. Ford, E. W. Plummer, and W. Eberhardt, 1985, Phys. Rev. B **32**, 8434.

Chen, C. T., Y. Ma, and F. Sette, 1989, Phys. Rev. A **40**, 6737.

Chen, C. T., L. H. Tjeng, P. Rudolf, G. Meigs, J. E. Rowe, J. Chen, J. P. McCauley, Jr., A. B. Smith III, A. R. McGhie, W. J. Romanow, and E. W. Plummer, 1991, Nature (London) **352**, 603.

Chiang, T. C., G. Kaindl, and T. Mandel, 1986, Phys. Rev. B **33**, 695.

Collin, J. E., and P. Natalis, 1968, Chem. Phys. Lett. **2**, 194.

Coville, M., and T. D. Thomas, 1991, Phys. Rev. A **43**, 6053.

Das Sarma, S., J. Fabian, X. Hu, and I. Zutic, 2000, *58th Device Research Conference* (IEEE, Piscataway, NJ), p. 95.

De Boeck, J., and G. Borghs, 1999, *International Electron Devices Meeting 1999. Technical Digest* (IEEE, Piscataway, NJ), p. 215.

Domcke, W., and L. Cederbaum, 1977, Chem. Phys. **25**, 189.

Dresselhaus, M. S., G. Dresselhaus, and P. C. Eklund, 1996, *Science of Fullerenes and Carbon Nanotubes* (Academic, San Diego).

Eberhardt, W., 1995, in *Applications of Synchrotron Radiation*, edited by W. Eberhardt, Springer Series in Surface Sciences Vol. 35 (Springer-Verlag, Berlin), Chap. 6, p. 203.

Elango, M., R. Ruus, A. Kikas, A. Saar, A. Ausmees, and I. Martinson, 1996, Phys. Rev. B **53**, R5978.

Enkvist, C., S. Lunell, B. Sjögren, S. Svensson, P. A. Brühwiler, A. Nilsson, A. J. Maxwell, and N. Mårtensson, 1993, Phys. Rev. B **48**, 14 629.

Fano, U., 1961, Phys. Rev. **124**, 1866.

Feifel, R., F. Burmeister, P. Salek, M. N. Piancastelli, M. Bässler, S. L. Sorensen, C. Miron, H. Wang, I. Hjelte, O. Björneholm, A. Naves de Brito, F. K. Gel'mukhanov, H. Ågren, and S. Svensson, 2000, Phys. Rev. Lett. **85**, 3133.

Föhlisch, A., N. Wassdahl, J. Hasselström, O. Karis, D. Menzel, N. Mårtensson, and A. Nilsson, 1998, Phys. Rev. Lett. **81**, 1730.

Fuggle, J. C., and S. F. Alvarado, 1980, Phys. Rev. A **22**, 1615.

Fulde, P., 1991, *Electron Correlations in Molecules and Solids* (Springer, Berlin).

Gadea, F. X., H. Köppel, J. Schirmer, L. S. Cederbaum, K. J. Randall, A. M. Bradshaw, Y. Ma, F. Sette, and C. T. Chen, 1991, Phys. Rev. Lett. **66**, 883.

Gel'mukhanov, F., and H. Ågren, 1994, Phys. Rev. A **49**, 4378.

Gel'mukhanov, F., and H. Ågren, 1999, Phys. Rep. **312**, 87, and references therein.

Glans, P., K. Gunnelin, P. Skytt, J.-H. Guo, N. Wassdahl, J. Nordgren, H. Ågren, F. Gel'mukhanov, T. Warwick, and E. Rotenberg, 1996, Phys. Rev. Lett. **76**, 2448.

Glans, P., P. Skytt, K. Gunnelin, J. Guo, and J. Nordgren, 1996, J. Electron Spectrosc. Relat. Phenom. **82**, 193.

Golod, A., M. S. Deleuze, and L. S. Cederbaum, 1999, J. Chem. Phys. **110**, 6014.

Gortel, Z. W., and D. Menzel, 2001, Phys. Rev. B **64**, 115416.

Gortel, Z. W., R. Teshima, and D. Menzel, 1998, Phys. Rev. A **58**, 1225.

Gortel, Z. W., R. Teshima, and D. Menzel, 1999, Phys. Rev. A **60**, 2159.

Gunnarsson, O., H. Handschuh, P. S. Bechthold, B. Kessler, G. Ganteför, and W. Eberhardt, 1995, Phys. Rev. Lett. **74**, 1875.

Gunnarsson, O., and K. Schönhammer, 1980, Phys. Rev. B **22**, 3710.

Hagfeldt, A., and M. Grätzel, 2000, Acc. Chem. Res. **33**, 269.

Halas, N. J., and J. Bokor, 1989, Phys. Rev. Lett. **62**, 1679.

Hannappel, T., B. Burfeindt, W. Storck, and F. Willig, 1997, J. Phys. Chem. B **101**, 6799.

Hentschel, M., R. Kienberger, C. Spielmann, G. A. Reider, N. Milosevic, T. Brabec, P. Corkum, U. Heinzmann, M. Drescher, and F. Krausz, 2001, Nature (London) **414**, 509.

Hjortstam, O., J. M. Wills, B. Johansson, and O. Eriksson, 1998, Phys. Rev. B **58**, 13 191.

Höfer, U., 1999, Appl. Phys. B: Lasers Opt. **68**, 383.

Huber, R., S. Spörlein, J. E. Moser, M. Grätzel, and J. Wachtveitl, 2000, J. Phys. Chem. B **104**, 8995.

Hüfner, S., 1996, *Photoelectron Spectroscopy* (Springer, Berlin).

Hummelen, J. C., B. Knight, J. Pavlovich, R. González, and F. Wudl, 1995, Science **269**, 1554.

Ichikawa, K., O. Aita, K. Aoki, M. Kamada, and K. Tsutsumi, 1992, Phys. Rev. B **45**, 3221.

Johansson, B., and N. Mårtensson, 1980, Phys. Rev. B **21**, 4427.

Jugnet, Y., F. J. Himpsel, P. Avouris, and E. E. Koch, 1984, Phys. Rev. Lett. **53**, 198.

Käämbre, T., 2002, Ph.D. thesis (Uppsala University).

Karis, O., A. Nilsson, M. Weinelt, T. Wiell, C. Puglia, N. Wassdahl, N. Mårtensson, M. Samant, and J. Stöhr, 1996, Phys. Rev. Lett. **76**, 1380.

Kassühlke, B., R. Romberg, P. Averkamp, and P. Feulner, 1998, Phys. Rev. Lett. **81**, 2771.

Keller, C., M. Stichler, G. Comelli, F. Esch, S. Lizzit, Z. W. Gortel, W. Wurth, and D. Menzel, 1999, Phys. Rev. B **60**, 16 143.

Keller, C., M. Stichler, G. Comelli, F. Esch, S. Lizzit, D. Menzel, and W. Wurth, 1998a, Phys. Rev. B **57**, 11 951, and references therein.

Keller, C., M. Stichler, G. Comelli, F. Esch, S. Lizzit, W. Wurth, and D. Menzel, 1998b, Phys. Rev. Lett. **80**, 1774.

Kempgens, B., H. Köppel, A. Kivimäki, M. Neeb, L. S. Cederbaum, and A. M. Bradshaw, 1997, Phys. Rev. Lett. **79**, 3617.

Keski-Rahkonen, O., and M. O. Krause, 1974, At. Data Nucl. Data Tables **14**, 139.

Kivimäki, A., A. Naves de Brito, S. Aksela, H. Aksela, O.-P. Sairanen, A. Ausmees, S. J. Osborne, L. B. Dantas, and S. Svensson, 1993, Phys. Rev. Lett. **71**, 4307.

Kjeldgaard, L., 2001, unpublished.

Klinkmann, J., D. Cappus, K. Homann, T. Risse, A. Sandell, T. Porwol, H.-J. Freund, K. Fink, R. Fink, and V. Staemmler, 1996, J. Electron Spectrosc. Relat. Phenom. **77**, 155.

Koch, E., O. Gunnarsson, and R. M. Martin, 1999, Phys. Rev. Lett. **83**, 620.

Koller, G., R. I. R. Blyth, S. A. Sardar, F. P. Netzer, and M. G. Ramsey, 2000, Appl. Phys. Lett. **76**, 927.

Köppel, H., F. X. Gadea, G. Klatt, J. Schirmer, and L. S. Cederbaum, 1997, J. Chem. Phys. **106**, 4415.

Kotani, A., and S. Shin, 2001, Rev. Mod. Phys. **73**, 203.

Krummacher, S., M. Biermann, M. Neeb, A. Liebsch, and W. Eberhardt, 1993, Phys. Rev. B **48**, 8424.

Kukk, E., S. Aksela, and H. Aksela, 1996, Phys. Rev. A **53**, 3271.

Kyrölä, E., and J. H. Eberly, 1985, J. Chem. Phys. **82**, 1841.

Lannoo, M., G. A. Baraff, M. Schlüter, and D. Tomanek, 1991, Phys. Rev. B **44**, 12 106.

Lanzafame, J. M., S. Palese, D. Wang, R. J. D. Miller, and A. A. Muenter, 1994, J. Phys. Chem. **98**, 11 020.

Li, Z. Y., K. M. Hock, and R. E. Palmer, 1991, Phys. Rev. Lett. **67**, 1562.

Lof, R. W., M. A. van Veenendaal, B. Koopmans, H. T. Jonkman, and G. A. Sawatzky, 1992, Phys. Rev. Lett. **68**, 3924.

Louie, S. G., and E. L. Shirley, 1993, J. Phys. Chem. Solids **54**, 1767.

Lunell, S., C. Enkvist, A. G. M. Agback, S. Svensson, and P. A. Brühwiler, 1994, Int. J. Quantum Chem. **52**, 135.

Luo, Y., H. Ågren, F. Gel'mukhanov, J. Guo, P. Skytt, N. Wassdahl, and J. Nordgren, 1995, Phys. Rev. B **52**, 14 479.

Ma, Y., P. Skytt, N. Wassdahl, P. Glans, D. C. Mancini, J. Guo, and J. Nordgren, 1993, Phys. Rev. Lett. **71**, 3725.

Maciejewski, P., U. Höfer, W. Wurth, and E. Umbach, 1993, J. Electron Spectrosc. Relat. Phenom. **62**, 1.

Magnuson, M., J. Guo, C. Såthe, J.-E. Rubensson, J. Nordgren, P. Glans, L. Yang, P. Salek, and H. Ågren, 1999, Phys. Rev. A **59**, 4281.

Mahan, G. D., 1977, Phys. Rev. B **15**, 4587.

Malinovskaya, S. A., and L. S. Cederbaum, 2000, Int. J. Quantum Chem. **80**, 950.

Mansour, A., S. E. Schnatterly, and R. D. Carson, 1985, Phys. Rev. B **31**, 6521.

Mårtensson, N., and R. Nyholm, 1981, Phys. Rev. B **24**, 7121.

Mårtensson, N., M. Weinelt, O. Karis, M. Magnuson, A. Nilsson, J. Stöhr, and M. Samant, 1997, Appl. Phys. A: Mater. Sci. Process. **A65**, 159.

Martins, J. L., N. Troullier, and J. H. Weaver, 1991, Chem. Phys. Lett. **180**, 457.

Matzdorf, R., A. Gerlach, F. Theilmann, G. Meister, and A. Goldmann, 1999, Appl. Phys. B: Lasers Opt. **B68**, 393.

Maxwell, A. J., P. A. Brühwiler, S. Andersson, N. Mårtensson, and P. Rudolf, 1995, Chem. Phys. Lett. **247**, 257.

Maxwell, A. J., P. A. Brühwiler, D. Arvanitis, J. Hasselström, M. K.-J. Johansson, and N. Mårtensson, 1998, Phys. Rev. B **57**, 7312.

Maxwell, A. J., P. A. Brühwiler, D. Arvanitis, J. Hasselström, and N. Mårtensson, 1996, Chem. Phys. Lett. **260**, 71.

Maxwell, A. J., P. A. Brühwiler, D. Arvanitis, J. Hasselström, and N. Mårtensson, 1997, Phys. Rev. Lett. **79**, 1567.

Maxwell, A. J., P. A. Brühwiler, A. Nilsson, N. Mårtensson, and P. Rudolf, 1994, Phys. Rev. B **49**, 10 717.

May, V., and O. Kühn, 2000, *Charge and Energy Transfer Dynamics in Molecular Systems* (Wiley-VCH, Berlin).

McCulloch, D. G., and R. Brydson, 1996, J. Phys.: Condens. Matter **8**, 3835.

Mele, E. J., and J. J. Ritsko, 1979, Phys. Rev. Lett. **43**, 68.

Menzel, D., G. Rocker, H.-P. Steinrück, D. Coulman, P. A. Heimann, W. Huber, P. Zebisch, and D. R. Lloyd, 1992, J. Chem. Phys. **96**, 1724.

Menzel, D., and W. Wurth, 2000, in *X-ray and Inner-Shell Processes, 18th International Conference*, Chicago, 1999, edited by R. W. Dunford, D. S. Gemmell, E. P. Kanter, B. Krässig, S. H. Southworth, and L. Young (AIP, New York), p. 372.

Merzbacher, E., 1970, *Quantum Mechanics* (Wiley, New York).

Michiels, J. J. M., M. Grioni, and J. C. Fuggle, 1992, J. Phys.: Condens. Matter **4**, 6943.

Miller, R. J. D., G. L. McLendon, A. J. Nozik, W. Schmickler, and F. Willig, 1995, *Surface Electron Transfer Processes* (VCH, New York).

Murphy, R., E. W. Plummer, C. T. Chen, W. Eberhardt, and R. Carr, 1989, Phys. Rev. B **39**, 7517.

Naves de Brito, A., A. Naves de Brito, O. Björneholm, J. S. Neto, A. B. Machado, S. Svensson, A. Ausmees, S. J. Osborne, L. J. Sæthre, H. Aksela, O.-P. Sairanen, A. Kivimäki, *et al.*, 1997, J. Mol. Struct.: THEOCHEM **394**, 135.

Neeb, M., J.-E. Rubensson, W. Biermann, and W. Eberhardt, 1994, J. Electron Spectrosc. Relat. Phenom. **67**, 261, and references therein.

Newns, D. M., 1969, Phys. Rev. **178**, 1123.

Nilsson, A., O. Björneholm, E. O. F. Zdansky, H. Tillborg, N. Mårtensson, J. N. Andersen, and R. Nyholm, 1992, Chem. Phys. Lett. **197**, 12.

Nyberg, M., Y. Luo, L. Triguero, L. G. M. Pettersson, and H. Ågren, 1999, Phys. Rev. B **60**, 7956.

O'Brien, W. L., J. Jia, Q.-Y. Dong, T. A. Callcott, D. L. Mueller, D. L. Ederer, N. D. Shinn, and S. C. Woronick, 1991a, Phys. Rev. B **44**, 13 277.

O'Brien, W. L., J. Jia, Q.-Y. Dong, T. A. Callcott, J.-E. Rubensson, D. L. Mueller, and D. L. Ederer, 1991b, Phys. Rev. B **44**, 1013.

Ohno, M., 1994, Phys. Rev. B **50**, 2566.

Osborne, S. J., A. Ausmees, S. Svensson, A. Kivimäki, O.-P. Sairanen, A. Naves de Brito, H. Aksela, and S. Aksela, 1995, J. Chem. Phys. **102**, 7317.

Park, J.-H., L. H. Tjeng, A. Tanaka, J. W. Allen, C. T. Chen, P. Metcalf, J. M. Honig, F. M. F. de Groot, and G. A. Sawatzky, 2000, Phys. Rev. B **61**, 11 506.

Patthey, L., H. Rensmo, P. Persson, K. Westermark, L. Vayssieres, A. Stashans, Å. Petersson, P. A. Brühwiler, H. Siegbahn, S. Lunell, and N. Mårtensson, 1999, J. Chem. Phys. **110**, 5913.

Pedio, M., M. L. Grilli, C. Ottaviani, M. Capozi, C. Quaresima, P. Perfetti, P. A. Thiry, R. Caudano, and P. Rudolf, 1995, J. Electron Spectrosc. Relat. Phenom. **76**, 405.

Piancastelli, M. N., 2000, J. Electron Spectrosc. Relat. Phenom. **107**, 1, and references therein.

Porwol, T., G. Dömötör, I. Hemmerich, J. Klinkmann, H.-J. Freund, and C.-M. Liegener, 1994, Phys. Rev. B **49**, 10 557.

Prince, K. C., I. Ulrych, M. Peloi, B. Ressel, V. Cháb, C. Crotti, and C. Comicioli, 2000, Phys. Rev. B **62**, 6866.

Prince, K. C., M. Vondrácek, J. Karvonen, M. Coreno, R. Camilloni, L. Avaldi, and M. de Simone, 1999, J. Electron Spectrosc. Relat. Phenom. **101-103**, 141.

Puglia, C., P. Bennich, J. Hasselström, C. Ribbing, P. A. Brühwiler, A. Nilsson, Z. Y. Li, and N. Mårtensson, 1998, Surf. Sci. **414**, 118.

Puglia, C., P. A. Brühwiler, J. Hasselström, P. Bennich, A. Nilsson, and N. Mårtensson, 1998, J. Chem. Phys. **109**, 1209.

Ramakrishna, S., and F. Willig, 2000, J. Phys. Chem. B **104**, 68.

Ramakrishna, S., F. Willig, and V. May, 2001, J. Chem. Phys. **115**, 2743.

Randell, J., S. L. Lunt, G. Mrotzek, D. Field, and J. P. Ziesel, 1996, Chem. Phys. Lett. **252**, 253.

Rotenberg, E., C. Enkvist, P. A. Brühwiler, A. J. Maxwell, and N. Mårtensson, 1996, Phys. Rev. B **54**, R5279.

Rubensson, J.-E., 2000, J. Electron Spectrosc. Relat. Phenom. **110-111**, 135.

Rubensson, J.-E., J. Lüning, S. Eisebitt, and W. Eberhardt, 1997, Appl. Phys. A: Mater. Sci. Process. **A65**, 91.

Rudolf, P., M. S. Golden, and P. A. Brühwiler, 1999, J. Electron Spectrosc. Relat. Phenom. **100**, 409.

Sałek, P., F. Gel'mukhanov, and H. Ågren, 1999, Phys. Rev. A **59**, 1147.

Sandell, A., 1993, Ph.D. thesis (Uppsala University).

Sandell, A., O. Björneholm, A. Nilsson, B. Hernnäs, J. N. Andersen, and N. Mårtensson, 1994, Phys. Rev. B **49**, 10 136.

Sandell, A., P. A. Brühwiler, A. Nilsson, P. Bennich, P. Rudolf, and N. Mårtensson, 1999, Surf. Sci. **429**, 309.

Sandell, A., O. Hjortstam, A. Nilsson, P. A. Brühwiler, O. Eriksson, P. Bennich, P. Rudolf, J. M. Wills, B. Johansson, and N. Mårtensson, 1997, Phys. Rev. Lett. **78**, 4994.

Sandell, A., J. Libuda, P. A. Brühwiler, S. Andersson, M. Bäumer, A. J. Maxwell, N. Mårtensson, and H.-J. Freund, 1997, Phys. Rev. B **55**, 7233.

Schmuttenmaer, C. A., M. Aeschlimann, H. E. Elsayed-Ali, R. J. D. Miller, D. A. Mantell, J. Cao, and Y. Gao, 1994, Phys. Rev. B **50**, 8957.

Schnadt, J., P. A. Brühwiler, L. Patthey, J. N. O'Shea, S. Södergren, M. Odelius, R. Ahuja, O. Karis, M. Bässler, P. Persson, H. Siegbahn, S. Lunell, 2002, unpublished.

Schön, J. H., C. Kloc, and B. Batlogg, 2000, Nature (London) **406**, 702.

Schulte, H. D., and L. S. Cederbaum, 1995, J. Chem. Phys. **103**, 698.

Schulz, G. J., 1973, Rev. Mod. Phys. **45**, 423.

Schwedhelm, R., L. Kipp, A. Dallmeyer, and M. Skibowski, 1998, Phys. Rev. B **58**, 13 176.

Sette, F., G. K. Wertheim, Y. Ma, G. Meigs, S. Modesti, and C. T. Chen, 1990, Phys. Rev. B **41**, 9766.

Shirley, E. L., 1998, Phys. Rev. Lett. **80**, 794.

Shirley, E. L., 2000, J. Electron Spectrosc. Relat. Phenom. **110-111**, 305.

Shirley, E. L., and S. G. Louie, 1993, Phys. Rev. Lett. **71**, 133.

Skytt, P., P. Glans, J.-H. Guo, K. Gunnelin, C. Såthe, J. Nordgren, F. Gel'mukhanov, A. Cesar, and H. Ågren, 1996, Phys. Rev. Lett. **77**, 5035.

Skytt, P., J. Guo, N. Wassdahl, J. Nordgren, Y. Luo, and H. Ågren, 1995, Phys. Rev. A **52**, 3572.

Smith, B. B., and A. J. Nozik, 1999, J. Phys. Chem. B **103**, 9915.

Sonntag, B., 1977, *Electronic Structure of Rare Gas Solids* (Academic, London), p. 1021.

Stöhr, J., 1992, *NEXAFS Spectroscopy* (Springer, Berlin).

Sundin, S., F. K. Gel'mukhanov, H. Ågren, S. J. Osborne, A. Kikas, O. Björneholm, A. Ausmees, and S. Svensson, 1997, Phys. Rev. Lett. **79**, 1451.

Themlin, J.-M., S. Bouzidi, F. Coletti, J.-M. Debever, G. Gensterblum, L.-M. Yu, J.-J. Pireaux, and P. A. Thiry, 1992, Phys. Rev. B **46**, 15 602.

Triguero, L., Y. Luo, L. G. M. Pettersson, H. Ågren, P. Väterlein, M. Weinelt, A. Föhlisch, J. Hasselström, O. Karis, and A. Nilsson, 1999, Phys. Rev. B **59**, 5189.

Tsuei, K.-D., J.-Y. Yuh, C.-T. Tzeng, R.-Y. Chu, S.-C. Chung, and K.-L. Tsang, 1997, Phys. Rev. B **56**, 15 412.

Ueba, H., 1991, Surf. Sci. **242**, 266.

Ueba, H., 1992, Phys. Rev. B **45**, 3755.

van Veenendal, M., and P. Carra, 1997, Phys. Rev. Lett. **78**, 2839.

Vinogradov, A. S., A. B. Preobrajenski, S. L. Molodtsov, S. A. Krasnikov, R. Szargan, A. Knop-Gericke, and M. Havecker, 1999, Chem. Phys. **249**, 249.

Vondrácek, M., K. C. Prince, J. Karvonen, M. Coreno, R. Camilloni, L. Avaldi, and M. de Simone, 1999, Synchrotron Radiat. News **12**, 27.

Walters, D. L., and C. P. Bhalla, 1971, Phys. Rev. A **3**, 1919.

Wang, H., J. C. Woicik, T. Åberg, M. H. Chen, A. Herrera-Gomez, T. Kendelewicz, A. Mäntykenttä, K. E. Miyano, S. Southworth, and B. Crasemann, 1994, Phys. Rev. A **50**, 1359.

Wästberg, B., S. Lunell, C. Enkvist, P. A. Brühwiler, A. J. Maxwell, and N. Mårtensson, 1994, Phys. Rev. B **50**, 13 031.

Wästberg, B., and A. Rosén, 1991, Phys. Scr. **44**, 276.

Weinelt, M., A. Nilsson, M. Magnuson, T. Wiell, N. Wassdahl, O. Karis, A. Föhlisch, N. Mårtensson, J. Stöhr, and M. Samant, 1997, Phys. Rev. Lett. **78**, 967.

Weng, X., P. Rez, and H. Ma, 1989, Phys. Rev. B **40**, 4175.

Wurth, W., 1997, Appl. Phys. A: Mater. Sci. Process. **A65**, 597.

Wurth, W., P. Feulner, and D. Menzel, 1992, Phys. Scr., T **T41**, 213.

Wurth, W., and D. Menzel, 1995, in *Spectroscopy and Dynamics of the Electronic Decay of Core Electron Excitations in Isolated and Chemisorbed Molecules*, edited by W. Eberhardt, Springer Series in Surface Science Vol. 35 (Springer, Berlin), Chap. 6, p. 171.

Wurth, W., and D. Menzel, 2000, Chem. Phys. **251**, 141.

Wurth, W., G. Rocker, P. Feulner, R. Scheuerer, L. Zhu, and D. Mentzel, 1993, Phys. Rev. B **47**, 6697.

Wurth, W., C. Schneider, R. Treichler, D. Menzel, and E. Umbach, 1988, Phys. Rev. B **37**, 8725.

Wurth, W., C. Schneider, R. Treichler, E. Umbach, and D. Menzel, 1987, Phys. Rev. B **35**, 7741.

Xu, S., J. Cao, C. C. Miller, D. A. Mantell, R. J. D. Miller, and Y. Gao, 1996, Phys. Rev. Lett. **76**, 483.

Zangwill, A., 1988, *Physics at Surfaces* (Cambridge, New York).

Zener, C., 1951, Phys. Rev. **81**, 440.